TECHNIQUE FOR RADIOLABELLING TRACERS WITH ^{64}Cu FOR POSITRON EMISSION PARTICLE TRACKING (PEPT) EXPERIMENTS

Cong Liu

Thesis presented in fulfilment of the requirements for the degree of Master of Science (Eng) at the University of Cape Town.

Department of Chemical Engineering

University of Cape Town

January 2015

DECLARATION

I, the undersigned, hereby declare that the work contained in this thesis is my own original work and that I have not previously submitted it at any university for a degree, neither in part nor in its entirety.

Signature: ……

Date: ……

ABSTRACT

Positron emission particle tracking (PEPT) is a non-invasive technique for studying the flow of particulate systems within industrial equipment. The technique tracks a tracer particle labelled with a positron emitting radionuclide moving within the field-of-view of a positron emission tomography (PET) scanner.

Two important components of the technique are a PET camera and PEPT tracers, which are particle tracers labelled with a positron emitting radionuclide. Currently, the majority of PEPT tracers are made with ^{68}Ga or ^{18}F. However, the relatively short half-life of these two radionuclides limits the application of PEPT to a maximum of 3 hours of experimental time. ^{64}Cu is a potential candidate for PEPT tracer fabrication due to its relatively long half-life (12.7 h) which could extend the experimental running time of PEPT experiments to two uninterrupted days.

The objective of the research described in this thesis was to develop a technique for radiolabelling tracers with ^{64}Cu, and to test their efficacy in PEPT experiment. The work was conducted at Radionuclide Production Department, iThemba LABS near Cape Town, where high purity ^{64}Cu was obtained by a two stages separation method using ion exchange chromatography. The purity of the final separated ^{64}Cu was analysed on a High Purity Germanium (HPGe) detector. And the ^{64}Cu tracer was manufactured via an ion exchange method. Finally, as the low positron emission branching ratio of ^{64}Cu might have produced lower tracking efficiency than common PEPT radionuclides such as ^{18}F or ^{68}Ga, comparison experiments were performed to determine the tracking efficiency of ^{64}Cu tracer relative to the common PEPT tracers.

Overall, the goals of this thesis were successfully achieved. High purity ^{64}Cu was produced from the ^{67}Ga production waste solution via the modified ion-exchange separation method. The modified method was proved to be more efficient and faster. A ^{64}Cu tracer was fabricated with a chelating ion-exchange resin particle. The tracer was tested and found to be capable of working in aqueous environments within a pH range of 3 to 13. The tracer showed good tracking efficiency when its activity was above 5 μCi and its long half-life would enable a tracking time of more than 100 hours without interruption.

ACKNOWLEDGEMENTS

I would like to express my gratitude to all those who assisted me throughout this research:

- My supervisors Prof. Jean-Paul Franzidis, Prof. Andy Buffler and Dr. Katie Cole for all their advice and whole hearted support throughout the project; the time spent on showing me how to conduct scientific research step by step; tirelessly editing my draft writing, and allowing me enough freedom to steer this work in my own direction. Without them, this work would not have been possible.

- My colleague at PEPT Cape Town, Michael van Heerden, for his support and assistance in running ^{64}Cu experiments in the PEPT Cape Town laboratory, and many conversations that helped to solve bumps in the research.

- My colleagues at the Radionuclide Production Department, iThemba LABS, Dr Clive Naidoo and Stuart Dolley, for giving me permission to conduct the ^{64}Cu separation and helping me through the practical experiments.

- The radiation protection team at iThemba LABS, for their help and advice to ensure the safety of this work.

- My friend Dr Yaodong Wang, for his advice in conducting ^{64}Cu PET plant research.

- Prof. Jolanta Mesjasz-Przybylowicz and Prof. Wojciech Przybylowicz from the Material Research Group, iThemba LABS, for their advice and contribution to ^{64}Cu PET plant imaging.

I would also like to thank the Mineral to Metals Initiative, the Department of Physics at UCT and iThemba LABS for their financial support.

CONTENTS

LIST OF FIGURES

CHAPTER 1 INTRODUCTION

Positron emission particle tracking (PEPT) is a non-invasive technique used for obtaining dynamic information of particle behaviour within engineering equipment. The basis of the technique is to radiolabel a tracer with a suitable positron emitting radionuclide. Positrons released from the tracer annihilate with local electrons to produce a pair of almost back-to-back 511 keV γ-rays. When both γ-rays are detected simultaneously, a line of response can be formed with the tracer located somewhere along that line. Multiple lines-of-response can be used to triangulate the tracer location [1], [2].

In theory, only three coincident pairs of γ-ray are needed for a 3D location, but in practice a large number of random gamma rays are also detected: thus many lines of response are needed to locate the tracer. A successful PEPT measurement crucially relies on whether the tracer has been labelled with sufficient activity to accurately locate it. In addition, the physical and chemical properties of the tracer need to be representative of a particle from the system bulk [3].

The PEPT technique has been used in science and engineering to obtain detailed information on the motion and flow fields of granular materials in industrial equipment. PEPT relies upon the detection of gamma rays which can penetrate opaque industrial equipment without interfering with the internal behaviour of the system. PEPT has been used to measure the dynamic behaviour of granular materials in a wide range of applications, including chemical reactors, granulators, mixers, dryers, rotating kilns, floatation cells and ball mills [4]–[8]. The information obtained by the PEPT technique, such as the occupancy of a rock particle in a tumbling mill as shown in Figure 1, can be used to optimize the design and operating conditions for a wide range of industrial process systems. It can also provide experimental data to validate fundamental physics based computational models [9].

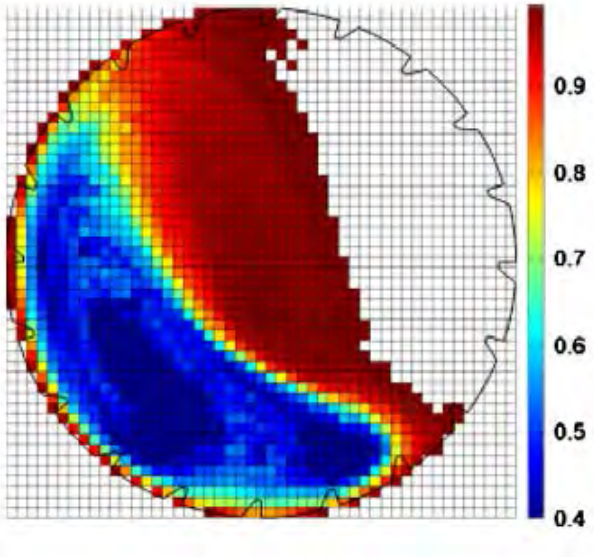

Figure 1: An example PEPT study: porosity distribution of a 5mm glass bead in tumbling mill for the mill rotating at 75% of critical speed [10]**.**

PEPT was developed in 1993 at the Positron Imaging Centre at the University of Birmingham, which has been the main PEPT facility in the world for the past 20 years. In 2009, the University of Cape Town established a second dedicated centre situated at iThemba LABS, Cape Town. PEPT Cape Town laboratory hosts a Siemens ECAD "EXACT 3D" PET scanner. This scanner has high sensitivity and resolution, which has made the tracking of extremely small sized and low activity tracers viable. The laboratory also benefits from being located at the iThemba LABS, which routinely produces radionuclides that can be used for labelling PEPT tracers.

1.1 Project motivation

Most current research in PEPT involves either validation of fundamental physics based models or granular industrial applications. Most of the tracer labelling methods in use are based on two papers published by Fan *et al.* in 2006 [2], [3]. PEPT is an increasingly popular technique; however, the existing tracer fabrication techniques are not sufficient to produce tracers for all PEPT applications. In particular, the following areas need further research:

- Labelling tracers with longer lived radionuclides;
- Controlling the physical properties of the tracers, *e.g.* density;

- Controlling the chemical properties of the tracers *e.g.* surface properties;
- Labelling sub-50 micron tracers with sufficient activity;
- Labelling tracer more quickly and effectively, to limit loss of activity due to the decay of the radionuclide, and minimize the exposure of the operators to radioactivity.

Most tracers for PEPT have been labelled with ^{68}Ga ($t_{1/2}$= 68 min) and ^{18}F ($t_{1/2}$= 109 min). Their relatively short half-lives have limited the PEPT tracking time to a few hours, because location errors tend to increase as the activity on the tracer decays. There is potential demand for longer lived tracers in order to extend the tracking time of PEPT experiments.

^{64}Cu decays via positron emission and has a half-life of 12.7 hours. It is a radionuclide that has been widely used in nuclear medicine for imaging and therapy [11]–[13]; therefor it could be also useful for PEPT experiments. iThemba LABS routinely produces ^{67}Ga by the bombardment of a natural zinc target with a 66 MeV proton beam. During this process, a substantial quantity of ^{64}Cu is co-produced by the ^{68}Zn(p, α)^{64}Cu reaction. After ^{67}Ga extraction, the zinc waste solution contains a significant amount of ^{64}Cu, which can be purified and used directly for tracer labelling.

1.2 Objectives

This work was focused on producing a tracer for PEPT with the longer lived radionuclide ^{64}Cu ($t_{1/2}$ = 12.7 h) using ion-exchange resins. The main aim of this work was to develop a new technique to label tracer particles with ^{64}Cu that are suitable for PEPT measurements. This was broken down into three steps:

1. Separation and purification of ^{64}Cu from ^{67}Ga production waste solution;
2. Development of a tracer labelling technique for ^{64}Cu tracer particles;
3. Comparison of the tracking efficiency of the ^{64}Cu tracer with ^{68}Ga, ^{18}F, ^{22}Na tracers in the PET scanner.

CHAPTER 2 LITERATURE REVIEW

Positron emission particle tracking (PEPT) is a technique that was developed originally at the University of Birmingham by Parker *et al.* [14]. Over the past 20 years, it has become a powerful tool for *in situ* characterization and visualization of particulate flow within aggressive industrial environments, such as tumbling mills and powder mixers. The basic principle of the PEPT technique is the tracking of a tracer particle which has been labelled with a suitable positron emitting radionuclide in a modified positron emission tomography (PET) camera.

This chapter gives an introduction to the PEPT technique, which includes the basic concept of PEPT; the development of PEPT at the University of Birmingham; a description of the new PEPT Cape Town laboratory; the radionuclides used for PEPT; three tracer labelling techniques; information about ion-exchange reins; and PEPT applications.

2.1 What is PEPT?

PEPT is derived from techniques developed for PET in the medical industry [15]. The basis of the technique is a tracer labelled with a radionuclide which decays by positron emission. Positrons emitted from the tracer annihilate with local electrons, which are the anti-particle of the positron. This annihilation event releases a pair of almost collinear 511 keV γ-rays (within ~0.5^{o}). If both of these gamma rays are detected in coincidence in an array of detectors, such as those found in a PET scanner or positron camera, this defines a “line of response” (LOR) at some point along which the annihilation occurred. A three-dimensional image of the distribution of the tracer can be constructed from a collection of such LORs, measured at many angles, using the analytical methods of tomography. Positron-emitting radionuclides are produced using particle accelerators, with the majority of medical PET facilities making use of the radiopharmaceutical [^{18}F]-fluorodeoxyglucose (FDG) which is administered to the patient in liquid form.

Practically, PEPT is the extension of PET imaging to particle tracers and was first developed in the late 1980s at the University of Birmingham [14], [16], [17]. The key

difference between PET and PEPT is that PET generates a three-dimensional image of the distribution of the radionuclide during an exposure time of several minutes, whereas PEPT locates a tracer particle in three dimensions many tens or hundreds of times per second.

In PEPT, the tracer particle must be labelled with a positron-emitting radionuclide. Then the location of this tracer particle can be determined by triangulating a small number of LORs within the field of view of a PET camera (Figure 2). Detection of a few such events in a very short time interval allows the position to be tracked with time.

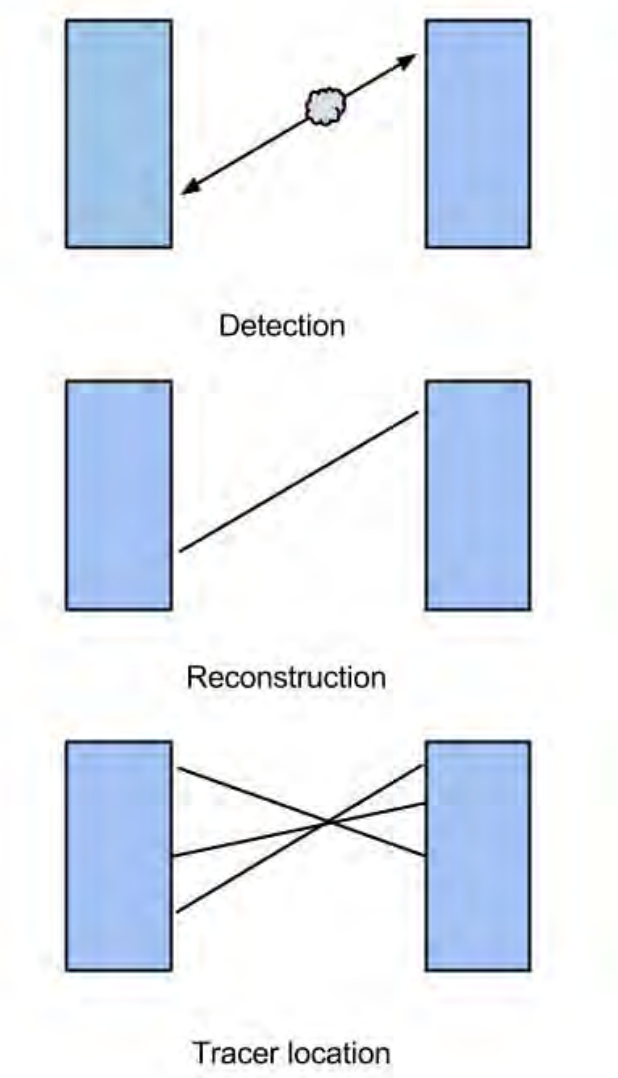

Figure 2: Schematic diagram of PEPT for a single tracer particle.

In principle only two LORs are necessary for a 3D triangulation, but practically a larger number of measured LORs are required to ensure an accurate measurement of the tracer location. Errors may arise from the detection of gamma rays after undergoing Compton scattering, and the coincident detection of two gamma rays which were not from the same annihilation event (Figure 3). However, since many thousands of coincidence events can be detected in a PET camera and processed each second, a particle moving at speeds of up to 10 m/s can be tracked.

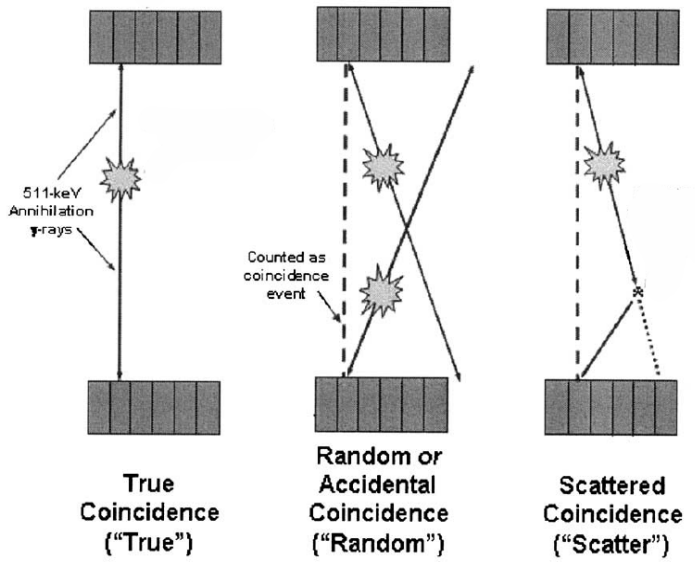

Figure 3: Error caused from random and scattered events in the detection of gamma rays [18]**.**

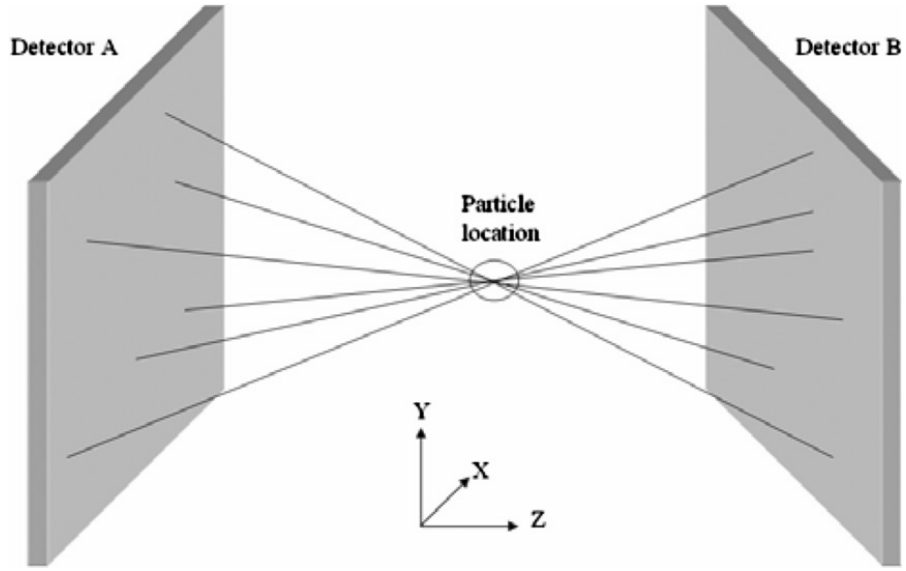

Figure 4: Schematic diagram of PEPT for a single particle [1]**.**

A location algorithm [14] is employed to calculate the position of the particle within the field of view based on the detection of a series of 511 keV back-to-back γ-rays. It is based on the notion that all true γ-ray pairs originating from the tracer at a given position should meet at a point in space, within limits set by the resolution of the camera. This meeting point of the LORs is the location of the particle, as shown in Figure 4.

The location algorithm calculates the point which minimizes the sum of perpendicular distances to the various LORs [1]. In practice, many of the detected events are scattered and random pairs (Figure 3). Thus, the location algorithm needs to discard these events, and then recalculate the location using only the true pair events.

2.2 The development of the Positron Imaging Centre at the University of Birmingham

The Positron Imaging Centre (PIC) at the University of Birmingham undertook research of positron detection in the early 1980s. In response to the need to develop a PET camera with a wide field of view at reasonable cost for non-medical studies, the original Birmingham Positron Camera (Figure 5) was designed and constructed at the Rutherford Appleton Laboratory [19]. It consisted of a pair of multi-wire proportional chambers, each having a sensitive area of 600 × 300 mm^2 and operated in coincidence. It was constructed in 1984 and carried on operating for the next 15 years.

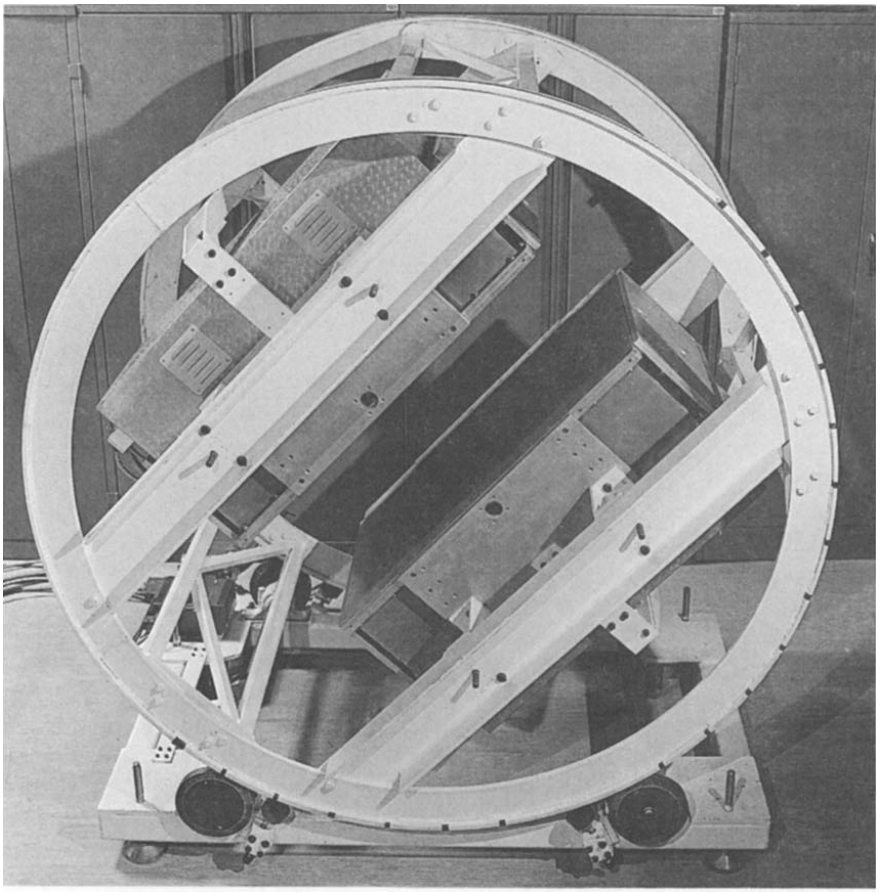

Figure 5: The two detectors of the original Birmingham positron camera on their rotating mount [17]**.**

The University of Birmingham employs positron imaging for science applications in three distinct ways: 3D PET imaging, 2D PET imaging and PEPT [20]. The 3D PET images are obtained by rotating detectors around the field of view; acquiring sufficient data takes at least an hour, so it is only applicable to steady-state systems. The 2D PET images are obtained when the detectors are stationary, and can be completed in a few minutes; this is particularly useful for tracers known to be confined to a relatively narrow band in the third dimension. The 2D and 3D PET imaging techniques are known collectively as Positron Emission Projection Imaging (PEPI) techniques, and have been used extensively to study liquid flow and distribution in oil extraction and waste disposal in geological applications [17]. It is also possible to use gas tracers such as ^{11}C labelled carbon monoxide for the study of gas pathways through saturated rock fractures [20]. PEPT is performed when the cameras are stationary, and the tracer can be located up to 1000 times per second [21].

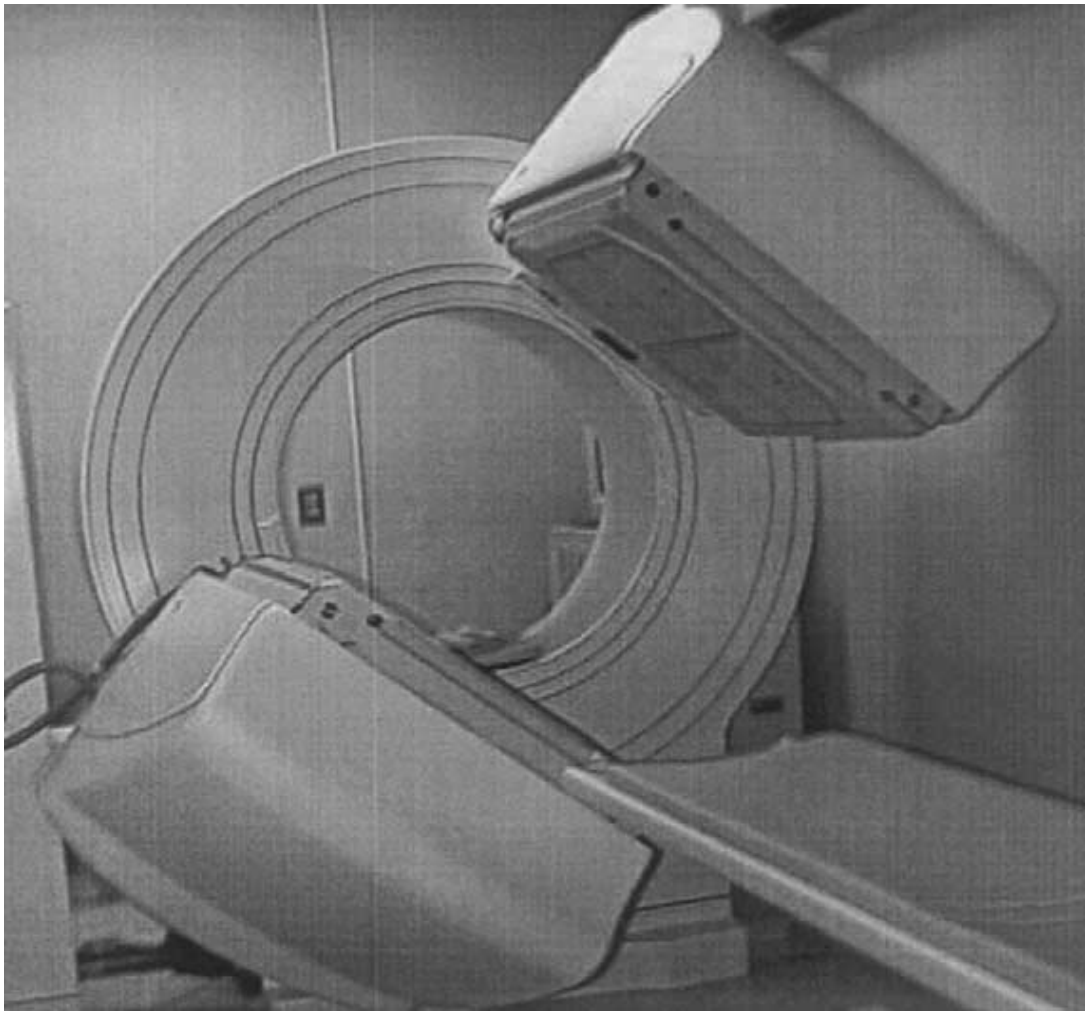

Figure 6: A medical ADAC Forte PET camera [20]**.**

The limitation of the original camera was a low quantum efficiency for detecting 511 keV energy level photon annihilation, hence the useful coincidence event rate was limited to less than 5000 s^{-1}. In 1999, the PIC upgraded their facility with a ADAC Forte gamma camera (Figure 6) manufactured by ADAC Laboratories. It consists of two heads, each containing a single crystal of NaI(Tl) scintillator, with size of 500 × 400 mm^2 and 16 mm thick. The scintillator is optically coupled to an array of 55 photomultiplier tubes, each channelled through a separate analogue-to-digital converter (ADC) [20].

The specifications of the ADAC Forte PET camera are given as follows: each head can operate at a single rate of over 2 million counts per second with the dead-time per pulse less than 170 ns. With a point source of gamma rays from electron-positron annihilation, a coincidence rate of over 100 k events per second can be achieved with a coincidence resolving time of 7.5 ns. The spatial resolution of the camera (full width

at half maximum (FWHM) of the back projected image of a point source) is approximately 6 mm. The data are recorded event by event on a computer for subsequent processing. The heads are mounted on a motorised gantry which permits rotation about a horizontal axis, and adjustment of the face-to-face separation of the detectors from 250 to 800 mm [22].

When using the ADAC Forte camera, a tracer labelled with a positron-emitting radionuclide moving with speed around 1 ms^{-1} can be located to within 0.5 mm over 250 times per second [23]. This allows the distribution of the instantaneous velocity of the tracer to be calculated with 10% uncertainty. Tracking is possible over a maximum field of view of 800 × 500 × 400 mm^3 within the space between the two detectors, although accurate tracking is not possible near the edges of the field of view. The camera is mounted on rails with a motorised drive under computer control so that a slowly moving tracer can be followed in real time.

Parker *et al.* [20] state that for the same camera geometry, the new camera offers improvements over the old camera. In particular, spatial resolution is at least 25% better, sensitivity is increased by a factor of 10, and the resolving time is reduced to 60%, enabling it to provide useful data rates between a factor of 20 and 40 higher. Specifically for PEPT, this result is an improvement by a factor of 10 in precision of location at optimum rates, enabling the tracking of faster moving particles. Practically, accurate tracking can be achieved using tracers with less activity; therefore there is scope for producing a wider range of tracers, including smaller tracer particles.

The ADAC Forte camera was originally designed to image human patients, which creates restrictions on the size and geometry of the experimental systems that can be used with PEPT. A new modular positron camera was developed in recent years to enable PEPT measurements in larger experimental systems [24]. The modular system was built using bismuth germinate (BGO) detector blocks from medical PET scanners. These blocks were grouped into modules (“buckets”), each comprised of four detector blocks with their associated electronics (preamplifiers, discriminators and ADCs) under the control of a “bucket controller” (Figure 7). A complete modular camera consists of 16 buckets, where each bucket is encased in a protective box, connected to a data processing system which identifies coincidences where gamma-rays are detected between two buckets. These data are recorded in list mode.

For most applications, the modular camera has been arranged in two modes: two opposite banks or four orthogonal banks, each four boxes high, with the experimental system in the centre (Figure 8). The maximum sensitivity is achieved when the blocks are closely packed.

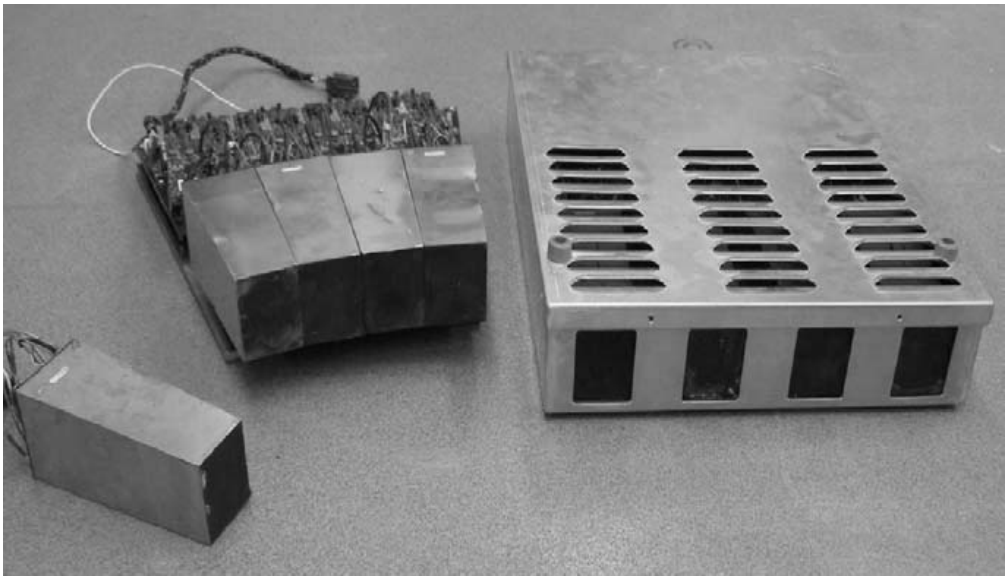

Figure 7: A single detector block (left), detector bucket (middle) and module mounted in protective box [24]**.**

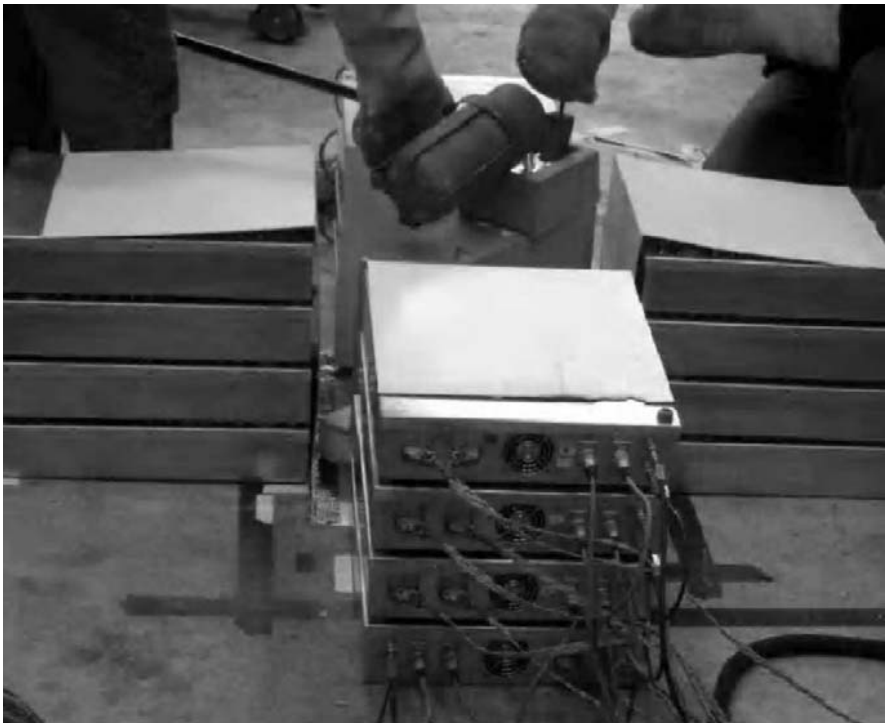

Figure 8: An example of modular camera application – study of molten aluminium [24]**.**

The advantages of this modular camera system are that it has flexible geometry; it is transportable, and capable of delivering high data rates. The limitation of this system, pointed out by Parker *et al.* [24], is that the effective count rate is limited by the speed of storing data from the PET camera. To overcome this, a new data storage system is currently under construction with the aim of being able to store all data from particles moving over 1 ms^{-1}.

2.3 PEPT Cape Town

PEPT Cape Town, of the University of Cape Town, is the world's second major operational PEPT facility after the PIC at the University of Birmingham. It was opened in 2009 and is situated at iThemba LABS national cyclotron centre in South Africa. The PEPT facility was installed at iThemba LABS due to the availability of radionuclides on-site. iThemba LABS operates a 200 MeV separated sector cyclotron, and a 6 MV van de Graaff accelerator. The cyclotron facility routinely produces both light and heavy particle beams for nuclear physics research, radiotherapy and radionuclide production. This location has advantages for PEPT Cape Town, through radionuclide production, handling and licensing.

PEPT Cape Town hosts an ECAD "EXACT 3D" HR++ (Model: CTI/Siemens 966) PET camera, which was donated to University of Cape Town by Hammersmith Hospital (now part of Imperial College London) in the UK. The camera was used for clinical research at Hammersmith Hospital from 1995 until it was decommissioned, and may still be the most sensitive 3D PET scanner in operation today.

The HR++ camera (Figure 9) was designed with the aim of achieving high sensitivity and resolution using available detector technology [25]. The detection system consists of 36 separated detector buckets, where each bucket is a group of 6 single bismuth germinate (BGO) detector blocks. The buckets are arranged around the ring geometry of the camera, which has a diameter of 82 cm, and produces an axial field of view of 23.4 cm. This is significantly larger than other "standard" ring geometries in PET cameras, which normally have a ring diameter of 50-70 cm [26]. The input/output and computing hardware can maintain a sustained acquisition rate of about 4 million coincidence events per second. The mean spatial resolution is 4.8 ± 0.2 mm FWHM (transaxial, 1 cm off-axis) and 5.6 ± 0.5 mm (axial, on-axis).

Figure 9: The "EXACT 3D" HR++ PET camera and control room at PEPT Cape Town laboratory [27]**.**

Compared to the Forte PET camera at the PIC, the advantage of the HR++ camera is its greater sensitivity and fast coincidence resolving time. In particular, the sensitivity is about 50 times greater; the coincidence resolving time is reduced to 53%; the spatial resolution is about 20% better; and the useful data rates are increased by a factor of 40.

The main limitation of the HR++ camera is the geometry of its field of view. The axial length determines the maximum apparatus size or area of imaging for PEPT studies, and the ring configuration limits access to the apparatus from the sides. However, the testing apparatuses can be specially designed for the camera geometry to overcome these issues.

2.4 Radionuclides for PEPT tracer fabrication

A radionuclide is an atom with an unstable nucleus, characterized by having excess energy. This energy is released as ionizing radiation through radioactive decay, and results in the emission of gamma rays and/or subatomic particles, such as alpha or beta particles [28]. There are different kinds of radioactive decay; some examples are:

- α decay, where the nucleus ejects an "alpha" particle which is a helium nucleus;
- β^- decay, where the nucleus emits an electron and an electron antineutrino;
- γ decay, where the excited nucleus releases a high-energy gamma ray;

- β^+ decay, where a nucleus emits a positron and an electron neutrino. In matter, the positron quickly annihilates with a nearby electron to produce a pair of almost back-to-back 511 keV gamma rays[1].

PEPT uses the detection of these 511 keV gamma rays to track the location of the tracer particle, therefore suitable radionuclides for PEPT must decay by β^+ decay and emit positrons. There are many potential radionuclides, with half-lives ranging from a few seconds to many years. A radionuclide suitable for PEPT study would have a half-life short enough to avoid persistent radioactive contamination in the experimental system, but long enough to enable sufficient detection over the experimental timescale. The most commonly used radionuclides in PEPT studies are ^{18}F, ^{68}Ga and ^{22}Na. There are also some potential candidates for further research, which are ^{66}Ga, ^{61}Cu, ^{64}Cu [3].

2.4.1 ^{18}F

^{18}F has a half-life of 109.7 minutes. It is an important radionuclide in nuclear medicine, and is primarily used to synthesize fluorodexyglucose (FDG) for use in medical PET scans.

At the PIC in the University of Birmingham, ^{18}F is the most frequently used radionuclide for PEPT study. It is produced by bombarding purified water using a 33 MeV ^{3}He cyclotron beam. The reactions happen as follows:

$$^{16}O(^{3}He, p)^{18}F \text{ and } ^{16}O(^{3}He, n)^{18}Ne\text{-}^{18}F \qquad \textbf{Equation 1}$$

The bombardment with the 33 MeV ^{3}He beam is performed at a current of 10 μA for 30 minutes, with a "cooling time" of around 20 minutes for the decay of any short-lived radionuclides produced during bombardment [3].

At PEPT Cape Town, ^{18}F is produced on-site by iThemba LABS, where fluoride ions are produced by the bombardment of ^{18}O enriched water with an accelerated proton beam. The nuclear reaction is via:

$$^{18}O(p, n)^{18}F^{-} \qquad \textbf{Equation 2}$$

[1] Positron has momentum when it travels in space, once the annihilation happened, the two opposite gamma rays would slightly bend toward the opposite direction of positron movement, and therefore the pair of gamma rays is not 100% back-to-back.

The bombardment of 4 ml of ^{18}O enriched water over 2 hours with a beam energy of 18 MeV leads to a ^{18}F yield as high as 6 Ci (222 GBq).

2.4.2 ^{68}Ga

^{68}Ga is the main radionuclide used for PEPT experiments at PEPT Cape Town. It has a half-life of 67.63 minutes. ^{68}Ga is produced from a $^{68}Ge/^{68}Ga$ generator (Figure 10) via electron capture. The principle of nuclear reaction is as follows: ^{68}Ge is the mother radionuclide which has a half-life of 270.84 days. It consists of 32 protons and 36 neutrons and decays via electron capture, during which one proton converts to a neutron and forms ^{68}Ga.

At iThemba LABS, ^{68}Ge is produced from a bombardment of gallium metal under a high energy 36 MeV proton beam. The nuclear reaction is:

$^{69}Ga(p, 2n)^{68}Ge$ **Equation 3**

The gallium metal has a low melting point and the element has a tendency to react and dissolve most metals; therefore, it is sealed inside a niobium canister, which is inert to gallium. After bombardment, the target is "cooled" for 10 days to allow some short lived radionuclides to decay. ^{68}Ga is then separated from the target material by anion exchange chromatography.

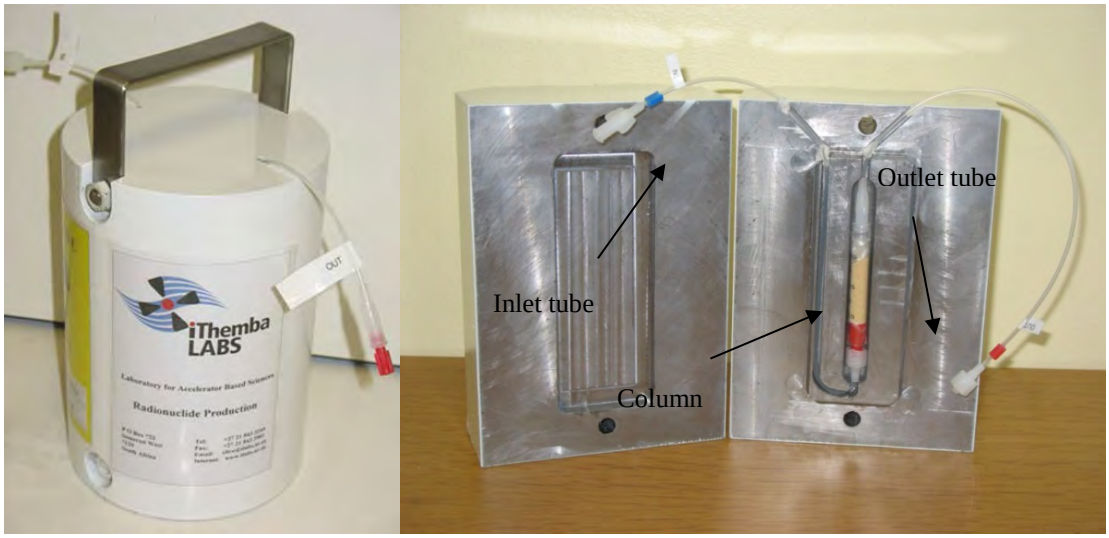

Figure 10: A$^{68}Ge/^{68}Ga$ generator.

From a practical perspective, the generator function is similar to chromatography as the column retains ^{68}Ge, but elutes the daughter radionuclide ^{68}Ga out. A small tin dioxide column is loaded with ^{68}Ge via the inlet tube using a dilute HCl solution, and then 3 – 6 ml 0.6 M HCl solution is used to elute ^{68}Ga out of the column via the outlet tube. The column is about 3 – 4 ml in volume and is placed inside lead shielding to protect users from radiation (Figure 10). The maximum amount of ^{68}Ga is available after 4 hours, so the generator can be eluted around twice a day.

2.4.3 ^{22}Na

^{22}Na is also used as a radionuclide for PEPT studies and has a much longer half-life of 2.6 years. Therefore, it is normally used as a point source in PEPT measurements. ^{22}Na is produced regularly at iThemba LABS, which is currently the sole producer of ^{22}Na positron sources. ^{22}Na is produced by bombarding a magnesium target under a 66 MeV proton beam. The nuclear reaction happens as follows:

$$^{24}\mathrm{Mg(d, \alpha)}^{22}\mathrm{Na} \qquad \textbf{Equation 4}$$

The bombardment takes several weeks at a beam current of 80 μA. After the bombardment, the target is allowed to cool down for few days to let the shorter half-life radionuclides decay. Then a standard ion-exchange procedure is employed to separate ^{22}Na from the magnesium target [29], with the whole procedure performed in a hot-cell.

^{22}Na is rarely used for labelling ion exchange resins for PEPT studies, due to the risk of contaminating users and equipment with a long-lived radionuclide. However, the ^{22}Na can be safely sealed in a button source for use in PEPT studies (see section 2.5.4).

2.4.4 ^{64}Cu

^{64}Cu is a radionuclide of copper which has unique decay properties making it useful in nuclear medicine for imaging and therapy. ^{64}Cu has a half-life of 12.7 hours and decays 17.86% by positron emission, 39.0% by β decay, 43.08% by electron capture and 0.48% gamma radiation / internal conversion.

^{64}Cu is commonly produced in a reactor or an accelerator. ^{64}Cu can be produced by several different nuclear reactions:

- the $^{63}Cu(n, \gamma)^{64}Cu$ reaction by using neutrons from a nuclear reactor;
- the $^{64}Zn(n, p)^{64}Cu$ reaction by using reactor fast neutrons; and
- the $^{64}Ni(p, n)^{64}Cu$, $^{64}Ni(d, 2n)^{64}Cu$,$^{64}Zn(d, 2p)^{64}Cu$,$^{66}Zn(p, 2pn)^{64}Cu$,$^{68}Zn(p, \alpha)^{64}Cu$ reactions by using a cyclotron [30]–[36].

At RPD, iThemba LABS, the waste solution from routine ^{67}Ga production contains a substantial amount of ^{64}Cu [2]. The ^{67}Ga is produced via bombardment of a tandem ^{nat}Zn-^{nat}Zn target under a 66 MeV proton beam for about 6 to 7 hours. After bombardment, the procedure of ^{67}Ga separation from a natural zinc target is completed as follows. The bombarded zinc target is dissolved in 10 M hydrochloric acid containing titanium(III) chloride solution (0.3%; 5 ml) to yield Zn(II), $^{67}Ga(III)$ and some other radionuclide ions in 7 M hydrochloric acid. A peristaltic pump is used to pass this solution through an Amberchrom^{TM} CG-71cd resin column (1.0 g) at 3.0 ml/min. The resin containing the absorbed $^{67}Ga(III)$ ion is washed with 7 M hydrochloric acid (200 ml) to remove residual Zn(II) ion and traces of Ti ion. Finally, the $^{67}Ga(III)$ ion is eluted with 0.5 M nitric acid (30 ml) and the solution is evaporated to dryness. The schematic diagram of the ^{67}Ga production is shown in Figure 11.

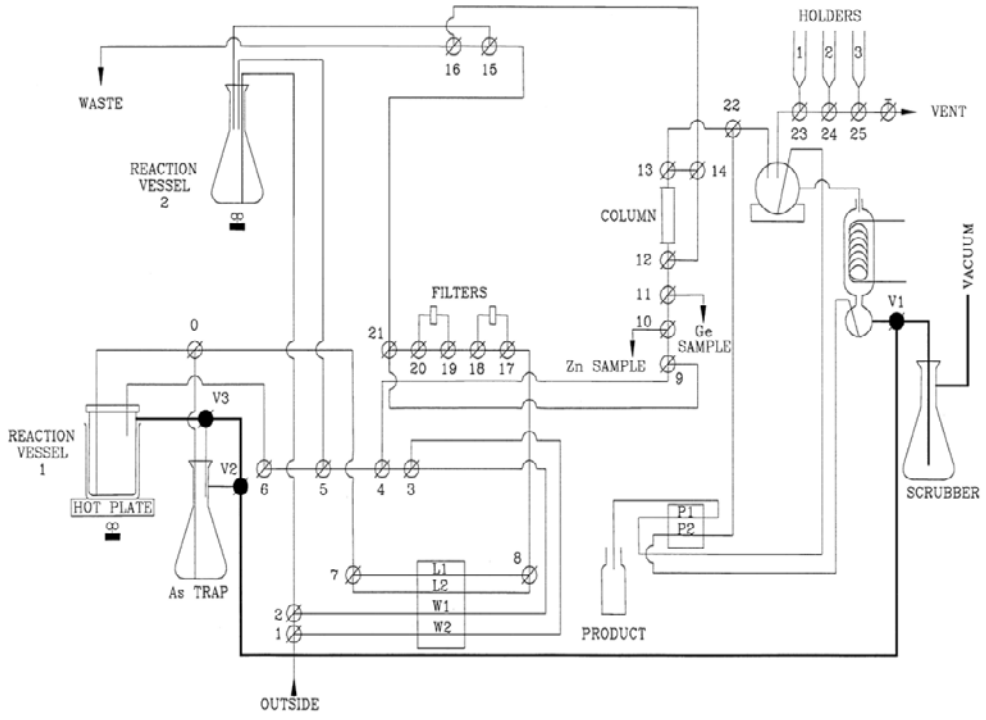

Figure 11: Schematic diagram of the hot-cell panel for the ^{67}Ga production.

[2] ^{67}Ga, which is not a PET tracer, is a useful radionuclide in tumor imaging. The nearly daily ^{67}Ga production is one of the most important products from iThemba LABS.

As mentioned above, the waste produced from the ^{67}Ga production at RPD, iThemba LABS, contains a substantial amount of radioactive copper in 7 M hydrochloride solution. However, a large amount of zinc, titanium and other radioactive ions need to be removed in order to obtain pure ^{64}Cu. Several techniques have been published for the separation of ^{64}Cu from zinc matrices, namely, dithizone extraction into CCl_4 [37], anion exchange chromatography [38]–[40] and electrolysis [32], [41]. By comparing these techniques, Schwarzbach *et al.* [42] indicated that the anion exchange method was the most effective way of separation. However, in order to obtain the acceptable level of purity, anion chromatography was normally combined with other methods. Smith *et al.* [43] tried to use an aqueous HCl / organic solvent mixture on AG1-X8 anion exchange resin to accomplish complete separation of ^{64}Cu, but suggested that only a small amount of enriched target (< 200 mg) was used as the target.

Dolley *et al.* [44] at iThemba LABS developed a two-stage method for purification of copper radionuclides, from up to 5 g of natural zinc and other radionuclides. The method is as follows. After the proton bombardment, the zinc is dissolved in concentrated HCl. After cooling the solution, the HCl concentration is adjusted to *ca* 7 M and the co-produced ^{66}Ga and ^{67}Ga are separated by passing the acidified solution through an ion exchange column containing 2.5 mL of Amberchrom CG-71 resin. The eluate, which contains ^{65}Zn, ^{64}Cu, ^{67}Cu, ^{56}Co, ^{57}Co and ^{58}Co is evaporated to incipient dryness and the salts dissolved in 300 mL 0.05 M HCl. This solution is then pumped through a 10 mL ion exchange column containing 10 mL dithizone-impregnated Amberchrom CG-71. The copper radionuclides are retained quantitatively on the ion exchange resin. Zinc and the cobalt radionuclides are eluted with 0.005 m HCl. The copper radionuclides are finally eluted with 40 ml 5 M HCO_3 at 50 ^{o}C. The copper yield is more than 97%. The entire procedure can be completed within 200 minutes.

^{64}Cu has not been studied in the field of PEPT previously, but there are many advantages of using ^{64}Cu for tracer labelling. ^{64}Cu has a relatively long half-life; therefore, a tracer can be used for a long period in an experimental run. Copper can be easily absorbed onto certain chelating resins, and leaching is minimal under normal experimental conditions. Since copper is recycled from production waste, the use of copper is economical, with no extra costs needed. However, the disadvantage of ^{64}Cu is that it has a lower percentage decay of positron emission, so in order to achieve the

same number of count in PET scanner, a larger dosage of ^{64}Cu might be needed in the experiment.

2.5 Fabrication of tracers for PEPT

PEPT tracers can be made by three different methods: direct activation, ion exchange and surface modification. Among these, ion exchange is the most widely used technique. The surface modification method previously only practiced at the PIC has been receiving wider application in recent years. Several different types of surface modified tracers have been fabricated to meet the requirements of particular PEPT experiments [45].

Beside the three "standard" tracer labelling methods, button source and drilling method can also be employed for fabrication of certain types of PEPT tracer.

2.5.1 Direct activation

Direct activation is used to produce tracer particles with a size greater than 1 mm. The particles used in this technique have to be heat resistant and must contain oxides. Particles from the system under study are used directly as the tracer material. The technique puts tracer particles directly in the 33 MeV ^{3}He beam from a cyclotron for about 60 minutes. After bombardment, some fraction of the oxygen content in the particles is converted to ^{18}F via the reaction:

$$^{16}O(^{3}He,p)^{18}F \qquad \textbf{Equation 5}$$

or

$$^{16}O(^{3}He,n)^{18}Ne \rightarrow {}^{18}F. \qquad \textbf{Equation 6}$$

Meanwhile, several short-lived radionuclides are co-produced from the structural elements of the materials, such as ^{10}C ($t_{1/2}$= 19.3 s), ^{12}N ($t_{1/2}$ = 11 ms), ^{27}Si ($t_{1/2}$ = 1.16 s), ^{29}P ($t_{1/2}$ = 4.1 s) and ^{26}Al ($t_{1/2}$ = 6.4 s) [3]. A cooling time of 20 minutes is employed to allow these radionuclides to decay, which does not significantly affect the amount of ^{18}F production. The ^{18}F in the tracer material exists as a structural element, and it forms within a layer approximately 0.3 mm deep [3].

The radioactivity (A) of ^{18}F produced in a single particle through this technique is determined by the bombardment time, the electrical current on the target and the cross-sectional area of the particle. Fan *et al*. [3] postulated an equation as shown below:

$$A = f_0(I, S, t) = f(I, d^2, t) \qquad \textbf{Equation 7}$$

where A is the radioactivity accumulated in a single particle (μCi), I is the electric current on the target (μA), S is the cross-sectional area of the particle (mm^2), d is the particle diameter (mm) and t is the irradiation time (minutes). When the irradiation time and electric current are fixed, the radioactivity accumulated in a single particle is proportional to the square of the particle diameter as shown in Figure 12.

The advantages of this method are that the tracer can be produced from materials that are identical to the bulk population in their physical and chemical properties, and ^{18}F is formed as part of tracer structure, making it unlikely to wear off. The disadvantages are that the tracer particle must contain oxygen; the size of particle is required to be greater than 1000 μm; and the tracer material must be able to resist the high temperature produced during the bombardment.

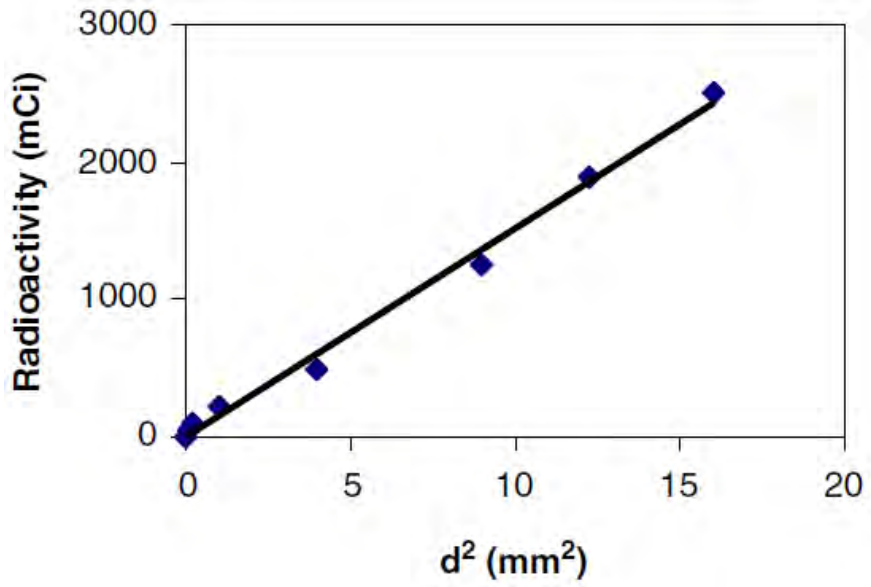

Figure 12: Effect of particle size on accumulated radioactivity via direct activation (33 MeV ^3He beam at a target current 10 μA for 60 min) [3].

2.5.2 Ion-exchange

Ion-exchange techniques are employed to make particle tracers with a size less than 1000 µm by using ion exchange resins. This is the most common labelling method for PEPT studies at both the PIC and PEPT Cape Town. The radionuclides used in the labelling process are normally ^{18}F and ^{68}Ga. The ^{18}F labelled tracers are made by sorbing ^{18}F onto anion exchange resins, whereas the ^{68}Ga tracers are made by absorbing ^{68}Ga onto cation exchange or chelating resins.

The basis of ion exchange labelling is to use radioactive ions to replace the counter ions attached to the functional groups on the resin surface. In order for the process to occur, the radioactive ions must have a higher affinity for the resin than the counter ions. This process normally happens in aqueous solution.

The practical processes of tracer labelling are quite similar for both ^{18}Fe and ^{68}Ga tracer fabrication. Several pre-treated resin beads are added to a small glass vial with a small volume of radioactive solution, after which the vial is placed on a digital shaker for a certain period of time. The labelled tracers are separated and the amount of activity is measured in an ionisation chamber. The amount of activity labelled on a single resin bead depends on the resin type, the particle size, the pH of the solution, the radioactivity concentration in solution and the shaking time.

Anion exchange resins can be classified as either weakly basic or strongly basic. Both of these resin types can be used to potentially absorb ^{18}F ions for ^{18}F tracer labelling. The uptake of ^{18}F in weakly basic anion exchange resins is strongly controlled by the solution pH. The free base amine functional group, e.g. $R\text{-}CH_2N(CH_3)_2$, interacts with water and forms $R\text{-}CH_2NH(CH_3)_2^+OH^-$, in which the OH^- acts as a counter ion. The dissociation of the "hydroxide" ions from the functional group is very weak, and as the process progresses, the hydroxyl concentration increases in solution. This causes the resin to convert back to the undissociated free base form $R\text{-}CH_2N(CH_3)_2$ immediately, as shown in Equation 8 below, resulting in the loss of its anion exchange capacity.

$$\mathbf{R\text{-}CH_2N(CH_3)_2 + H_2O \leftrightarrow R\text{-}CH_2NH(CH_3)_2^+OH^-} \qquad \textbf{Equation 8}$$

(weak dissociation)

Strongly basic anion exchange resins are preferred for the uptake of ^{18}F. They are less affected by the concentration of hydroxyl ions, as the affinity for ^{18}F is stronger than that of hydroxyl ions. Strongly basic anion exchange resins normally contain quaternary ammonium derivatives as the functional group. The resins are usually shipped in chloride form, such as $R\text{-}CH_2N(CH_3)_3^+Cl^-$ or $R\text{-}CH_2N(CH_3)_2(CH_2CH_2OH)^+Cl^-$, where R is the organic backbone (polystyrene mostly), $\text{-}CH_2N(CH_3)_3^+$ and $–CH_2N(CH_2CH_2OH)^+$ are functional groups, and Cl^- is the counter ion.

The affinity order of ^{18}F to the functional groups is much weaker than the affinity of the Cl^- ion as shown in the affinity sequence below [46].

$$\mathbf{SO_4^{2-} > HSO_4^- > I^- > NO_3^- > Br^- > Cl^- > HCO_3^- > HSiO_3^- > F^- > OH^-} \qquad \textbf{Equation 9}$$

Therefore, the resins in chloride form are not used directly for ^{18}F tracer labelling. They have to be converted into fluoride form or hydroxide form before use, as shown in Equations 10 and 11.

$$\mathbf{R\text{-}CH_2N(CH_3)_3^+Cl^- + OH^- \leftrightarrow R\text{-}CH_2N(CH_3)_3^+OH^- + Cl^-} \qquad \textbf{Equation 10}$$

$$\mathbf{R\text{-}CH_2N(CH_3)_3^+Cl^- + F^- \leftrightarrow R\text{-}CH_2N(CH_3)_3^+F^- + Cl^-} \qquad \textbf{Equation 11}$$

The main advantage of ^{18}F as a positron imaging radionuclide is that it does not emit any gamma rays directly (in this case, the positron emission branching ratio[3] of ^{18}F is 100%, ^{68}Ga is 87.7%, ^{64}Cu is 17.6%), and only produces pairs with energy 511 keV due to positron annihilation. Therefore it produces minimal corrupt gamma ray pairs, which provides a high level of coincidence accuracy in positron imaging techniques. The disadvantage of ^{18}F is that it tends to leach from labelled ion exchange resins as soon as the tracer is placed in water. This has the potential to cause serious contamination in a PEPT experiment, and therefore the labelled tracers have to be coated with glue or waterproof paint.

Cation exchange resins can also be classified as either strongly acidic or weakly acidic. Strongly acidic cation resins typically contain a sulfonic acid functional group, while weakly acidic cation resins typically contain a carboxylic acid functional group.

[3] The branching ratio is the fraction of particles which decay by an individual decay mode with respect the total number of particles which decay from a particular radionuclide.

The strongly acidic cation exchange resins are normally used for ^{68}Ga labelling. The resins are usually shipped in sodium form and, according to the table of relative selectivity (Table 1), the sodium counter ion has third lowest selectivity. Thus the resins can be used directly for labelling, and no pre-treatments are needed.

Table 1: **Relative selectivity of various counter ions** [47]**.**

Counter ion	Relative selectivity[4] for AG 50W resin	Counter ion	Relative selectivity for AG 50W resin
H^+	1.0	Fe^{2+}	2.55
Li^+	0.85	Zn^{2+}	2.7
Na^+	1.5	Co^{2+}	2.8
NH_4^+	1.95	Cu^{2+}	2.9
K^+	2.5	Cd^{2+}	2.95
Rb^+	2.6	Ni^{2+}	3.0
Cs^+	2.7	Ca^{2+}	3.9
Cu^+	5.3	Sr^{2+}	4.95
Ag^+	7.6	Hg^{2+}	7.2
Mn^{2+}	2.35	Pb^{2+}	7.5
Mg^{2+}	2.5	Ba^{2+}	8.7

The specific resins used in the ^{68}Ga labelling are NRW-100 (manufactured by Purolite) and the AG 50W series (manufactured by Bio-Rad) as they have the same sulphonic acid functional group. The ion exchange reaction happens as follows:

$$\mathbf{3(R\text{-}SO_3\text{-}Na^+) + {}^{68}Ga^{3+} \rightarrow (R\text{-}SO^{3-})3{}^{68}Ga^{3+} + 3Na^+} \qquad \textbf{Equation 12}$$

Chelating[5], also called amphoteric, resins are ion exchangers where the counter ions are bound to the resin by coordinate covalent bonds or by electrostatic interactions. This makes the chelating resins highly selective for target metal ions. However, in the case of ion exchange, the electrostatic forces between oppositely charged functional groups and ions in solution play the main role. Different types of chelating resins consist of different functional groups. The chelating resins used in tracer labelling are Purolite S950 (manufactured by Purolite) and Chelex 100 (manufactured by Bio-Rad). Their functional groups are aminophosphonic acid and iminodiacetic acid, respectively.

[4] The selectivity coefficients are a measurement of a resin's preference for an ion. In this case, the coefficient is over the hydrogen ion. The greater the selectivity coefficient, the stronger the preference for the ion.

[5] Please see section 2.6 for more detailed information regarding to chelating resins.

There are two advantages of using ^{68}Ga as a tracer for PEPT studies: firstly, the tracer does not leach in most aqueous solutions, and previous studies have shown that the ^{68}Ga labelled ion exchange resins are quite stable in solutions of pH 1 – 11 [48]. This reduces the risk of radioactive contamination in PEPT experiments, and the tracer can be used without coating. Secondly, ^{68}Ge/^{68}Ga generators are readily available at iThemba LABS and re-grow every 4 hours, so the tracer production can be performed twice every day.

The short half-life of ^{68}Ga tracer is both an advantage and a disadvantage for PEPT studies. Any contaminated equipment will decay to safe levels within 24 hours, but the practical length of experiments is limited before the tracer has too little activity to be located accurately. This is exacerbated by a maximum safety limit of 1.5 mCi for radioactive material used in and transported to the PEPT laboratory.

Overall, ion exchange is the most important technique for radioactive tracer fabrication in PEPT, as it is possible to make tracers sized between 150 – 1000 μm. Therefore this technique is used for daily tracer fabrication at both PIC and PEPT Cape Town. Improvements have been made to meet requirements for specific PEPT experiments, e.g. coatings which provide the tracer with specific surface properties for flotation studies, and drilling which implants the tracer inside drilled glass or metal balls for milling studies.

2.5.3 Surface modification

Surface modification has been used to improve the sorption of ^{18}F onto particle surfaces other than resin beads. Through this technique, ^{18}F adsorption onto solids can be significantly improved, leading to a considerable extension in the range of materials which can be labelled adequately for PEPT measurement.

In this process, metallic ions are firstly introduced to the solid surfaces as active sites, and then anions bind with the metallic ions on the solid surface. After the modification of the surface chemistry of the solid, the absorption of ^{18}F can be significantly improved as shown in Figure 14. For example, under optimized experimental conditions, the radioactivity labelled on a single particle was increased from 67 to 600 μCi for hydroxyapatite, from 2 to 400 μCi for quartz and from 2 to 152 μCi for polyethylene [1].

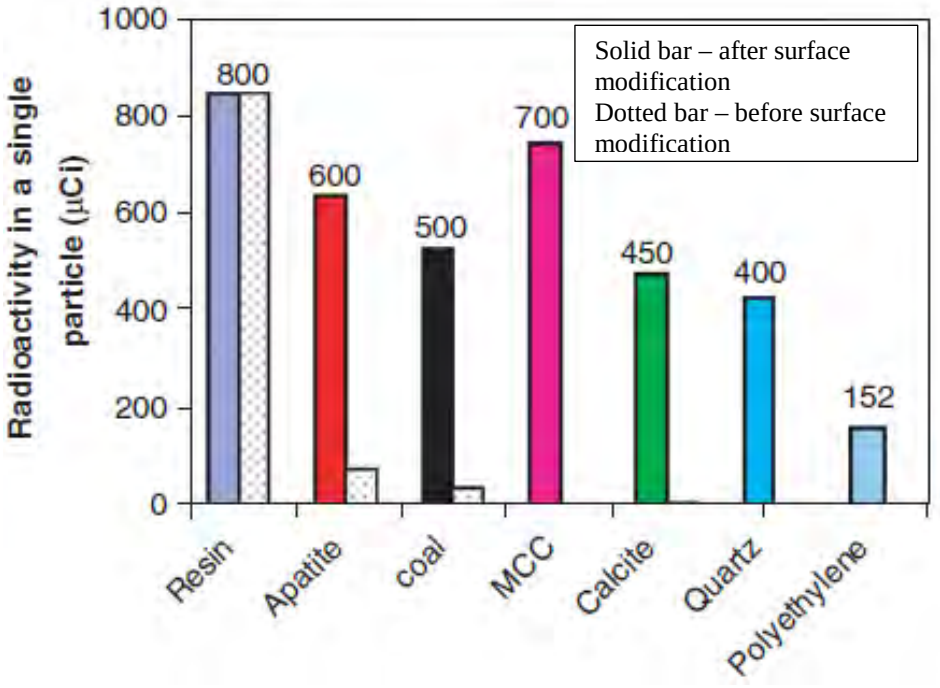

Figure 13: Comparison of activity labelled on a single particle between surface modification and ion exchange methods (particle size: 212 – 250 μm) [1].

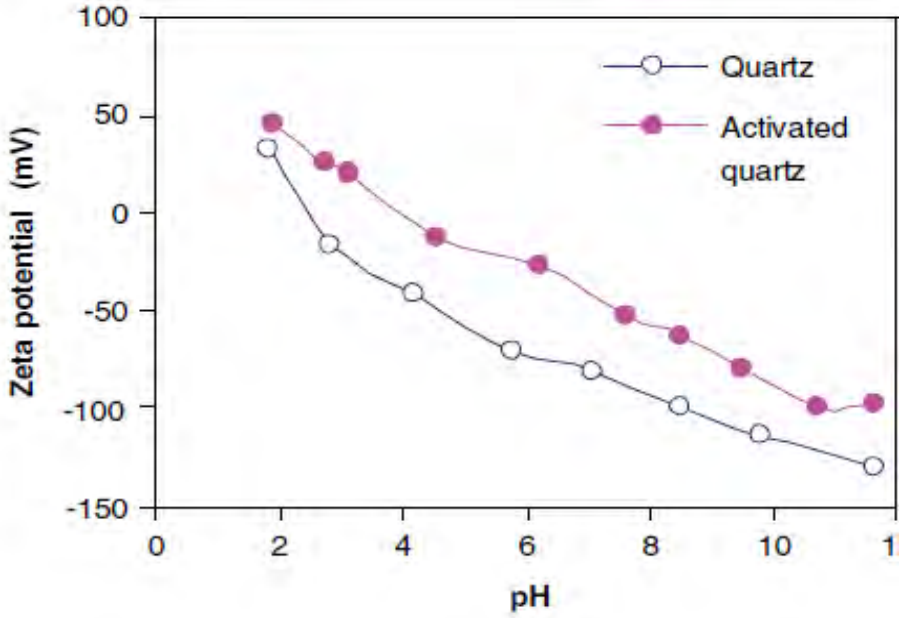

Figure 14: Effect of Fe^{3+} on quartz zeta potential [2].

It is still unknown how the metallic ions improve the absorption of ^{18}F onto the solid surfaces. A possible explanation offered by Fan *et al.* [2] is that the absorbed metallic ions alter the surface charges of quartz and microcrystalline cellulose, or act as bridges. For example, quartz interacts with water and forms a saline group in aqueous solution, with a negative zeta potential above pH 2.6. This zeta potential decreases by

increasing the pH of the aqueous solution and reaches approximately -100 mV at pH 11.5 (Figure 15).

After modification, the metallic ions were sorbed onto quartz surfaces, and the zeta potential of quartz increased by approximately 30 mV over the whole pH range. The increase in zeta potential could result in the impact of more $^{18}F^-$ anions into the surface double layer of the solids. The absorption of metallic ions on solid surfaces also enhances the absorption of hydroxides. The absorbed hydroxides are further replaced by ^{18}F, therefore the radioactivity labelled in a single particle increases significantly [1].

This "chemical activation" surface modification method has been practiced mostly at the PIC. The advantage of this method is its ability to label tracers made from a wide range of materials, such as mineral ore particles and plastics. The disadvantage is that ^{18}F can leach out from the tracers in solution, thus coating is essential. Unfortunately the details of the surface modification process have not been disclosed yet, so this method has not been repeated anywhere else.

In recent years, a new type of surface modification method was developed at PEPT Cape Town to alter surface properties of labelled tracers. The method involves coating a tracer with materials to represent hydrophobic mineral particles in froth flotation PEPT experiments [45]. Density modified tracers have also been made available at PEPT Cape Town.

2.5.4 Button source and "Drill and fill" method

Button sources are made by concentrating a liquid radionuclide in a sealed cylinder, known as a "button source". This type of radioactive source is used as reference standard or a location marker, and is placed on the surface of equipment.

Button sources have 1 cm diameter and height, and are made of Plexiglas. They consist of two parts (Figure 16), with a small concave depression at the centre of the bottom part in which to deposit the ^{22}Na solution before sealing with superglue.

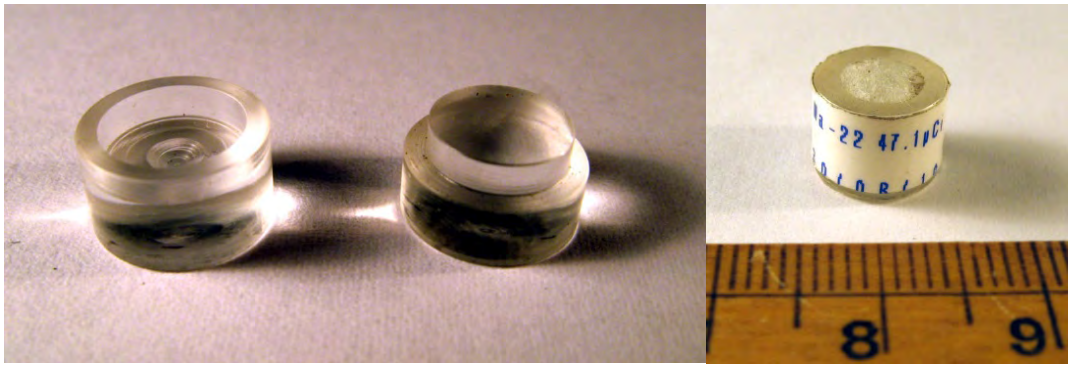

Figure 15: The open structure of a button source (left) and a final sealed source (right).

The main radionuclide used in button sources for PEPT studies is ^{22}Na. The main advantage of a ^{22}Na button source is its long half-life. One point source can be used for the duration of a series of PEPT experiments (several weeks), and ensures a consistent activity for calibration. The ^{22}Na point sources have been used to investigate the efficiency of tracking algorithms [14] and for location markers to orientate PEPT data within an experimental vessel [49]. The disadvantages of ^{22}Na as a PEPT radionuclide are that it has a low maximum activity limit, as laboratory safety regulations only allow a maximum of 100 µCi per tracer. Sealing the ^{22}Na inside a button source minimises the risk of contamination of equipment and the environment with a long lived radionuclide. However any radionuclide can be used to make a button source.

Some PEPT experiments require tracers to represent the movement of larger particles, such as large beads or mineral ore chips. In this case, a labelled ion-exchange resin is imbedded into a larger particle directly from the system bulk. By placing the tracer inside of a larger particle can also provide extra protection of the tracer, thus it reduces the chances of tracer breakage in aggressive environments, thus minimising the risk of contamination.

The technique is rather simple: a hole of approximately diameter 0.8 mm is drilled into the mineral ore chip or bead. One or two labelled tracers, with approximately diameter 0.5 mm are inserted inside the drilled hole. A drop of superglue is used to seal the hole. After 5 minutes drying under a heating lamp, the activity of the tracer is measured in an ionisation chamber. The “drill and fill” method has been successfully performed in several projects at PEPT Cape Town. Two examples of drilling tracer particles are shown in Figure 17. The top one is a ceramic bead tracer used in an

IsaMill experiment, while the bottom one is a hematite chip tracer used in an industrial gravity separator.

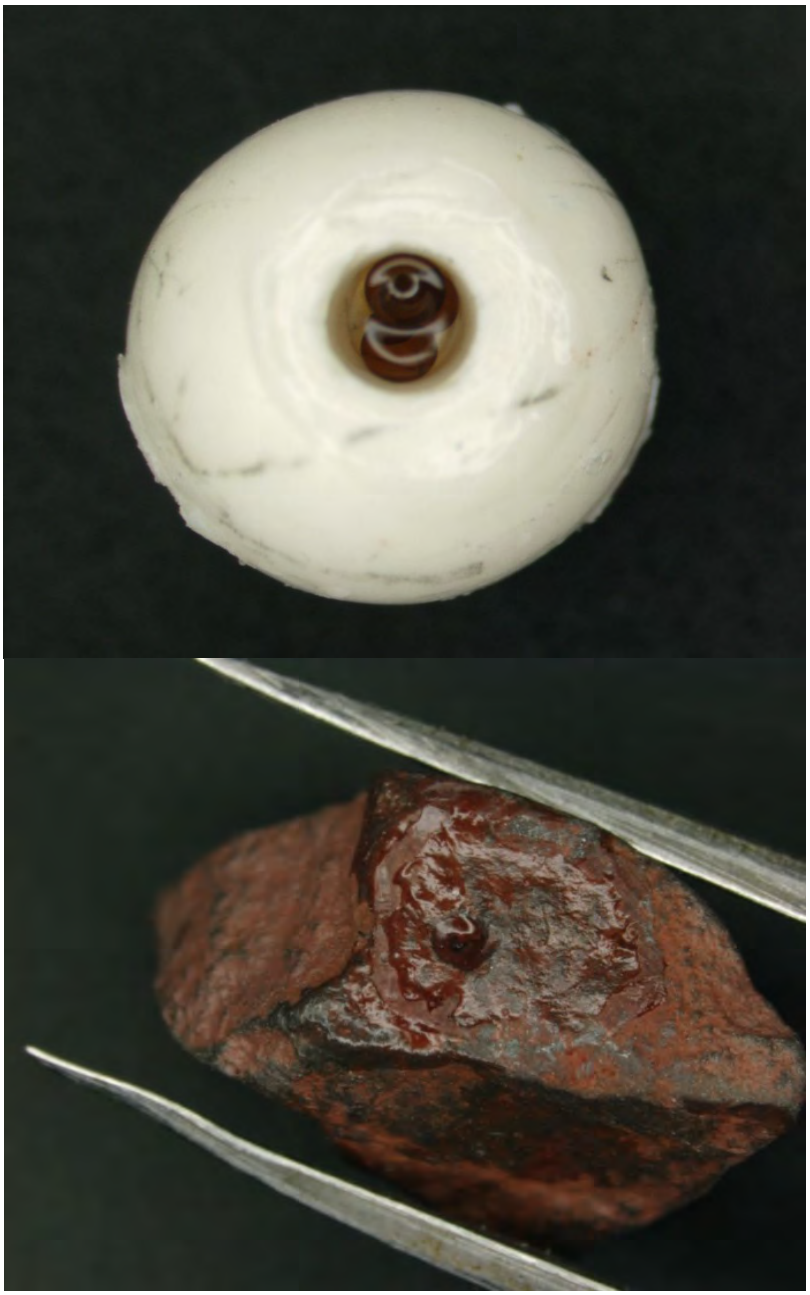

Figure 16: Tracers made using the "drill and fill" method, (top) a ceramic bead tracer, (bottom) a hematite chip tracer [50]**.**

2.6 Ion exchange resins

Ion exchange resins are essential for radionuclide production and PEPT tracer labelling due to their ability to separate different ionic species. Several different types of resins are used in this study for radionuclide separation and tracer production.

An ion exchange resin is an insoluble matrix (or support structure) [51] which is fabricated from an organic polymer substrate, normally in the form of small beads (≤ 2 mm diameter) which are white or yellowish in appearance (Figure 18). The material has an intricate structure of pores on the surface which are sites with easily trapped and released ions. The trapping of ions takes place only with the simultaneous release of other ions, thus the process is called ion exchange. Many different types of ion exchange resin are fabricated with selectivity for one or several different types of ions. Ion exchange resins are widely used in different separation, purification and decontamination processes. The most common examples are water softening and water purification.

Most typical ion exchange resins are based on a structure of cross-linked polystyrene. The required functional groups can be introduced after polymerization, or substituted monomers can be used. For instance, the cross-linking is often achieved by adding 0.5 to 25% of divinylbenzene to styrene in the polymerization process. Non-cross-linked polymers are rarely used in ion exchange resins because they are less stable mechanically. When the percentage cross-linking is increased, the ion exchange capacity of the resin is decreased. This prolongs the time needed to accomplish the ion exchange processes, with the exception of macroporous resins.

Figure 17: Ion exchange resins beads – AG 50W.

2.6.1 Types of resins

There are four main types of ion exchange resins:

- Strongly acidic cation – typically with sulphonic acid functional groups, e.g. sodium polystyrene sulphonate or polyAMPS;
- Strongly basic anion – with quaternary amino groups or trimethylammonium groups, e.g. polyAPTAC;
- Weakly acidic cation – mostly with carboxylic acid groups;
- Weakly basic anion – with primary, secondary, or tertiary amino groups, e.g. polyethylene amine.

There is also a special type:

- Chelating resins – with iminodiacetic acid, thiourea, and other functional groups.

2.6.2 Ion-exchange resin properties

The performance of any ion exchange resin is dependent on its chemical and physical properties. The functional groups of the resin give it unique chemical properties. The physical properties of an ion exchange resin include ionic form, the distribution of particle size, cross linkage, swelling and porosity, the matrix and particle shape.

a) Ionic form

Most resins are available in several ionic forms and can be converted from one form to another. In the simplest case the resin is used in an ionic form, with a lower selectivity for the counter ions than the sample ions to be exchanged. The sample ions are exchanged with the counter ion on the functional group when introduced to the resin, and can be replaced by introducing an ion with a higher affinity order, or a high concentration of an ion with equivalent or lower affinity. In many cases, a high concentration of the original counter ion can be used for regenerating the resin.

In general, the lower the selectivity of the counter ion, the more readily it will exchange for another ion with a similar charge. The order of selectivity can be used to estimate the effectiveness of the ion exchange process, with the most highly selective ions being the most efficient in exchange. The order of selectivity can also be used to

estimate the difficulty in converting the resin from one form to another; therefore, conversion from a highly selective to a less highly selective ionic form would require an excess of the ion to be introduced in solution [52].

b) Particle size

Most ion exchange resins are available as spherical porous beads. The particle size of the resin beads is mostly given as a standard mesh size through which the resin can pass. This mesh size, as stated by the U.S. Standard Screen, is determined as follows:

Mesh ≈ 16 / diameter of resin bead in mm **Equation** 13

Analytical Grade resin particle size is generally specified as dry mesh where mesh describes the number of openings per inch on the screens used to size the ion exchange resin.

Most Analytical Grade (AG) resins are available in several particle size ranges for laboratory uses. In general, 200 – 400 mesh and finer resins are used for high-resolution chromatography, whereas 100 – 200 mesh resins are used for general-purpose ion exchange techniques. The coarser resins, such as 50 – 100 mesh, are used for large scale applications and batch operations, where a slurry of resin and sample is used[6]. The large mesh sizes are also suitable for small-scale applications, such as the removal of a cationic species by converting it to an anionic complex in the presence of an uncomplexed cation, or as in this study, to make tracers by labelling resin particles with radionuclides.

c) Cross-linking

Ion exchange resins consist of a matrix to which functional groups are attached. The number of individual monomers used in the synthesis of the three dimensional matrix determines the properties of the elastic matrix. These elastic, three dimensional polymers do not have a pre-determined pore size. The grade of cross-linkage in a polymer exchanger is indicated by the fraction of divinylbenzene (DVB) contained in the styrene-divinylbenzene resin beads, which is usually between 1 and 25%. The 4% and 8% cross linkage are regarded as ideal for general use.

[6] Even larger size range, such as 1 – 5 mm resins are used in industry for metallurgical separations.

2.7 Summary

In this chapter, a comprehensive review of PEPT was presented, beginning with the history of PEPT from its first development at the University of Birmingham in 1993 to the establishment in 2009 of PEPT Cape Town at iThemba LABS, which hosts the Siemens HR++ PET camera which is still considered one of the world's most sensitive PET cameras ever built. The radionuclides used in PEPT tracer fabrication were discussed: of the commonly used ones, their half-lives are either too short (^{68}Ga and ^{18}F) or too long (^{22}Na) for some applications.

^{64}Cu had been considered as a potential candidate for longer lived tracer fabrication. The waste solution of ^{67}Ga production at the Radionuclide Production Department (RPD), iThemba LABS, contains a substantial amount of ^{64}Cu. A novel method has been developed by Dolley *et al.* [44] to separate the copper from the waste solution. The conjunction of these resources provides a good opportunity to evaluate and modify the method to recover ^{64}Cu from the ^{67}Ga waste solution and use it for tracer labelling.

The three "standard" methods of tracer fabrication, namely, direct activation, ion-exchange and surface modification were reviewed. Ion-exchange is the most used tracer labelling technique at PIC and PEPT Cape Town. This technique could be investigated for ^{64}Cu tracer labelling. Besides the "standard" method, radionuclides can be made into button sources or implanted into a larger object; such a button source could be used for the comparison of tracers.

Since the ion-exchange resins are the foundation of this study, a short introduction to ion-exchange resins was also presented, including the theory of ion-exchange, the types of ion-exchange resins and the general properties of resins.

2.8 Scope

This work was focused on the separation of ^{64}Cu from ^{67}Ga production waste solution produced routinely at RPD, iThemba LABS, and the fabrication of ^{64}Cu tracer. The experimental work was limited to ^{64}Cu separation; the determination of the purity of the final ^{64}Cu; tracer fabrication using an ion-exchange method; and testing the

tracking efficiency of the tracers in the Siemens HR++ PET camera at stationary and rotating positions. The data analysis was carried out using MatLab software.

2.9 Key questions

1. Is it possible to separate and purify ^{64}Cu from ^{67}Ga production waste solution more quickly and with a greater efficiency by evaluating and modifying the existing ion-exchange chromatography technique (which is a relatively slow process and designed for large scale ^{64}Cu separation)?

2. Is it possible to develop a tracer labelling technique for ^{64}Cu tracer particles using the ion-exchange technique?

3. Do labelled ^{64}Cu tracers leach in aqueous environments?

4. How does the ^{64}Cu tracer tracking efficiency compare with that of ^{68}Ga, ^{18}F, ^{22}Na tracers in the PET camera? If poorly, how can this problem be overcome in the PEPT experiments?

CHAPTER 3 EVALUATION AND MODIFICATION OF ^{64}Cu SEPARATION METHOD

3.1 Introduction

In the past 5 years, tracers made with ^{68}Ga and ^{18}F have been successfully used for PEPT experiments at PEPT Cape Town on a daily basis. However, despite the great success of these tracers, their application is ultimately restricted by their half-lives to experiments lasting several hours. Since ^{64}Cu has a half-life of 12.7 hours, it is a potential candidate to produce longer lived tracers and extend the tracking time with PEPT.

iThemba LABS routinely produces ^{67}Ga via the reaction ^{68}Zn(n, 2p)^{67}Ga by the bombardment of a natural zinc target by 66 MeV proton beam. During this process, substantial quantities of ^{64}Cu are co-produced by via the ^{68}Zn(p, α)^{64}Cu reaction. After ^{67}Ga extraction, the zinc waste solution contains significant amounts of ^{64}Cu, which need to be purified to be used for tracer labelling.

A novel method has been developed to separate radioactive copper via ion exchange from the production waste solution at iThemba LABS in recent years [44]. This chapter presents the work done to evaluate and modify this method to produce purified ^{64}Cu for the labelling of PEPT tracers.

3.1.1 ^{64}Cu separation

As discussed in section 2.4.4, natural zinc is used for the ^{67}Ga production at RPD, iThemba LABS. The waste solution from ^{67}Ga production contains approximately 0.075 g/mL zinc and other co-produced radionuclides. These radionuclides include $^{62, 65, 69}$Zn, $^{56, 57, 58}$Co, and $^{64, 67}$Cu. The estimated amount of ^{64}Cu content in solution is approximately 9.2 mCi/mL at the end of bombardment (EOB), which converted into mass per volume is equivalent to 2.4×10^{-9} g/mL.

This is a very small amount of ^{64}Cu compared to the zinc ions in the solution. If used directly for tracer fabrication, the substantial amount of zinc ions in solution will mask the functional groups on the resin surface, which can cause the failure of tracer labelling. The presence of other radionuclides can also interfere in the PEPT measurement: gamma rays from non-positron emitters may be scattered and lead to

random events, resulting in less accurate PEPT measurements. Thus, it is essential to separate the ^{64}Cu completely from the other elements in the waste solution.

Dithizone (diphenylthiocarbazone) is a sulfur-containing organic compound. It is a strong ligand and forms complexes with many metals. It is also very selective for copper in certain pH ranges. The pH ranges for dithizone complex formation of specific ions are Co: 6.5 to 10.5, Cu: 2 to 5, Fe: 7.5 to 8.5, Ni: 6 to 9, and Zn: 6.5 to 9.5 [53]. Therefore copper can be separated from any of these metal ions in solutions of low pH or dilute acid solution.

The matrix of Amberchrom CG-71 resin is an acrylate polymer; it does not have any functional groups on its surface. Therefore it serves as an ideal organic backbone for the immobilization of chelating ligands onto stationary phase supports, while retaining the ability to selectively form chelates and thus remove them from solution.

Dithizone does not dissolve in water at pH<7, therefore an organic solvent such as CCl_4 is firstly introduced to dissolve dithizone [44]. In this thesis, a modification was made to that design, to use 0.5 M NaOH solution instead of organic solvent [44]. This gives the same impregnation results, but removes the need for the operator to deal with flammable solvents and to complete the experiment in a fume hood.

3.1.2 Flow diagram of the sequence of events

The flow diagram of the experimental work is listed below:

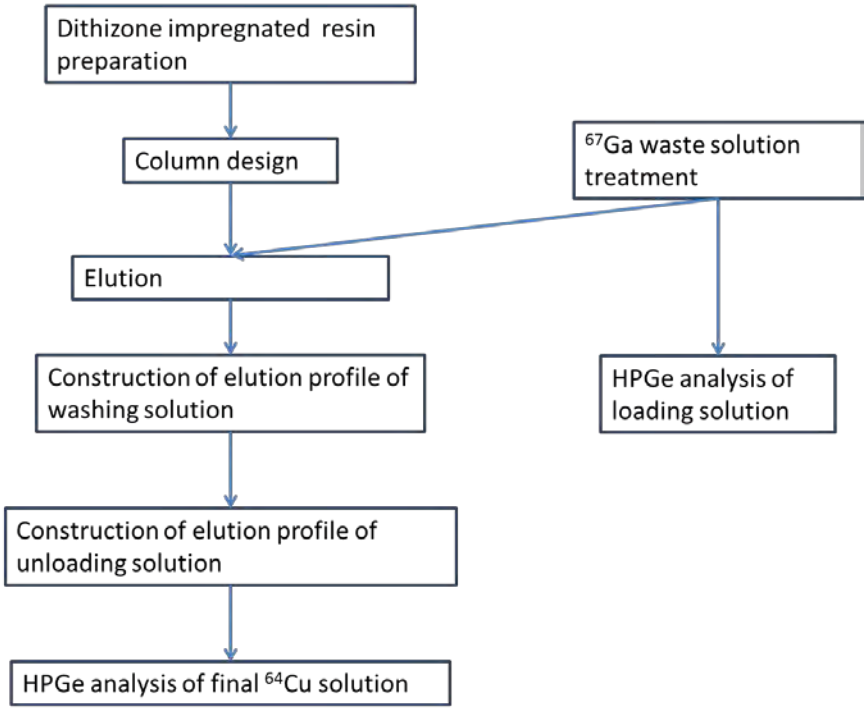

Figure 18: The flow diagram of the experimental work.

3.2 Experimental methods

Analytical grade reagents were used throughout this work and were obtained from Merck (SA) Pty. Ltd or Sigma-Aldrich products. The Amberchrom CG-71 adsorption resin was purchased from Sigma-Aldrich. De-ionised water was used for all the experimental work; it was obtained from a Millipore MilliQ Reagent Grade Water System, to a conductivity of greater than 10 megaohm.cm^{-1}.

3.2.1 Resin preparation

Dithizone (diphenylthiocarbazone) impregnated Amberchrom CG-71 (7% cross-linked) methacryclate-based resin was used to purify ^{64}Cu from the ^{67}Ga production waste solution. The dithizone impregnated resin was prepared as follows: 20 mg dithizone was dissolved in 200 mL 0.5 M NaOH solution. Approximately 20 mL of Amberchrom CG-71 resin (in water) was then added to the rapidly stirred solution which was orange in colour (the natural colour of dithizone). This mixture was stirred for 2 hours to allow for the impregnation of dithizone into the resin pores and on the resin surface. This was indicated by the steady disappearance of the orange colour of the solution.

The solution was then acidified to approximately 0.5 M HCl by the slow addition of 21 mL of 32% HCl, while stirring. The resin turned black as soon as the dithizone molecule was reconstituted. 100 mL water was added and the solution stirred for 15 minutes. The mixture was allowed to stand about 2 to 3 minutes to let the black resin settle, and the supernatant liquid poured off. Another portion of 300 mL water was added and the resin stirred for 5 minutes.

The resin was again allowed to settle and the supernatant discarded. The addition of water, stirring, and discarding of the supernatant were repeated two more times. The solution was then acidified to obtain a 0.05 M HCl concentration. The resin was stored in 0.05 M HCl so it could be used for up to three weeks when stored away from light.

3.2.2 Separation column design

The column was made by completely removing the plunger from a 5 mL medical syringe, and severing the top of its cylindrical tube with a scalpel blade. A circular frit filter was fitted to the bottom of the syringe. 5 mL of previously prepared dithizone impregnated resin was inserted into the syringe and the top was sealed with a specially designed Teflon plunger (Figure 19). Then inlet and outlet tubes were attached to the top and bottom of the syringe via luer locks. Finally, a piece of black insulation tape was wrapped around the column to hold the Teflon plunger and cylindrical tube together. 50 mL of 0.05 mL HCl solution was pumped through the column using a peristaltic pump (102U, *Watson Marlow*) to equilibrate the resin and check whether there was a leak in the system.

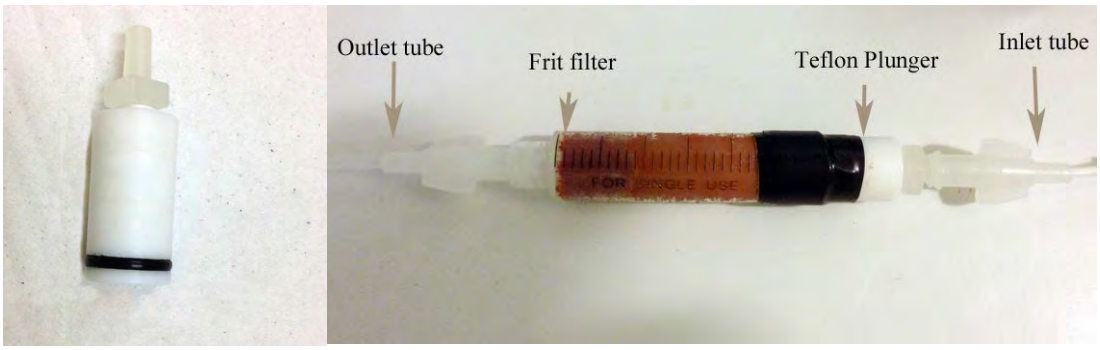

Figure 19: Photographs of the ^{64}Cu separation column: (left) Teflon plunger, (right) assembled column.

3.2.3 Column operation

The following step involved handling of highly radioactive materials, and was performed in the high radiation zone - red area - at the Radionuclide Production Department (RPD) at iThemba LABS, where the radiation protection procedure was strictly implemented. 5 mL of ^{67}Ga production waste solution was obtained from the RPD 24 hours after the end of bombardment (EOB). It was heated in a Teflon beaker on a hotplate at 300 ^{o}C until dryness; 20 mL of 0.05 M HCl solution was then added to dissolve the residual radionuclides. This solution was pumped through the pre-made 5 mL column at approximately 2 mL/min to load radioactivity onto the column. HCl was chosen because, in 0.05 M HCl solution, copper is retained in a dithizone column. After loading, the column was washed with 150 mL of 0.05 M HCl solution to rinse off impurities. Finally 15 mL of warm (approx. 50 ^{o}C) 5 M HNO_3 solution was eluted through the column to wash out the ^{64}Cu. Because oxidizing acids such as nitric acid react vigorously with the acrylate polymer backbone, this step removed dithizone and copper completely from the resin.

3.2.4 Method to determine the radiopurity of ^{64}Cu

During each step, a small sample of the solution was taken for measurement on a high purity germanium detector (HPGe detector, *CANBERRA*). During the washing step, the wash solution was sampled in 10 mL fractions after washing, and the total count of each sample was measured in the HPGe detector (Figure 20). During the unloading step, the final solution was collected and activity of each successive 1 mL was measured in an ionization chamber (CRC-25 R, *Capintec Inc*., NJ). The gamma spectrum of 2 mL of the final ^{64}Cu solution was measured using a calibrated HPGe detector to examine the radiopurity of copper.

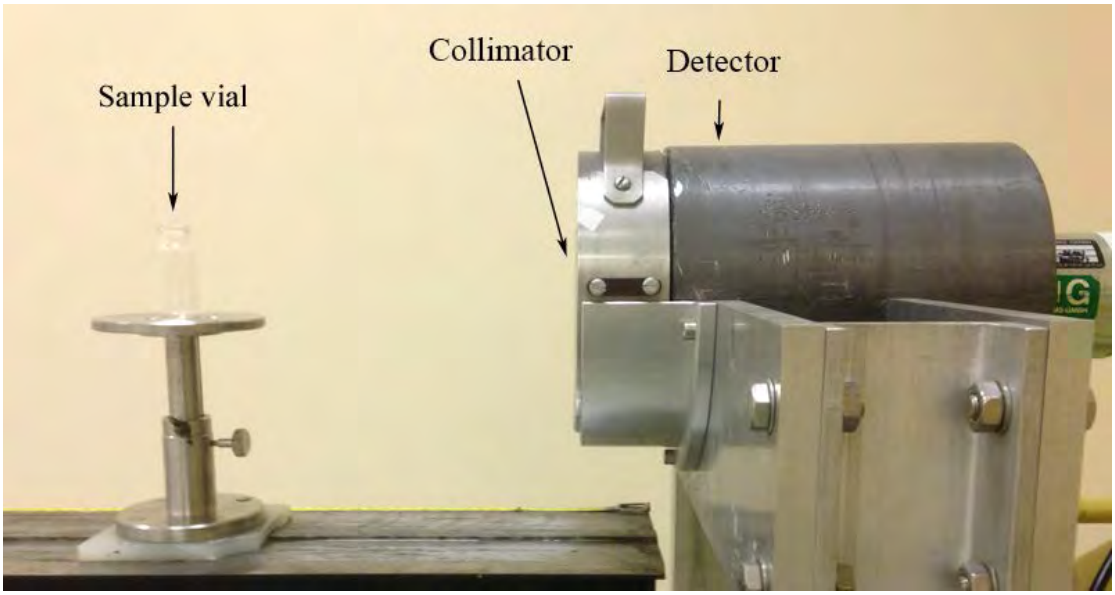

Figure 20: The HPGe detector in the counting room, iThemba LABS.

3.3 Results and discussion

3.3.1 Gamma ray spectrum of ^{67}Ga production waste solution

Figure 21 shows the gamma spectrum of the ^{67}Ga production waste solution before the copper separation process. This measurement was made by placing a 100 µL sample of the ^{67}Ga production waste solution in front of the HPGe detector. The sample solution was contained in a 10 mL clear glass vial at a distance of 50 cm to the detector with a lead collimator. The acquisition time was 200 seconds and the detector dead time was 4.19%.

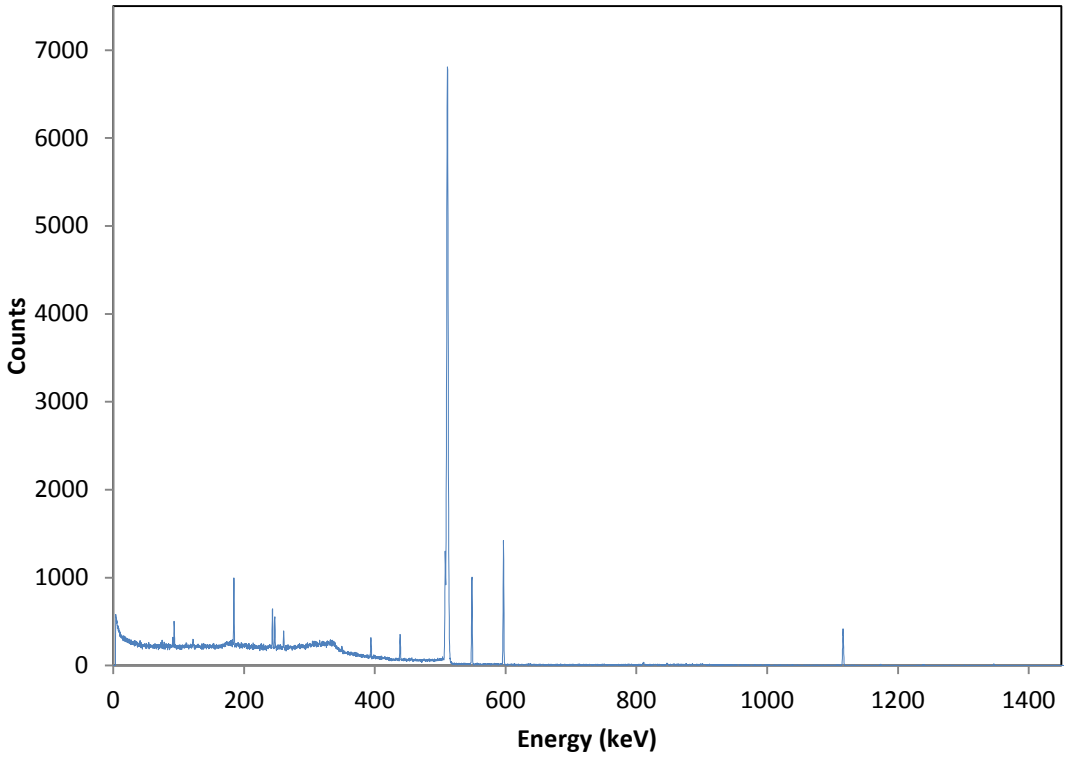

Figure 21: Gamma spectrum of the ^{67}Ga waste solution.

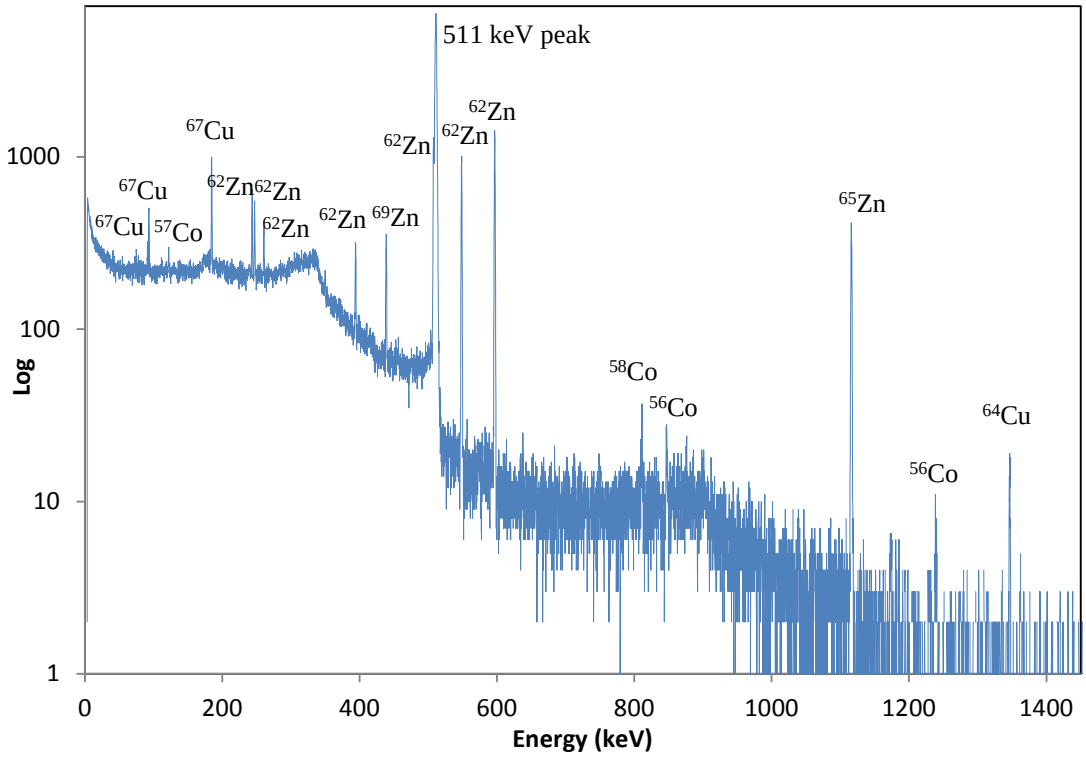

Figure 22: Gamma spectrum of ^{67}Ga waste solution on log scale.

The production waste solution was analysed 24 hours after EOB, which allowed most of the "short" lived radionuclides to decay. The plateau on the left of the graph (Figure 21) was caused by Compton scattering, which is an inelastic scattering of a photon by a free charged electron. The largest peak is at 511 keV caused by the emission and annihilation of positrons. In this spectrum, the large 511 keV peak could be contributed by various radionuclides, this peak alone cannot be used to determine which specific radionuclide was present in the waste solution. Due to the relatively low intensity and low count of some peaks in the gamma spectrum, some of the peaks are impossible to see in Figure 21. Thus the spectrum is re-plotted on a log scale in Figure 22 to illustrate all the peaks in the spectrum.

The peak at 1115 keV indicates the presence of ^{65}Zn which has a half-life of 244.26 days. The intensity of this peak is moderate compared with the 511 keV peak, and the intensity of this peak is 50.60%. The 243 keV, 246 keV, 260 keV, 394 keV, 507 keV, 548 keV and 596 keV peaks represent ^{62}Zn which has a half-life of 9.186 hours. The 507 keV peak is quite small, and so near the 511 keV peak that it is almost indistinguishable from the 511 keV peak; however, at an enlarged size, this peak merges into the 511 keV peak and forms a little "shoulder" on its left. The intensity of the ^{62}Zn peaks are 2.52%, 1.90%, 1.35%, 2.24%, 14.8%, 15.3% and 26% respectively. A small peak at 438 keV indicates the presence of ^{69}Zn, which has a half-life of 13.8 hours, and the peak intensity is 94.85%. A small peak at 122 keV indicates the present of ^{57}Co ($t_{1/2}$ = 271.3 d), with an intensity of 85.60%.

The gamma spectrum also shows the presence of trace amounts of ^{56}Co and ^{58}Co. ^{56}Co ($t_{1/2}$ = 77.24 d) has 511 keV, 846.7 keV and 1238 keV peaks, and the peak intensity are 39%, 99.9% and 66.5%. ^{58}Co ($t_{1/2}$ = 9.1 h) has 511 keV and 810 keV peaks; the peak intensity are 29.8% and 99.45%.

The characteristics of the ^{67}Ga ($t_{1/2}$ = 3.26 d) gamma spectrum are 91 keV, 93 keV, 184 keV, and 300 keV peaks; the intensity of these peaks are, respectively, 3.16%, 39.2%, 21.1% and 16.8%. As shown on the graph, the 91 keV, 93 keV and 184 keV peaks can be confused with ^{67}Cu, because it has the same peaks on the gamma spectrum. However, ^{67}Ga has a peak at 300 keV, with a 21.1% intensity; therefore, it should have similar peak size as 184 keV. The absence of such a peak at 300 keV indicates there was no ^{67}Ga present in the solution.

The peaks at 91 keV, 93 keV, 184 keV, 300 keV and 394 keV are characteristic of ^{67}Cu ($t_{1/2}$ = 61.83 h). The intensity of these peaks are, respectively, 7.0%, 16.1%, 48.7%, 0.797% and 0.22%. The ratios of peak intensity match the ratio of ^{67}Cu gamma spectrum shown on the graph, although the intensity of 300 keV and 394 keV peaks are quite small, and consequently they do not appear on the diagram due to the relatively low acquisition time.

The peak at the highest energy level of 1345 keV is considered to be ^{64}Cu. Because of its low intensity of 0.437%, the net peak size appears to be very small. The detailed spectrum analysed intensity is shown in Table 2.

Table 2: Detailed peak analysis of gamma spectrum of the ^{67}Ga waste solution.

Nuclides	Energy (keV)	Intensity (%)	half-life
^{65}Zn	511	2.85	243.93 d
	1115	50.04	
^{62}Zn	243	2.52	9.19 h
	246	1.9	
	260	1.35	
	394	2.24	
	507	14.8	
	511	16.4	
	548	15.3	
	596	26.0	
^{69}Zn	438	94.85	13.75 h
^{57}Co	122	85.6	271.74 d
^{67}Cu	91	7.0	61.83 h
	93	16.01	
	184	48.7	
^{64}Cu	511	35.2	12.70 h
	1345	0.475	
^{56}Co	511	39.0	77.23 d
	846.7	99.93	
	1238	66.46	
^{58}Co	511	29.8	9.10 h
	810	99.45	

These results show that there are several zinc nuclides present in this sample solution. They were produced during the bombardment of natural zinc; their presence indicates a large amount of “cold” zinc remaining in the waste solution from the ^{67}Ga

production procedure. During the production process after EOB, the 5 g natural zinc target is completed dissolved into HCl solution. After ^{67}Ga is extracted for the final product, the rest of the zinc remains in the waste[7]. There are also three types of cobalt nuclides present in solution, although their amounts are very minimal.

Another major metal ion contained in the solution is Ti^{3+}. Visually the waste solution appeared to be purple; this is because Ti^{3+} is added during the ^{67}Ga separation step to avoid the production of Fe^{3+}. Fe^{3+} behaves similarly to gallium ions which would be retained in the separation column, causing contamination of Fe^{3+} in the final ^{67}Ga product. By adding Ti^{3+}, Fe^{3+} ions are reduced to the +2 oxidation state, which does not interfere with the ^{67}Ga separation. The added Ti^{3+} ions also remain in the waste solution and result in the purple colour. Since it is a stable nuclide, there are no corresponding peaks showing in the gamma spectrum. In order to obtain high purity ^{64}Cu, all of these metal ions need to be removed completely.

3.3.2 Gamma spectrum of loading solution

The ^{64}Cu separation process began with heating the waste solution until dryness. This was necessary because 7 M HCl solution is used as a washing solution to remove zinc, titanium and other contaminating ions during ^{67}Ga production and the acid remains in the waste solution. As the dithizone impregnated column requires a more dilute (0.05 M) HCl solution to retain copper, an evaporation step was implemented to obtain a loading solution at the right HCl concentration. A Teflon beaker was used for the evaporation as it has good acid and radiation resistance and, most importantly, Teflon does not absorb metal ion on its surface. This makes easier to “pick up” (dissolve) the residual ions after evaporation. In order to “pick up” the maximum amount of residual ions, the beaker was gently shaken for a few minutes when the solution was added. In Dolley’s original paper, 300 mL of 0.05 M HCl was added to dissolve the dried residual [44]. However, in that work, 5 g zinc was used in the experiment and a 10 mL dithizone impregnated resin column was employed for the retention of copper. In this study, the estimated zinc in 5 mL waste solution was about 0.375 g. The amount of other contaminant ions was also much lower, thus it was possible to use a smaller column (5 mL) and a smaller volume (20 mL) of 0.05 M HCl solution in the experiment. In future work, the size of the separation column and the

[7] For more details of the ^{67}Ga production process, see section 2.4.4 above.

volume of the pick-up solution could be reduced further to shorten the operating time and minimise the loss of ^{64}Cu due to radioactive decay.

From a practical perspective, the ^{67}Ga waste solution emitted a very high level of radiation 24 hours after EOB, thus the experiment needed to be performed in the red area (high radiation zone) of the Radionuclide Production Department (RPD) with very good shielding in place. Radioactive copper, zinc and cobalt are not volatile, so a fume hood was not necessary.

Figures 23 and 24 show the gamma spectrum of the 5 mL loading solution collected from the column outlet tube[8]. In this process, the useful ^{64}Cu and ^{67}Cu should be retained in the column, while the other radionuclides should exit via the outlet tube.

The distance of the solution was 1 m from the detector with a collimator (Figure 20 above). The acquisition time was 200 s and the detector dead time was 5.47%. 20 mL loading solution was pumped through the column at approximately 2 mL/min and the loading step was complete after 10 minutes. 5 mL solution was sampled for the measurement.

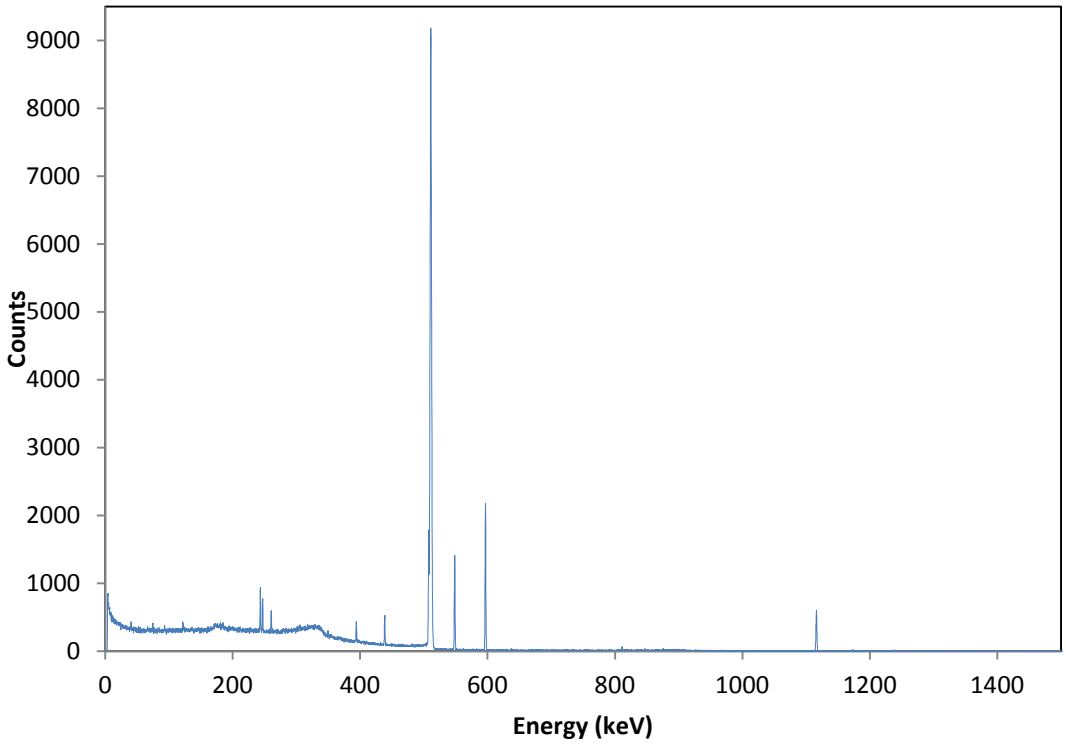

Figure 23: Gamma spectrum of loading solution from the ^{64}Cu separation process.

[8] For more details of the column operation, see section 3.2.2 and 3.2.3 above.

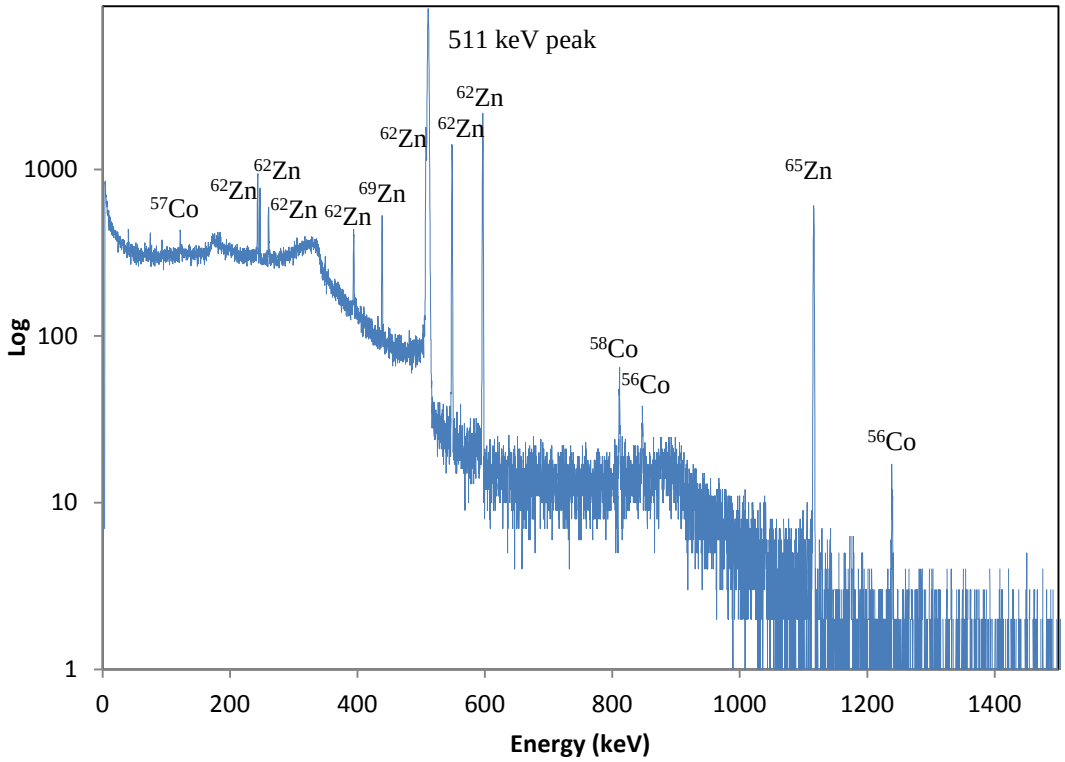

Figure 24: Gamma spectrum of loading solution from the ^{64}Cu separation process on log scale.

Figures 23 and 24 clearly show the disappearance of ^{67}Cu and ^{64}Cu peaks at 91 keV, 93 keV, 184 keV and 1345 keV. The positions of the other radionuclide (^{62}Zn, ^{65}Zn, ^{69}Zn, ^{56}Co, ^{57}Co, ^{58}Co) peaks remain the same, and the peak intensity and peak ratios are all the same. The 511 keV positron emission peak still shows as strong as in Figure 22 compared to the other peaks on the graph, due to the contributions of ^{62}Zn, ^{65}Zn, ^{56}Co and ^{58}Co, because these radionuclides are also positron emitters. Thus Figures 23 and 24 prove that radioactive copper (^{64}Cu and ^{67}Cu) ions were completely removed from the solution after loading, while all the other known radionuclides passed through the column without any retention.

3.3.3 Elution profile of washing solution

After the loading step, 0.05 M HCl washing solution was pumped through the column to further wash off the contaminant ions. In Dolley's paper [44], the experimental data indicated that the zinc ion should be completely washed out after 340 mL elution for 5 g zinc in a 10 mL column. This study narrowed down the experimental conditions down to 0.375 g zinc and a 5 mL column, thus a smaller volume washing solution was required for this process.

Figure 25 shows the elution profile built to determine the best suitable washing volume. This was done by taking samples of every 10 mL of washing solution coming out of the column. The total count of each sample was measured on an HPGe detector. All the samples were placed 15 cm away from the detector with a collimator. The acquisition time was 100 s for all samples, the detector dead times ranged from 5.02% to 0.41% due to the decreased activity of the samples.

Figure 25 shows the total number of counts from all the peaks on the gamma spectrum. Each bar on the graph represents the overall gamma count of a single sample, since all the samples were placed the same distance from the detector. The entire graph illustrates the change in the activity count in the profile of the washing solution.

The graph shows that the first 10 mL of the washing solution contained the most activity. As more washing solution was pumped into the column, less activity was measured in each successive fraction of solution. After 30 mL of washing, the sample counts became quite low, and remained relatively constant until the seventh sample. After 70 mL of washing, the activity of the washing solution became very low, as there were only a few hundred counts on the HPGe detector over a period of 100 seconds acquisition.

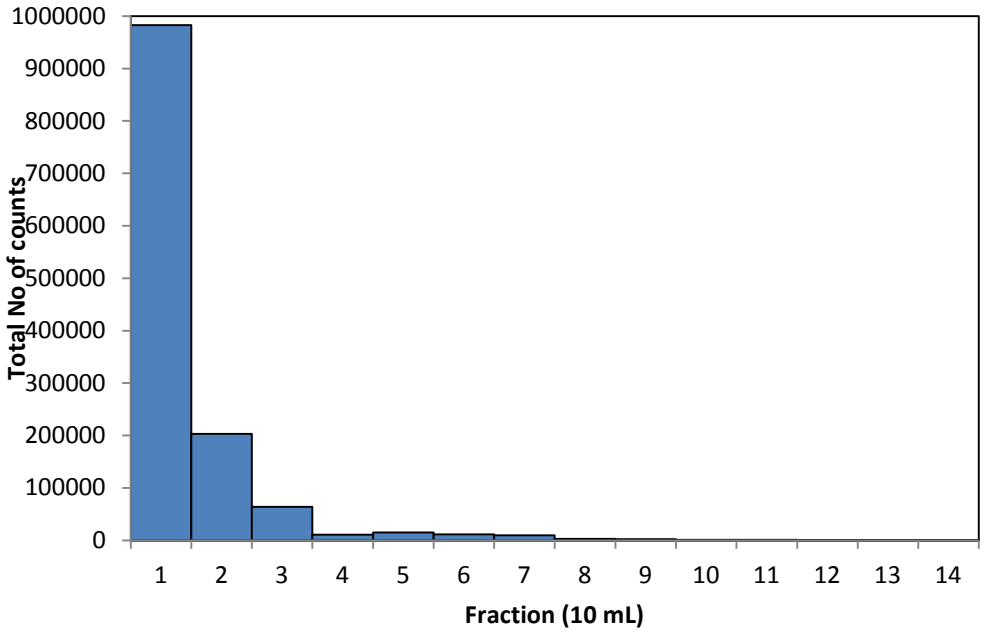

Figure 25: The elution profile of the washing solution from the separation column.

This showed that less than 150 mL of 0.05 M HCl washing solution was needed for the total rinsing of the 5 mL column. 70 mL washing solution was sufficient to wash nearly all the unwanted ions out of the system.

3.3.4 Elution profile of unloading solution

In the unloading step, warm 5 M HNO_3 was used to completely break the bond between the dithizone and copper ions to enable the removal of the copper ions from the column. The temperature of the nitric acid was about 50 ^{o}C. A discoloration of the column was observed during the experiment, as the dark red/black colour of the dithizone impregnated resin column changed to the white/milky colour associated with the colour of Amberchrom CG-71. This colour change happened initially at the top of the column once the nitric acid solution was pumped in, and then moved gradually from the top toward the bottom of the column until the whole column was completely changed back to its original colour. This also broke the impregnation of dithizone to Amberchrom CG-71; therefore, the column could not be used again.

Dolley *et al.* [44] employed 40 mL of warm HNO_3 solution to wash radioactive copper out from the previously loaded column. For the smaller column, 15 mL of warm HNO_3 solution was pumped through the column for unloading.

Figure 26 shows the elution profile of ^{64}Cu in the unloading solution. The activity of ^{64}Cu in each successive 1 mL of eluate solution was measured in an ionization chamber (CRC-25 R, *Capintec Inc.*). The final solution contained both ^{64}Cu and ^{67}Cu radionuclides; as they have the same chemical properties, it is impossible to separate them using a chemical method. They also have different half-lives, so the ratio of ^{64}Cu and ^{67}Cu in a solution will constantly change from EOB (detailed calculations will be shown in the next section). The ionization chamber was set with calibration number 015 to determine the activity of ^{64}Cu. The readout was calculated from the ^{64}Cu gamma energy level, therefore the presence of ^{67}Cu in the solution should not have interfered with the ^{64}Cu measurement. A comparison calculation is presented in next section.

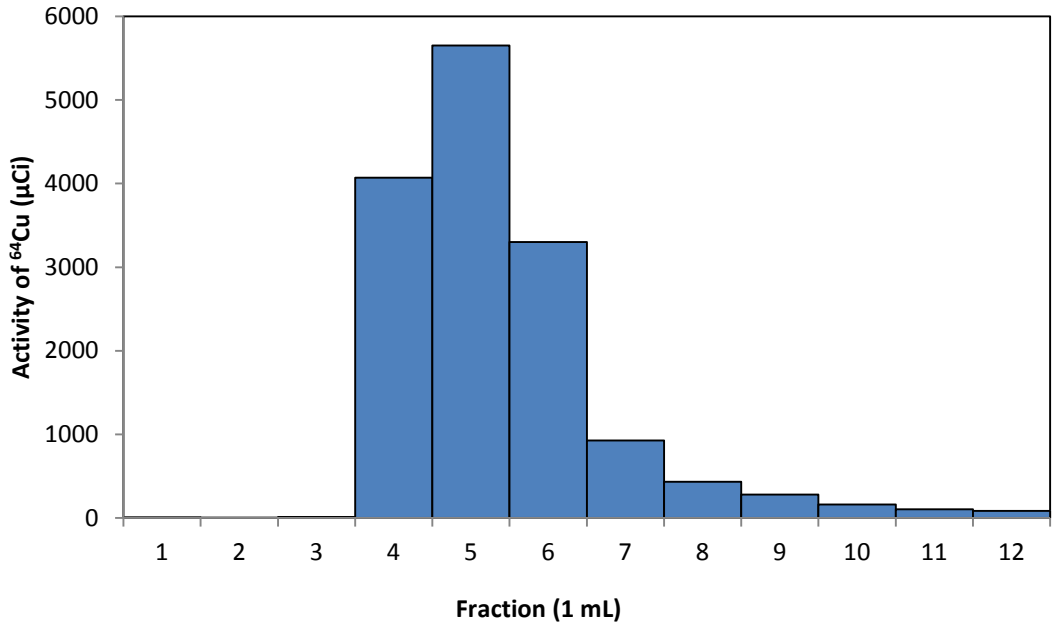

Figure 26: Elution profile of the unloading solution.

Figure 26 shows that there was almost no ^{64}Cu unloaded from the column in the first 3 mL of unloading solution. This is due to the dead volume of the system: the washing solution contained in the volume of the column and pipes came out first, containing no radioactive copper. The fourth millilitre of solution contained 4070 µCi activity and the fifth millilitre reached the maximum of 5650 µCi. The activity then decreased, as the sixth millilitre of solution contained about 3300 µCi activity and the seventh millilitre 929 µCi. From the eighth millilitre onward, the copper activity tailed off with each consecutive millilitre. The graph is plotted up only to the twelfth millilitre because the activity washing out of the column became very low, and it was not worth eluting further.

A total of 15.04 mCi ^{64}Cu was produced in 12 mL of the 5 M HNO_3 unloading solution. According to the estimated production yield of ^{64}Cu, the waste solution contained 9.2 mCi/mL at the time of EOB. At the time when ^{64}Cu was successfully separated, more than 24 hours had passed, which represented approximately two half-lives of ^{64}Cu – this should give a value of 2.3 mCi/mL. Since 5 mL of waste solution was processed in the experiment, the total theoretical value of ^{64}Cu should be 11.5 mCi. The results surprisingly show that the actual separation yield was more than 100% of theoretical value. A possible explanation for this is that the time of the zinc target bombardment might have been longer than usual in this particular ^{67}Ga

production. And in general radionuclide production, the production yield does show differences from time to time, even when the bombardment times are the same.

The results also show that a smaller amount of unloading solution was needed to wash the copper off the column. The fourth to seventh millilitre of eluting solution contained 92.8% of overall copper yield, thus if high specific activity of copper is needed, 4 mL of solution can be used to elute the copper out of the column. This reduction in the volume of nitric acid would be beneficial for the remainder of the labelling process.

3.3.5 Gamma spectrum of purified copper solution

Figures 27 and 28 show the gamma spectrum of the final copper solution. The fifth millilitre of the final copper solution was measured at a 50 cm distance from a detector with a collimator. The acquisition time was 100 s and the detector dead time was 4.63%.

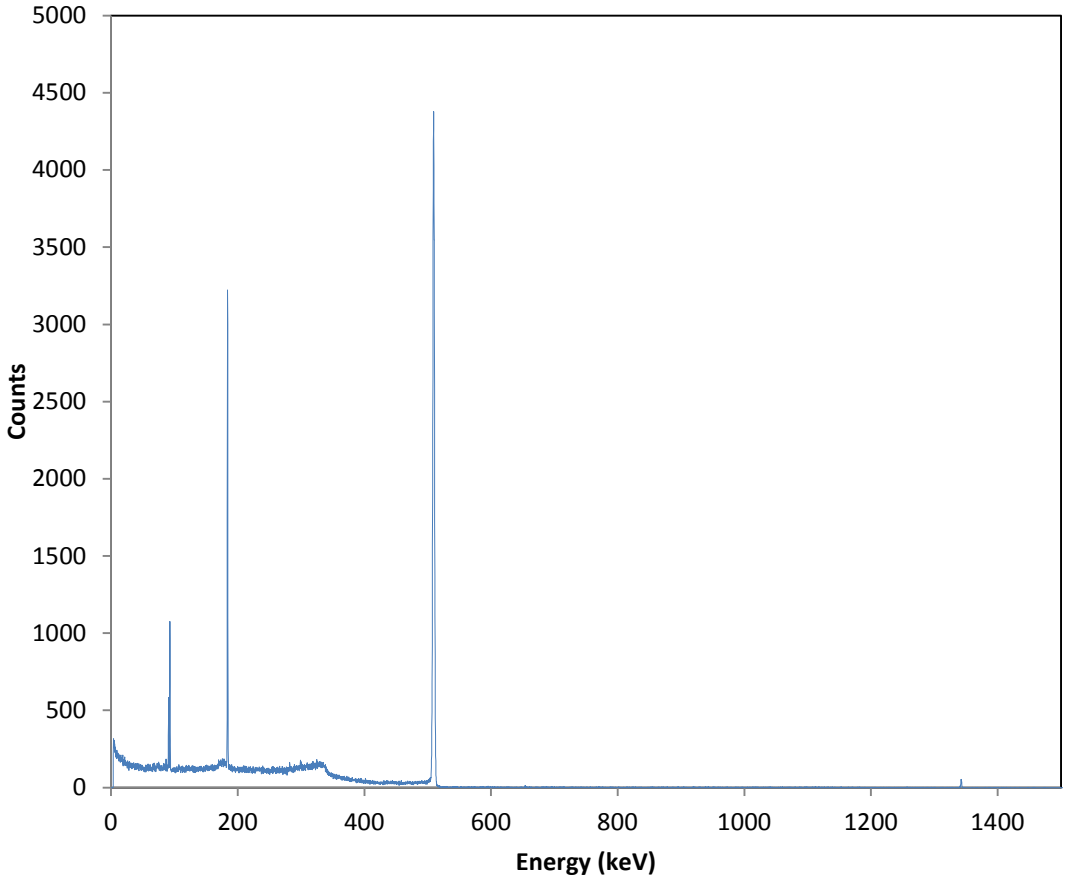

Figure 27: Gamma spectrum of the purified ^{64}Cu solution.

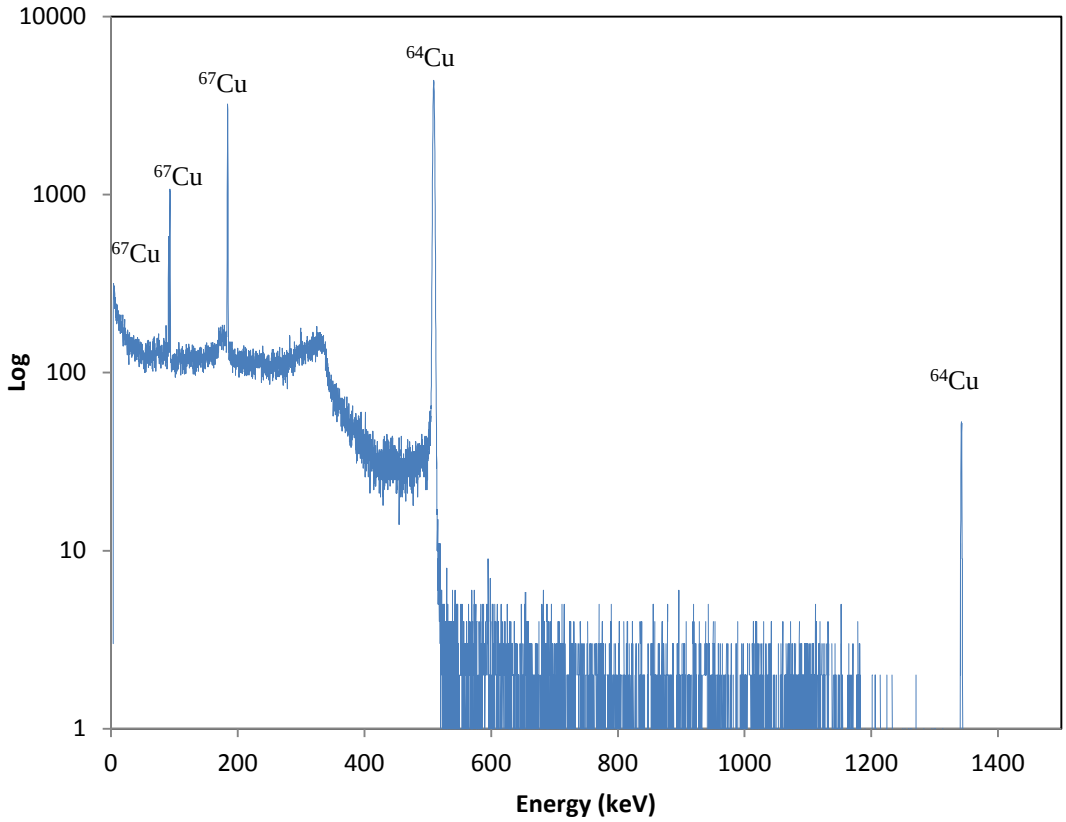

Figure 28: Gamma spectrum of the purified ^{64}Cu solution on log scale.

The position of peaks at 90.8 keV, 93.3 keV and 184.5 keV indicate the presence of the radionuclide ^{67}Cu, which is co-produced during the bombardment above the 40 MeV energy level. The largest peak at 511 keV is the target peak for PEPT measurement which is produced from ^{64}Cu radionuclide positron emission. The small peak at 1345.7 keV represents ^{64}Cu gamma ray emission. Due to its low natural abundance (0.473%), it is indicated by an extremely small peak on the graph. The absence of other peaks indicates there are no other radionuclide contaminants in the solution, i.e. the solution contained a high radiochemical purity of copper after the purification process.

The activity of each radionuclide was calculated from the gamma spectrum using the following equation:

$$A_d = \frac{A_p}{\varepsilon_d v_b T_l} \qquad \textbf{Equation 14}$$

where A_d is the activity of the radionuclide, A_p is the photo-peak area, ε_d is the detector efficiency at the photo-peak energy, v_b is the peak intensity or branching ratio of the particular gamma peak and T_l is the live counting time.

When the live counting time was 100 seconds, the intensity of the ^{64}Cu 1345 keV peak was 0.457%. The net peak area was read as 470 from the analysed gamma spectrum results. The detector efficiency is quite unique for each individual detector, as it depends on the sample shape and a sample matrix. The detector efficiency curve was obtained from RPD, iThemba LABS. The approximate detector efficiency for the ^{64}Cu 1345 keV peak was read as 4.819×10^{-6} from the curve. Thus, the activity of ^{64}Cu was calculated as 205.32 MBq, which is equivalent to 5.55 mCi. The ionization chamber readout of sample was 5.65 mCi. By comparing these two values, the calculated result may be seen to be very close to the readout. The small difference (1.7%) might arise from the value of detector efficiency: as it read manually from a graph, the exact value is hard to determine.

For the calculation of ^{67}Cu activity, the intensity of the 184.5 keV peak was 48.7%. When the live counting time was 100 seconds, the net peak area was analysed as 14900 and the detector efficiency was about 3.657×10^{-5}. The activity of ^{67}Cu was calculated as 8.367 MBq, which is equivalent to 0.226 mCi. This gives the ^{67}Cu/^{64}Cu activity ratio about 4% at 30 hours after EOB. Because ^{67}Cu has a longer half-life than ^{64}Cu, this ratio will keep increasing with time.

The result shows that the final solution contained a high radiochemical purity of copper, and that the main contaminants (such as zinc ions) were completely removed. The titanium ions cannot be detected by the HPGe detector; however, the clear colour of the solution indicated the absence of titanium. The ^{67}Cu/^{64}Cu ratio is relatively low even 30 hours after EOB. The ^{67}Cu has peaks at 91 keV, 93 keV and 184.5 keV energy levels, which should not interfere with PEPT experiments, because these peaks are outside of the detection energy window on the PET camera which is above 350 keV at the low end [54].

3.4 Final purification method

In this chapter, a method was described to separate ^{64}Cu out of the waste solution from the ^{67}Ga production at RPD, iThemba LABS. The ion exchange separation

method developed originally by Dolley *et al.* [44] was evaluated by taking samples from each step of the experiments, and analysing them with an HPGe detector and ionisation chamber. From the evaluated results, the original method was modified to make it simpler. The final solution contained highly purified ^{64}Cu. The final ^{64}Cu yield was 15.04 mCi from 5 mL production waste solution, approximately 30 hours after EOB. This was considered a very good yield, especially as the cost of production was nearly nothing, and a valuable product was recovered from production waste.

The ^{64}Cu separation method may be simplified as follows: a small volume (5 – 10 mL) of ^{67}Ga production waste solution is obtained from the RPD 24 hours after the EOB. It is heated in a Teflon beaker on a hotplate at 300 ^{o}C until dryness, then 10 mL of 0.05 M HCl solution is added to dissolve the residual radionuclides. This solution is pumped through a 3 mL column of dithizone impregnated resin at approximately 2 mL/min to load radioactivity onto the column. After loading, the column is washed with 100 mL of 0.05 M HCl solution at 5 mL/min to rinse off impurities. Finally 7 mL of warm (approx. 50 ^{o}C) 5 M HNO_3 solution is eluted through the column to wash out the ^{64}Cu, after discarding the first 3 ml as dead volume. Using this method, approximately 20 mCi of high purity ^{64}Cu can be produced with an operating time of less than one hour (the timing is carefully calculated by adding all the time consumption at each single steps).

CHAPTER 4 RADIOLABELLING OF TRACER PARTICLES WITH ^{64}Cu

4.1 Introduction

After obtaining purified ^{64}Cu solution, the radionuclide needs to be loaded onto a small particle to be able to track with PEPT. The ion-exchange method has been well studied and practised for PEPT at both the PIC, University of Birmingham, and PEPT Cape Town for many years [1], [55]. The method involves loading radionuclide onto a small resin particle via ion-exchange in an aqueous environment.

The optimal labelling conditions of cation and chelating resins with ^{68}Ga were determined previously [50]. This can be served as a guideline for the following labelling experiment with purified ^{64}Cu solution. A chelating resin with high selectivity for copper was chosen for the tracer labelling. ^{64}Cu has a low positron emission branching ratio, and emits fewer positrons than ^{18}F and ^{68}Ga. This may cause higher errors in the location of the tracer measurement in PEPT experiments. Therefore the tracer location measurements were compared with results using tracers labelled with other radionuclides.

This chapter describes how a copper-selective chelating resin was labelled with ^{64}Cu, the leaching test of labelled ^{64}Cu tracer in acidic and basic aqueous environments, the method to determine the tracking accuracy of the copper tracer, and the comparison to other PEPT tracers. Due to the difficulty of controlling the activity of tracers, button sources were used in the tracer comparison experiments.

4.1.1 Tracer labelling conditions

The ion-exchange method has proven to be the most effective method of tracer labelling at PEPT Cape Town, and has been employed for the majority of tracer fabrications. As described in Chapter 2, a standard labelling procedure has been used for tracers labelled with ^{18}F and ^{68}Ga; this method is also assumed to apply for the copper tracer.

The procedure is carried out in a small glass vial. Several resin particles are added to the glass vial with a small volume of radioactive solution. The vial is then placed on a

digital shaker, and shaken for certain time period. The resin particles are then separated and the amount of activity on each can be measured in an ionisation chamber. The amount of activity labelled on a single resin tracer depends on the resin type, the particle size, the chemical composition of the solution, the activity concentration in solution and the shaking time [50].

The effect of a number of parameters on the labelling efficiency (the ratio of amount of activity labelled on a tracer with initial total activity[9]) of a single tracer has been determined previously by the author [48]. Figures 29 to 31 show the effect of the HCl concentration of the solution, the concentration of activity in the solution, and the shaking time on the labelling efficiency of a single resin particle with a cationic radionuclide.

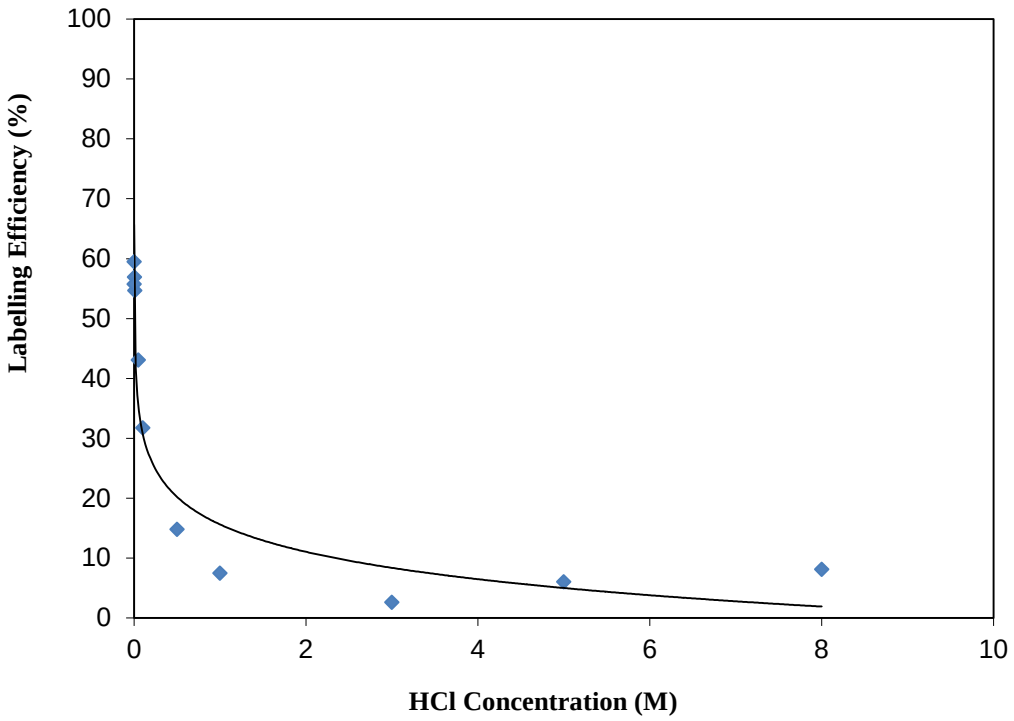

Figure 29: Effect of HCl concentration on the labelling efficiency of ion exchange tracers [55]**.**

[9] The total activity is the activity of labelled tracers plus the activity remained in labelling solution.

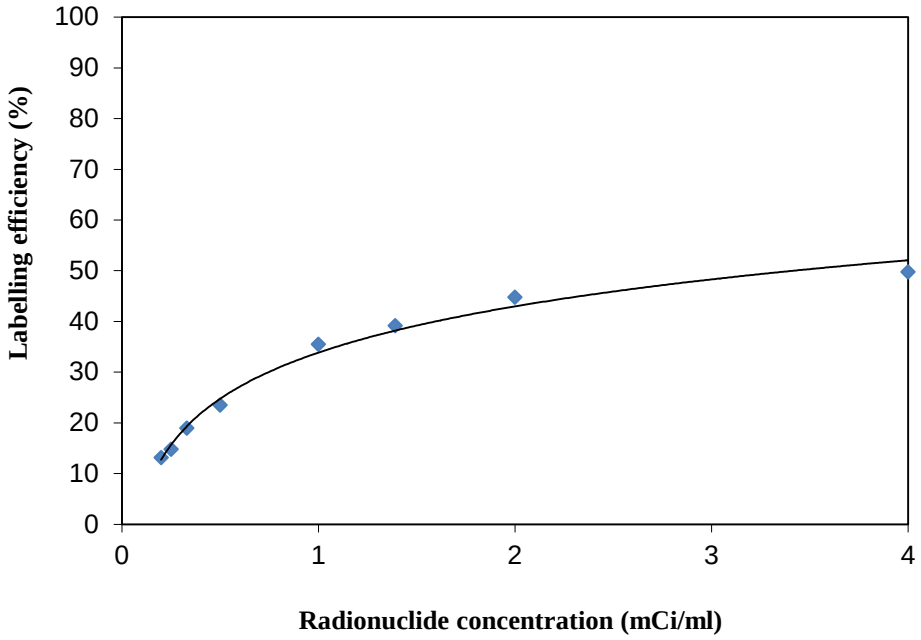

Figure 30: Effect of radionuclide concentration on the labelling efficiency of ion exchange tracers [55]**.**

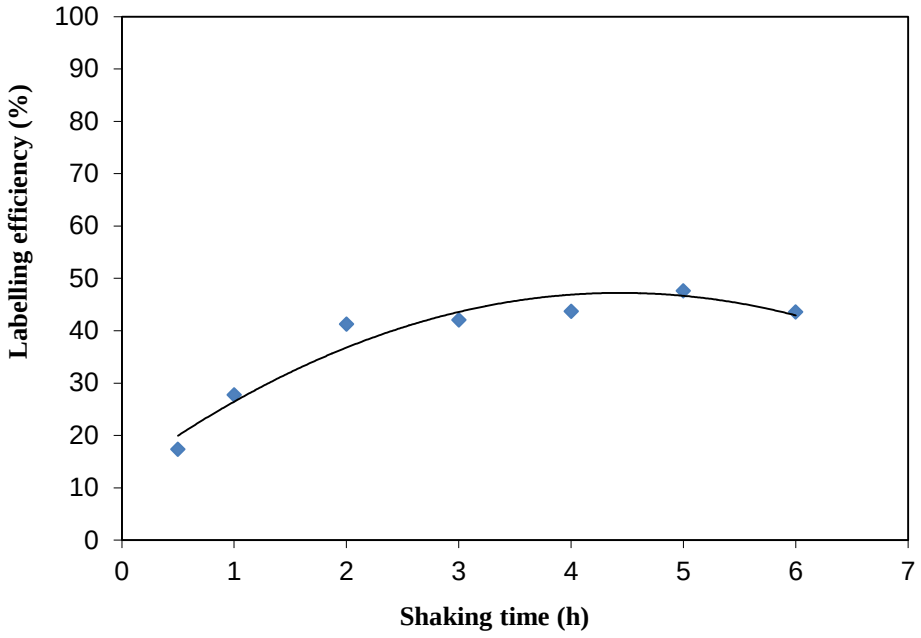

Figure 31: Effect of shaking time on the labelling efficiency of ion exchange tracers [55]**.**

Figure 29 shows that when the activity concentration and shaking time are fixed, the labelling efficiency decreases logarithmically with an increase in hydrochloric acid concentration. Therefore optimum labelling should be achieved in weakly acidic or

neutral solution. Figure 30 shows that when the labelling process occurs at low fixed HCl concentration, and the shaking time is fixed, the labelling efficiency increases with an increase in activity concentration, and does not approach a maximum value at the highest concentration of 4 mCi/mL; this suggests that a greater labelling efficiency would be achieved by using a higher activity concentration. Figure 31 shows that when the HCl concentration and activity concentration in the solution are optimised, the tracer particle sorbs greater activity as the shaking time increased, with an equilibrium reached after 2–3 h. However, due to the loss of activity associated with the short half-life radionuclides (^{68}Ga), it is not feasible to shake the particle over such a long period. Therefore, 30 minutes shaking time is considered to be ideal for the labelling of short lived tracers.

4.1.2 Selection of resin for tracer labelling

As discussed in Chapter 2, there are three main groups of resins: cation exchange resins, anion exchange resins and chelating resins. In PEPT research, cation exchange resins and chelating resins are normally used for labelling metal ions and the anion exchange resins are usually used for labelling anions. More specifically at PEPT Cape Town, Purolite NRW-100 strong cation exchange resin is used for ^{68}Ga tracer labelling, and AG-1 strong anion exchange resin is used for ^{18}F tracer labelling. The reaction equations happen as follows :

$$\mathbf{R\text{-}(SO_3H)_2 + {}^{68}Ga^{2+} \rightarrow R\text{-}[(SO_3)_2][{}^{68}Ga] + 2H^+} \qquad \textbf{Equation 15}$$

$$\mathbf{R\text{-}CH_2N(CH_3)_3{}^+OH^- + {}^{18}F^- \leftrightarrow R\text{-}CH_2N(CH_3)_3{}^{+18}F^- + OH^-} \qquad \textbf{Equation 16}$$

According to the theory, strong cation exchange resins can also be used for labelling tracers with ^{64}Cu. However, a special chelating resin, Purolite S930, was initially chosen for this work, due to its high copper exchange selectivity.

Purolite S930 chelating resin is a macroporous styrene divinylbenzene polymer matrix with iminodiacetate ions as the functional groups. These ions act as chelating agents in binding polyvalent metal ions. In industry, this resin is used for the extraction and recovery of metals from ores, refining the salt solutions of transition metals, and purification of organic or inorganic chemical products [56].

The spherical resin beads have an opaque beige physical appearance, and a specific gravity of 1.17 g/cm^3 in moist hydrogen form. 90% of the resin particles are sized between 1.2 – 0.3 mm. The resin is particularly suitable for the sorption of heavy metals which are held according to the following order of affinity:

Cu >> Ni > Zn ≥ Co ≥ Cd >Fe(II) > Ca **Equation 17**

In weakly acidic or neutral solutions, iminodiacetic acid would dissociate from R-$HN(CN_2CO_2H)_2$ to R-$[HN(CH_2CO_2)_2H]^-$ or R-$[HN(CH_2CO_2)_2]^{2-}$, where R is the styrene divinylbenzene matrix and $[HN(CH_2CO_2)_2]^{2-}$ is the functional group. The ion exchange reaction of copper occurs in the following regime:

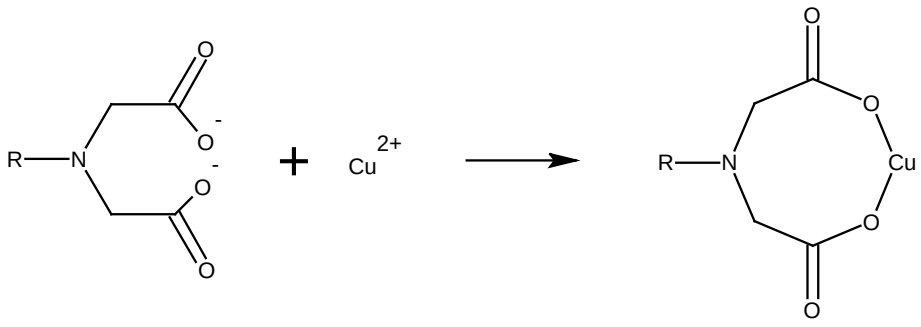

Equation 18

4.2 Experimental method

Analytical grade reagents were used throughout this work and were obtained from Merck (SA) Pty. Ltd or Sigma-Aldrich products. The AG 50W-X2 cation exchange resin used in this work was obtained from BioRad Laboratories, Richmond, USA. The Purolite S930 and S950 chelating resins were obtained from Purolite International, United Kingdom. ^{68}Ga was obtained from the elution of a ^{68}Ga/^{68}Ge generator and ^{67}Ga production waste solution was acquired from RPD at iThemba LABS.

De-ionised water was used for all the experimental work; it was obtained from a Millipore MilliQ Reagent Grade Water System, to a conductivity of greater than 10 megaohm.cm^{-1}.

4.2.1 Radiolabelling of tracer particles

Three different types of resins were tested under the same experimental conditions: Purolite S950 chelating resin, AG 50W-X2 strong cation exchange resin and Purolite S930 chelating resin.

The tracer labelling was performed as follows: 1 mL of the radioactive copper solution obtained according to the method described in Chapter 3 was heated in a Teflon beaker until the solution had evaporated to complete dryness. The residue was dissolved in 1 mL of 0.01 M HCl solution. Several similar sized organic resin particles (500 – 600 μm) were added to the solution and shaken at 1500 rpm for 30 minutes (MS 3 digital shaker, *IKA*). The labelled tracers were then separated using fine-tipped tweezers and the activity of each tracer was measured using an ionisation chamber (CRC-25 R, *Capintec Inc*., NJ).

To compare with the conventional tracer labelling method for ^{68}Ga, these three resin types as well as the NRW-100 cation exchange resin were tested under the same experimental conditions.

4.2.2 Leaching test

Since the labelled tracers were to be used in different media during the PEPT experiment, a leaching test was performed on the labelled Purolite S930 resin tracer. After the labelling process, one labelled Purolite S930 resin tracer was shaken in 1 mL of HCl and NaOH solution of different concentrations at 1500 rpm for 20 minutes. The activities of each tracer and solution were measured separately after shaking and the percentage of leaching was determined by comparing the activity of the solution to total activity. This procedure was repeated for 0.001 M, 0.01 M, 0.1 M, 1 M NaOH solutions and 0.001 M, 0.01 M, 0.1 M, 0.5 M, 3 M HCl solutions respectively.

4.2.3 Comparison of different radionuclides for PEPT studies

The PEPT measurements were conducted using the ECAT “EXACT3D” (Model: HR++) PET camera at the PEPT Cape Town laboratory. In order to maintain the exact amount of activity on each tracers for comparison, the button sources were used in this experiments, due to the difficulty of controlling the amount of activity labelled on a resin tracer.

A 60 μCi ^{64}Cu button tracer was made and placed at the centre of the field-of-view of the PET camera. The tracer was tracked in a stationary position for 2 minutes. The same procedure was repeated with 60 μCi ^{68}Ga, ^{18}F and ^{22}Na button tracers.

A moving test was performed on a wooden circular rotating disc (Figure 32). The apparatus was made at the workshop in the Department of Physics, University of Cape Town. It had a radius of 150 mm, and was powered by a 5 V DC motor. The speed of the motor was adjusted by altering the input voltage from the power supply unit. The actual rotating speed of disc was determined by a digital photo tachometer (RS 163-5348, *Tachometer*).

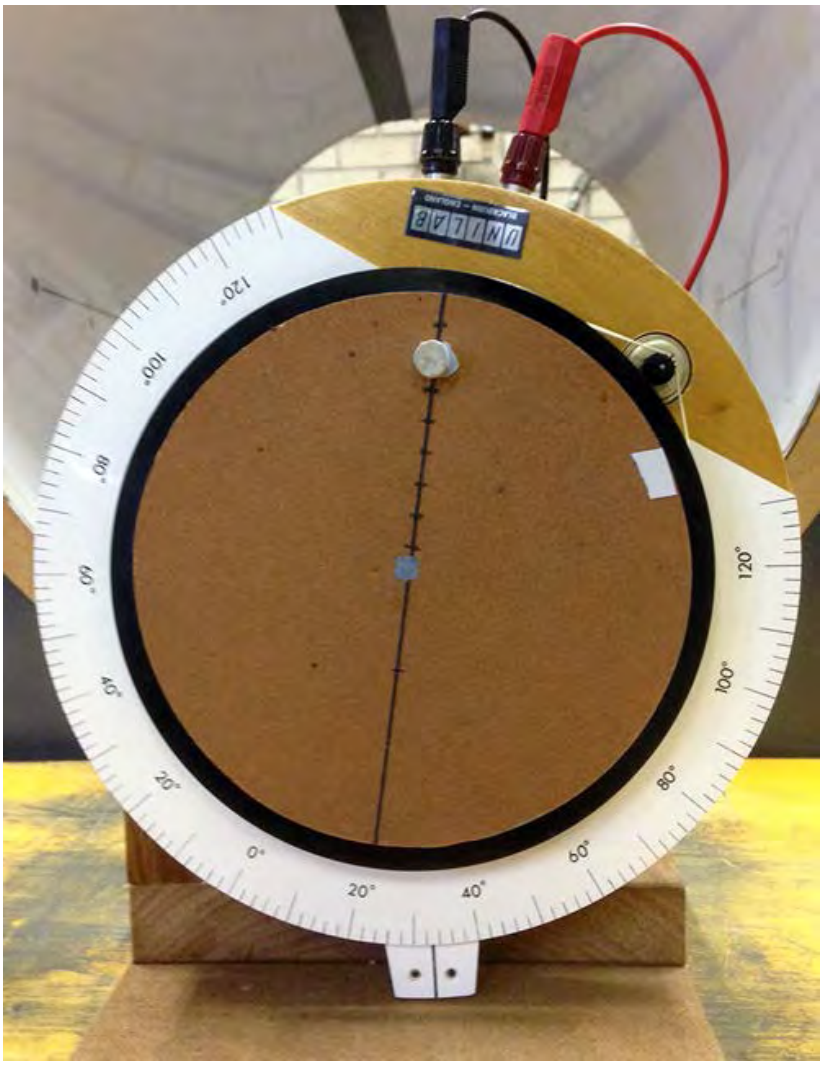

Figure 32: The wooden rotating disc used for PEPT with the button source attached.

A labelled tracer was fixed to the edge of a circular wooden disc of radius 120 mm and the whole set-up was placed at the centre of the field-of-view of the PET camera. The tracer was tracked while the disk was rotating, over a tracking time of 2 minutes.

This experiment was performed with ^{64}Cu and ^{68}Ga button tracers. A range of tracer activities and rotating speeds were tested.

4.3 Results and discussion

4.3.1 Tracer labelling tests

The ion-exchange theory of Purolite S930 with copper was discussed in section 4.1.2. The other chelating resin, Purolite S950, is a macroporous styrene divinylbenzene (DVB) polymer matrix with weakly acidic aminophosphonic functional groups, and a sodium counter ion. In weakly acidic or neutral solution, the $R\text{-}CH_2NHCH_2PO_3Na_2$ dissociates to form $R\text{-}CH_2NHCH_2PO_3^{2-}$. The 2- functional group would attract Cu^{2+} ions in solution as in Equation 19.

$$R\text{-}CH_2NHCH_2PO_3Na_2 + {}^{64}Cu^{2+} \rightarrow R\text{-}CH_2NHCH_2PO_3^{2-}[{}^{64}Cu^{2+}] + 2Na \qquad \textbf{Equation 19}$$

AG 50W-X2 strong acid cation exchange resin is composed of sulfonic acid functional groups attached to a styrene divinylbenzene copolymer lattice. X represents the percentage of cross linkage of the resin. A resin with a lower cross linking has a more open permeable structure than a highly cross linked resin, which allows more metal ions get into the resin and results in a quick ion exchange reaction. The resin is supplied in the hydrogen form. In weakly acidic or neutral solution, the $R\text{-}SO_3H$ dissociates to $R\text{-}SO_3^-$ where R is the organic backbone, and $-SO_3H$ is the functional group. The reaction of Cu^{2+} ions with AG 50W-X2 happens as in Equation 20.

$$R\text{-}(SO_3H)_2 + {}^{64}Cu^{2+} \rightarrow R\text{-}[(SO_3)_2][{}^{64}Cu] + 2H^+ \qquad \textbf{Equation 20}$$

The labelling experiment was designed as follows: the final copper solution obtained according to the method described in Chapter 3 was in 5 M nitric acid solution, which is too high to conduct an efficient labelling according to the optimized radiolabelling conditions described in section 4.1.1. It was necessary to reduce the acid concentration to the desired solution condition. The evaporation method was

implemented. For comparison purposes, these resins were also radiolabelled with ^{68}Ga under exactly the same experimental conditions. NRW-100 cation exchange resin was also put into the test, to serve as a baseline, and a point of comparison for the ^{64}Cu against the best possible labelling with ^{68}Ga.

Figure 33 compares the labelled activities of different types of resin particle with purified ^{64}Cu and ^{68}Ga solutions. The initial activity of ^{64}Cu and ^{68}Ga was measured approximately as 2 mCi and 3 mCi at the beginning of each experiment. Due to the short half-life of ^{68}Ga, slightly more gallium was added initially in order to match the activity with that of ^{64}Cu for the PEPT tests, as ^{68}Ga decays more rapidly than ^{64}Cu during the shaking process. Four particles of each resin were added to each solution, and after shaking the activity of each labelled tracer was measured, and the average value was used to plot the graph.

As shown in Figure 33, the average activity of the Purolite S950 chelating resin tracer labelled with ^{64}Cu was 22 µCi; that of the AG 50W-X2 strong cation exchange resin was 33 µCi, and that of the Purolite S930 chelating resin was 126 µCi. Thus the Purolite S930 resin particle showed a higher activity than the other two resins when the same optimised experimental conditions were applied.

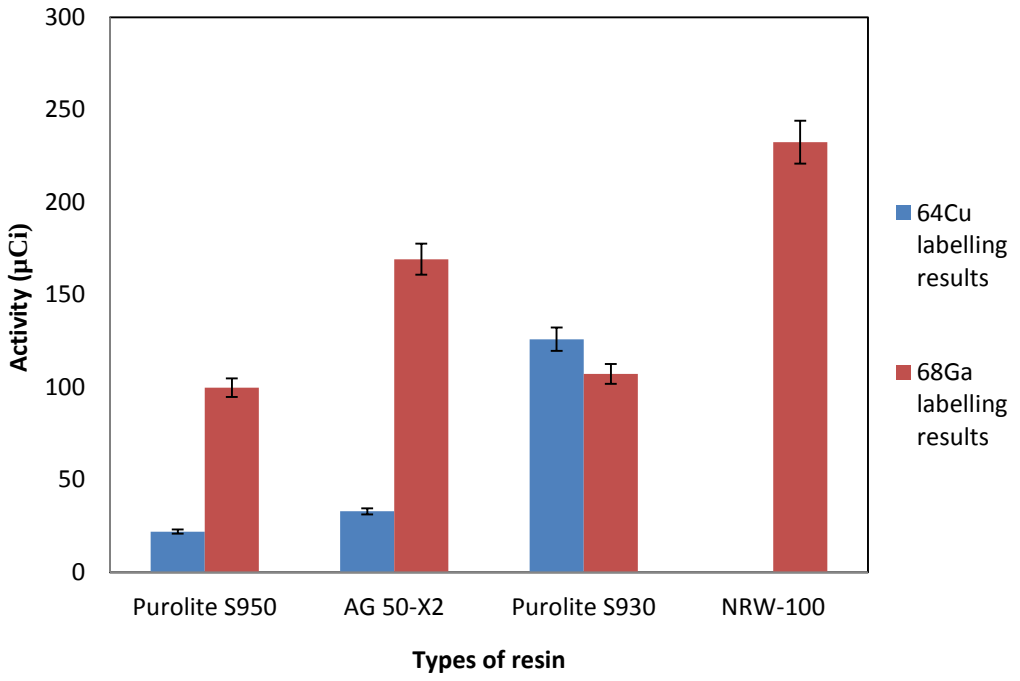

Figure 33: Average activities of different types of resin labelled with ^{64}Cu and ^{68}Ga, the standard deviation of mean error bars have been added on top of the columns.

This can be explained by the affinity order and relative selectivity of the resins. Cu^{2+} has the highest affinity order with Purolite S930 in Equation 17. However, the copper selectivity is not specifically high for Purolite S950.

The relative selectivity of AG 50W-X2 cation exchange resin for various ions is shown in Table 1 at section 2.5.2 above. The value is 2.9 for Cu^{2+}, which is moderate in comparison with other metal ions shown in the table. Cation exchange resins are not specialised in retaining certain metals, therefore, AG 50W-X2 resin had lower labelling ability than Purolite S930 in the experiments.

In the ^{68}Ga labelling tests, the two cation exchange resins showed better labelling ability than the two chelating resins, because these chelating resins do not have particularly high gallium selectivity. Comparing the ^{64}Cu and ^{68}Ga labelling results overall, all the resins labelled higher with ^{68}Ga except for Purolite S930. The ^{64}Cu labelling result of Purolite S930 was lower than the activity of the commonly used NRW-100 cation exchange resin labelled with ^{68}Ga. Under optimal labelling conditions, a 500 μm NRW-100 resin can be labelled with ^{68}Ga as high as 10 mCi[10]. This indicates that Purolite S930 should have a much higher ^{64}Cu labelling result under optimised experimental conditions.

4.3.2 Tracer leaching test

During a PEPT experiment, a radiolabelled tracer is normally placed inside industrial equipment, where the chemical and physical environment may result in leaching of the radionuclide from the tracer. This can cause inefficient tracking results and contamination of the equipment, requiring the abortion of the experiment and shutdown of the laboratory in some cases. This is of particular importance for the ^{64}Cu labelled tracer due to its long half-life in comparison with ^{18}F and ^{68}Ga. With the shorter lived radionuclides, if any contamination occurs, the contaminated environment can be cleared out the next day due to the decay of the radionuclides to safe levels. However, this would not be possible with ^{64}Cu due to its longer half-life. Therefore, it is appropriate to assess the risk of contamination by testing the leaching of ^{64}Cu in different media.

[10] Based on the data from the experimental log book.

Tracers made from anion exchange resin always leach in aqueous solutions due to its ion exchange nature. Regarding the order of the affinity sequence in Equation 9, the fluoride ion is the second lowest in the sequence, only slightly higher than the hydroxide ion. Therefore it can be easily replaced with other ions in the solution. On the other hand, labelled cation exchange and chelating resins are quite stable in solution. The commonly used ^{68}Ga tracers at PEPT Cape Town can endure pH ranges of 1 to 11 without any leaching in aqueous solutions [50]. In the same pH range, ^{64}Cu tracers should give the same stable results as other chelating resin tracers. The leaching experiment was designed to determine how much leaching would occur in both acidic and basic solutions for a labelled ^{64}Cu tracer.

Figure 34 shows the percentage leaching of Purolite S930 tracers labelled with ^{64}Cu in HCl and NaOH solutions of different concentrations. After 20 minutes of shaking, the tracer showed no leaching in de-ionised water and very low leaching in 0.001 M HCl and 0.001 M, 0.01 M, 0.1 M NaOH solutions. However, the leaching was considerable in 0.01 M, 0.1 M, 0.5 M, 3 M HCl and 1 M NaOH solutions. This shows that the ^{64}Cu labelled tracer can be used for PEPT experiments in neutral, weakly acidic and moderately basic aqueous environment, within a practical working pH range of pH 3 to pH 13.

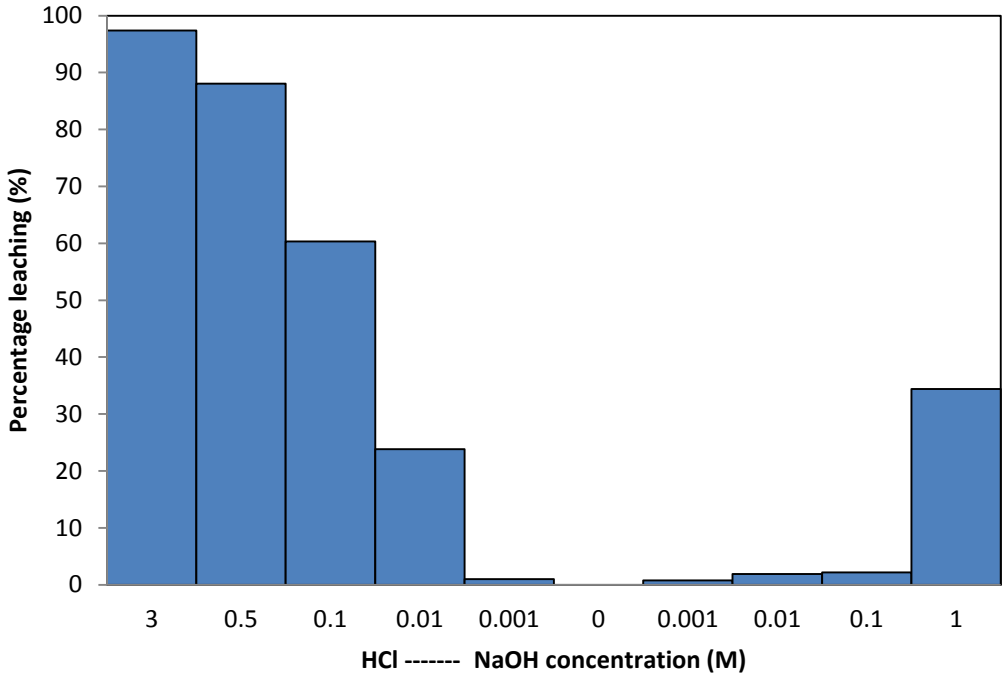

Figure 34: Percentage leaching of labelled Purolite S930 in acidic and basic solutions.

4.3.3 Comparison of ^{64}Cu tracer with other tracers in PEPT tests

A series of experiments was designed to determine the practicality of ^{64}Cu tracers in actual PEPT experiments. The tracer was first placed in the centre of the PET camera for tracking in a stationary position, and then it was tracked in a circular motion on a rotating disk at various speeds. The acquired data were analysed with the Birmingham location algorithm [14]. ^{68}Ga, ^{18}F and ^{22}Na tracers were also tested to enable comparisons based on the different nuclear properties of each radionuclide.

a) PEPT measurement of ^{64}Cu tracer on a rotating disk

As discussed in Chapter 2, pairs of 511 keV gamma rays acquired in the PET camera contain a large number of random gamma rays. These random gamma ray pairs come from either one or both of a pair of gamma rays which has undergone Compton scattering before detection, or two detected gamma rays which are not from the same annihilation event.

A location algorithm was developed at the Positron Imaging Centre (PIC), University of Birmingham, to remove the corrupted gamma rays and calculate the location of the tracer particle more accurately. This is done by finding the closest point of intersection of all the gamma ray paths in a short time interval. The mathematical representation is shown as follows:

$$\bar{\boldsymbol{d}}_{\boldsymbol{N}} = \frac{\mathbf{1}}{\boldsymbol{N}} \sum_{\boldsymbol{i}} \boldsymbol{d}_{\boldsymbol{i}} \qquad \textbf{Equation 21}$$

where N is the number of "line of response" (LORs) and d_i is the minimum distance from a LOR to the tracer (i = 1, 2, 3…, N). The minimum distance is perpendicular to the trajectory.

During the calculation, all the LORs satisfying $d_i > \bar{\boldsymbol{d}}$ are rejected as they are considered to be random events. The remaining events are used to calculate the mean minimum distance in a second iteration, then any paths larger than the mean value are discarded again. This process is repeated until only un-scattered events are assumed to remain.

As this iteration continues, a large number of acquired events would be discarded, yet in an ideal situation, only three events are necessary to have accurate location of the tracer. From a practical perspective, a certain number of events are needed in order to obtain an accurate measure of the tracer location. Therefore an *f* value is introduced into the algorithm, which is the fraction of LORs remaining in the final location measurement after iteration. The *f* value needs to be optimised for each tracer.

When tracking a moving tracer particle, the location algorithm needs to calculate a new location after a short period of time. This is achieved by repeating the location process using a new set of trajectories. This is controlled by the *N* value which is the number of trajectories in each set initially. The *N* value represents the number of events in each set of calculations. The optimum value varies according to the speed of the tracer and the level of attenuation in the equipment. When a tracer is stationary, a large *N* value can be used to calculate an accurate location. When the tracer is moving, a smaller *N* value is used to increase the number of tracking points and to give more accurate representation of the tracer trajectory.

Overall, the choice of *N* and *f* depends on the total LORs recorded in the run, and the proportion which have been random events.

In the experimental design of this thesis, the PEPT tracking data of ^{64}Cu tracers were first analysed to determine whether ^{64}Cu tracers are suitable for PEPT applications. Two ^{64}Cu button tracers were used, one with 30 µCi activity and another with 170 µCi. The 30 µCi tracer was tracked on the rotating disk at 1.33 Hz, and the 170 µCi tracer was tracked at 0.92, 1.40 and 3.67 Hz.

Figure 35 shows the processed PEPT tracking result of a 30 µCi ^{64}Cu tracer attached on the edge of the rotating wooden disc. The values of $N = 100$ and $f = 30\%$ were chosen for a rotational frequency of 1.33 Hz. The data are plotted as individual spatial dimensions, *X, Y,* and *Z* versus time, for the first five seconds of tracking. The regular sinusoidal shapes represent the cyclic up and down movement of the tracer on the *X* and *Y* axes. The movement of the tracer on the *Z* axis is minimal, but shows a slight up and down shift due to the slight bending of the wooden disk during rotation.

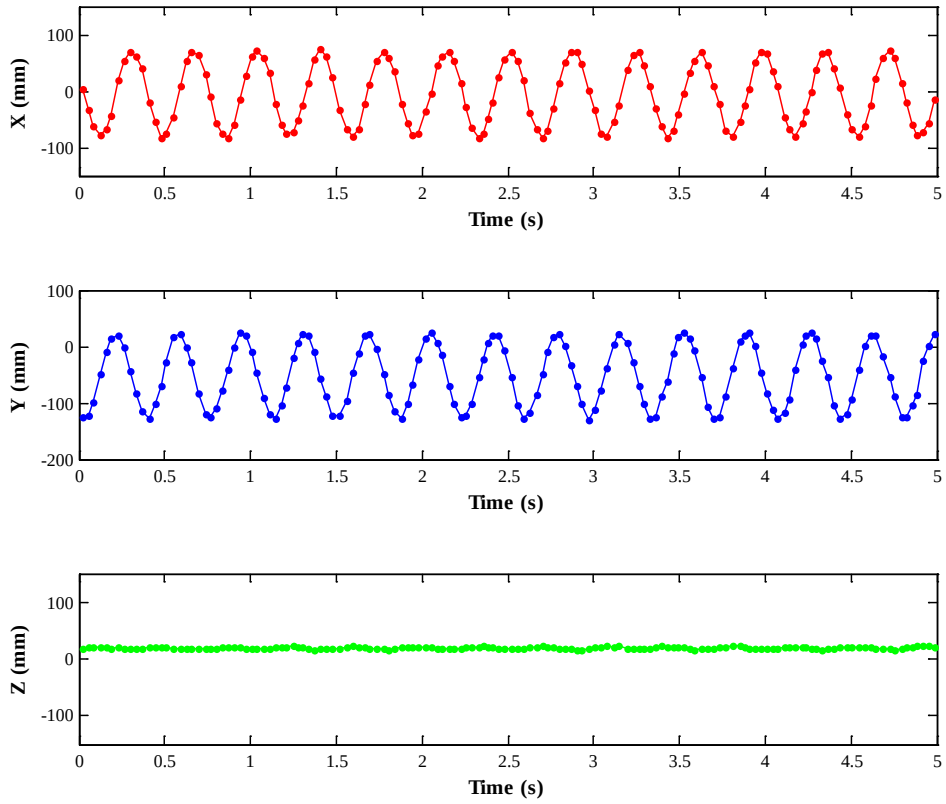

Figure 35: Coordinate measurements of ^{64}Cu tracer attached to a rotating wooden disc. Frequency 1.33 Hz, activity 30 µCi, *N* = 100, *f* = 30%.

Figure 36 shows the tracking trajectories of a 170 µCi ^{64}Cu tracer at two different rotational speeds: 0.92 Hz (left) and 3.67 Hz (right). The disk was also placed in the *XY*-plane. Due to the volume of data, only the first 2.5 seconds of tracking are used for this illustration. The two graphs show significant differences in frequency on the *X* and *Y* axes. For an *N* value of 100 and an *f* value of 30%, both of these diagrams show sufficient locations to match the circular motion of the tracer. The average speed of the tracer (left) was analysed as 410 mm/s, and the average speed of the tracer (right) was 1600 mm/s.

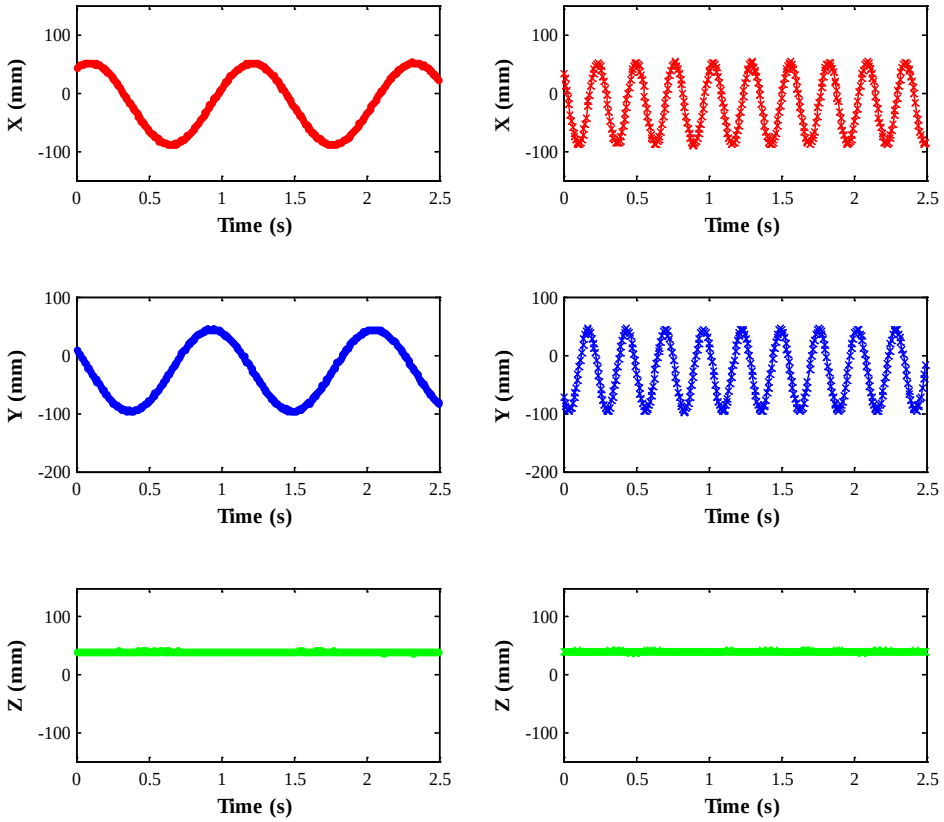

Figure 36: Coordinate measurements of the ^{64}Cu tracer attached to a rotating wooden disk. Frequencies (left) 0.92 Hz and (right) 3.67 Hz.

The circular trajectory of the tracer can be represented by a mathematical sinusoidal function as follows:

$$\boldsymbol{S(t) = Acos(\omega t + D)} \qquad \textbf{Equation 22}$$

where A is the amplitude, ω is the angular frequency, θ is the phase angle and D is the displacement. The location errors of a tracer trajectory can be calculated as the difference between each measured location and the expected location predicted by the circular path of the rotation. A "root mean squared error" (r.m.s.) was used to calculate the location error for runs in which the tracer rotated with a constant radius. The r.m.s. error is given symbol δr. This is calculated as in the following equation:

$$\boldsymbol{\delta r = \sqrt{\frac{\sum_i^n (\Delta r_i)^2}{n}}} \qquad \textbf{Equation } 23$$

where Δr_i is the perpendicular distance between each positional datum measured via PEPT and the expected position of the tracer, given by the least squares fit to the set of data, and n is the total number of triangulated locations obtained for the total run. For each PEPT measurement, Δr_i was calculated for 150 locations (Equation 23). An algorithm written in Matlab software by Cole *et al.* [55] was used to facilitate the calculation. In order to find the best match, several different parameters were tried in Equation 23 until the results closely represented the sinusoidal cycle. Then the r.m.s. location errors were calculated using Equation 24 for the 30 µCi and 170 µCi ^{64}Cu tracers. The results are given in Table 3.

Table 3: R.m.s. location errors of the 30 µCi and 170 µCi tracers.

Tracer activity (µCi)	Disk rotational frequency (Hz)	Mean location frequency (Hz)	δX (mm)	δY (mm)	δZ (mm)
30	1.33	29	3.90	3.60	0.81
170	0.92	131	1.36	0.97	0.53
170	1.40	131	1.43	1.05	0.51
170	3.67	131	1.62	1.26	0.48

Table 3 shows that the r.m.s. location error of the 30 µCi tracer was higher than that of the 170 µCi tracer on all (*X, Y* and *Z*) axes. This is a result of the lower tracer activity, as fewer location points are acquired. The number of locations decreased from 131 locations per second for 170 µCi tracer to 29 locations per seconds for 30 µCi tracer.

Table 3 also shows that the r.m.s. location error increased in the *X*- and *Y*-directions with increasing rotational speed. For the 170 µCi tracer, when the velocity of the tracer increased from 410 mm/s to 1600 mm/s, the r.m.s. location errors in the *X* and *Y* directions increased from 1.36 to 1.62 mm and 0.97 to 1.26 mm respectively. However, the increase in r.m.s. location errors was not significant in relation to the normal errors expected for a PEPT measurement. The r.m.s. location error was lower in the *Z*-direction as the tracer did not have any significant motion in this direction, but the low activity tracer did show a higher value than the higher activity tracer. Figure 38 shows the relationship between r.m.s. location error and rotational speed in

the experiments: only X and Y coordinates were plotted, for N = 100, f = 30%. The solid lines represent a least square linear fit for the data (R^2 = 0.988 for X coordinate and R^2 = 0.986 for Y coordinate).

The current data shows (three data points) linear correlation between r.m.s. location error and tracers speed, however, it is hard to say for sure that the relationship is linear as we do not have enough data points to prove it. Overall, the determination of relationship of tracking efficiency with tracer speed is not part of this study, as it involves more complicated factors, such as detector efficiency, tracer activity, attenuation, position of tracers in the field of view etc.

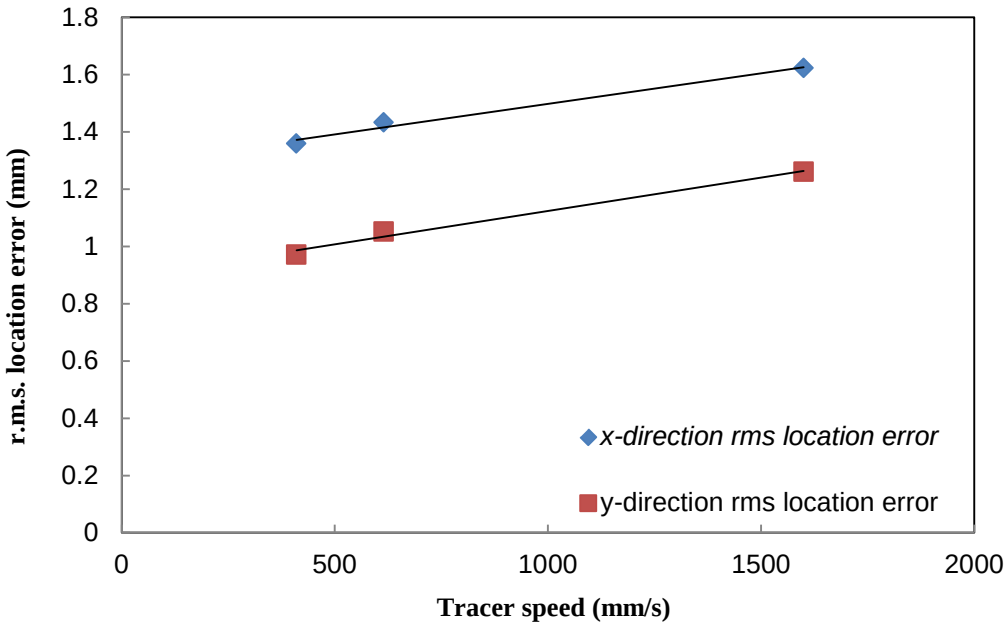

Figure 37: R.m.s. location error of the 170 µCi ^{64}Cu tracer moving at different speeds.

b) Comparison of PEPT measurements using ^{64}Cu tracer with other radionuclide tracers.

This section of the experimental work was designed to compare the ^{64}Cu tracer with other common radionuclide tracers used at PEPT Cape Town. The activities of the radionuclide tracers were kept constant to track each tracer under the same experimental conditions. Different N and f values of each radionuclide were analysed.

Figures 38 to 40 show measurement results for a 60 µCi tracer placed in a stationary position at the centre of the field-of-view of the PET camera, over two minutes of tracking.

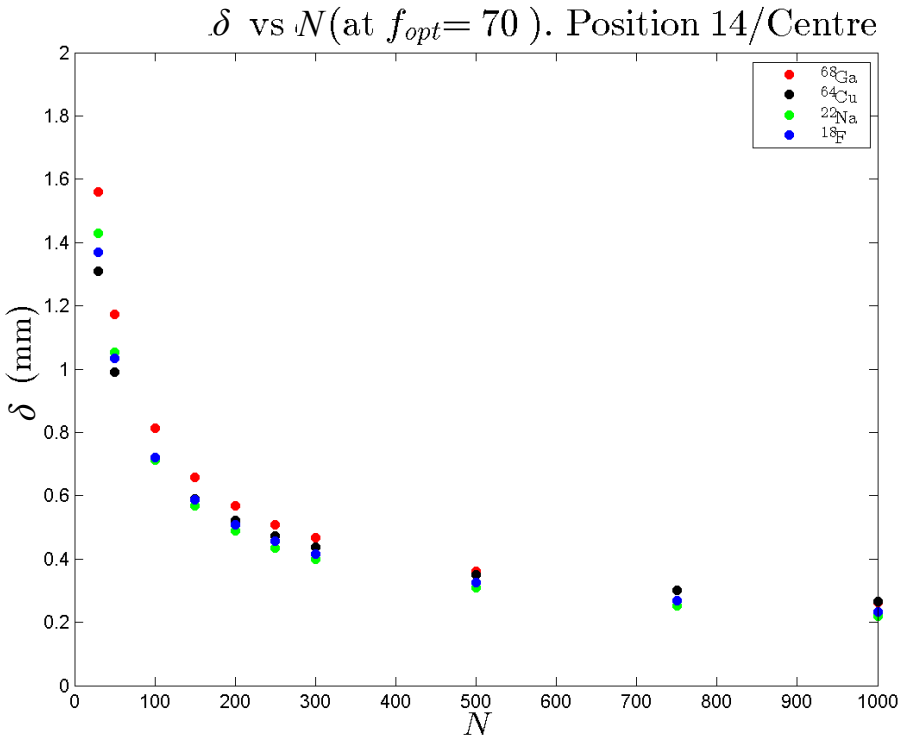

Figure 38: *r.m.s.* versus *N* location error for different tracers at stationary position.

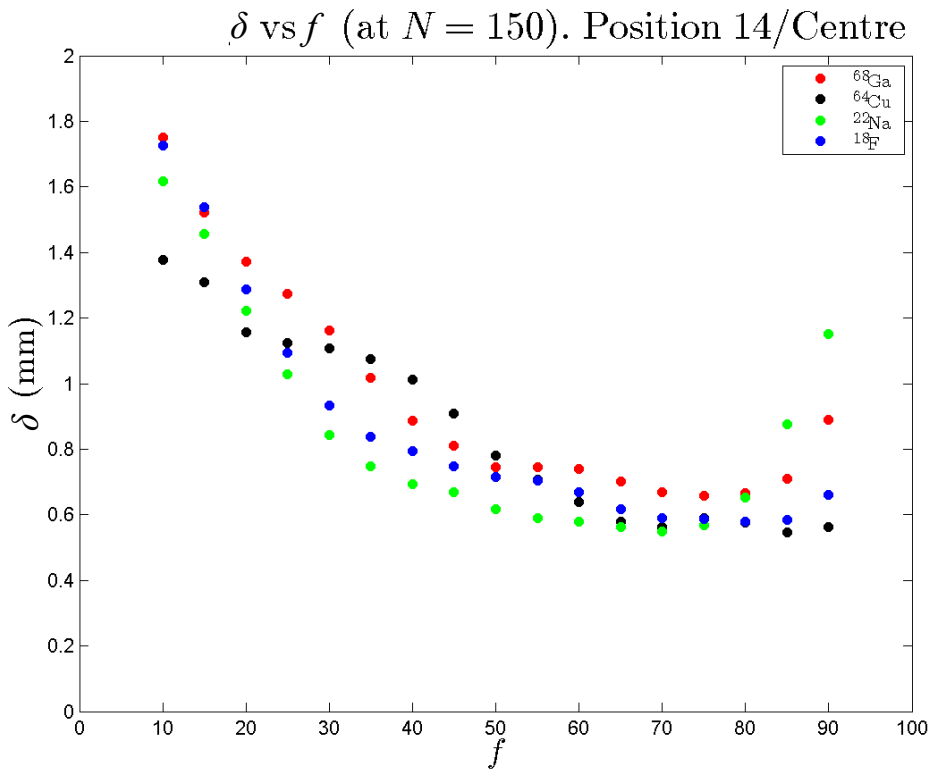

Figure 39: *r.m.s.* versus *f* location error for different tracers at stationary position.

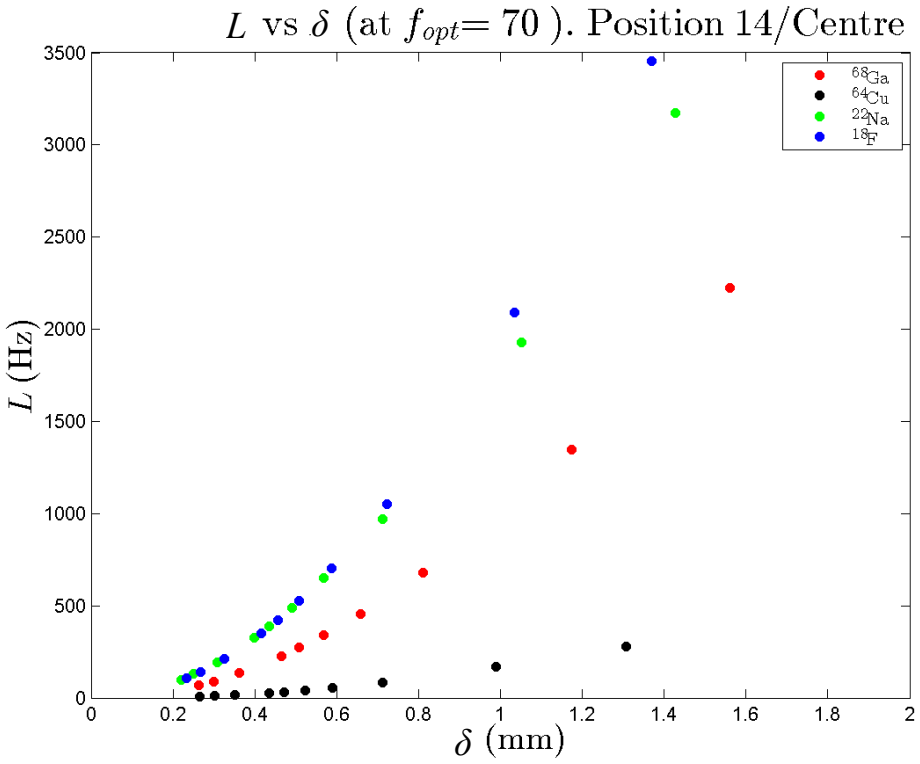

Figure 40: Number of location points per second versus r.m.s. location error for different tracers at stationary position.

In Figure 38, the collected binary data for each tracer were processed by the location algorithm with f = 70, and different N values ranging from 20 to 1000. Then one second of analysed data was used to calculate the r.m.s. location error Δr_i as the difference between each measured location and the average values of all locations. As the N value increased, the r.m.s. location error decreased. Between 20 and 100, the r.m.s. location error dropped sharply, and then tended to be constant with further increases in the N value. All four radionuclide tracers showed similar trends, and there was no large deviation for any tracer.

As discussed in section (a) above, N is a set of initial LORs chosen for the calculation of a particular location point, by using the iterative location algorithm. When a large number of LORs are chosen, the location error should be lower for a stationary tracer and more events are used to increase the accuracy of the calculation. As seen in Figure 38, when the N value increased, the r.m.s. location error decreased. The number of LORs is related to the activity of the tracer; therefore the analysis of stationary and moving tracer locations must be treated differently. In order to determine the accurate location of moving tracer, a moderate N value is needed. If the N value is too large, the tracer may move a significant distance during this set of LORs, with the effect of increasing the location error. If the N value is too small, it may not provide enough number of LORs for analysis and be strongly affected by the inclusion of random gamma rays.

In Figure 39, the collected data were processed as follows: with the N value fixed at 150, different f values from 10% to 90% were used in the location algorithm, and the r.m.s. location errors were calculated and plotted in the graph. The graph shows that the r.m.s. location error decreased when the f value increased, reached its lowest at 60%, and then was constant from 60% to 80%. It then increased from 85% to 90%. All the tracers followed a similar trend, with small fluctuations.

The f value is the fraction of obtained LORs remaining in the location calculation after iteration. If the f value is too large, many random events are included in the calculation which increases the location error. If the f value is too small, there are not enough statistical data for analysis and the location algorithm cannot calculate a location. This can be clearly seen in the Figure 39, where the tracer location errors increase when the f values are too large or too small.

From Figure 39, the optimal *f* value is about 70% for all tested tracers. This suggests that 20% to 30% of acquired LORs were random. However, this only applies to stationary tracers at the centre of the field of view without any shielding. In situations such as tracking moving tracers, or in highly attenuated media, the number of random LORs may increase, which would lead to a decrease in the optimal *f* value.

In Figure 40, the same set of data was processed in a different way. With the *f* value set at the optimal 70%, different *N* values were used to analyse the data in location algorithm. After calculating the r.m.s. location errors, these were plotted against the number of location points per second in the graph. This figure shows that when the number of location points increased, the r.m.s. location error increased. Each tracer behaved differently, with the ^{18}F curve on top, followed by the ^{22}Na and ^{68}Ga curves, and the ^{64}Cu curve at the bottom.

In PEPT measurement, *L* is the location frequency and the value of *L* is related to the *N* value and tracer activity. If the tracer activity is fixed, leading to a constant number of events (LORs) acquired, a larger *N* value would generate smaller *L* and a lower location error. Practically a large *L* is required to have enough locations to closely track the path of a moving tracer. If a smaller *N* value is taken in order to get larger *L* (see Figure 38), the location error increases correspondingly. Therefore, the radionuclide tracers with large *L* value (up to maximum about 1 kHz) and small location error would be the best choice for a PEPT measurement. ^{18}F tracer appears be the most suitable radionuclide for PEPT, because for the same tracer activity it provides the highest number of locations per second.

The differences in *L* value for each tracer can be explained by each radionuclide having a different positron emission branching ratio. Branching ratio (or branching fraction) is the fraction of particles which decay by an individual decay mode with respect to the total number of particles which decay. This happens because some radionuclides have more than one decay mode. According to the chart of radionuclides, the branching ratios of positron emission for ^{18}F, ^{22}Na, ^{68}Ga and ^{64}Cu are listed below:

Table 4: Branching ratios of certain radionuclides.

Radionuclides	^{18}F	^{22}Na	^{68}Ga	^{64}Cu
Branching ratio for β^+ decay	96.7%	90.3%	87.7%	17.6%

The number of positron emissions depends on the branching ratio for β^+ decay: when the radionuclides have the same activity, a high branching ratio tracer would give higher count readings in a PET camera. This has been supported by experimental observation in the table below:

Table 5: Count rates of a 60 µCi tracer of certain radionuclides on a PET camera (Siemens HR++).

Radionuclides	^{18}F	^{22}Na	^{68}Ga	^{64}Cu
Count rate (s^{-1})	105515	97014	67670	7600

For fixed values of N and f values, the count rate is directly proportional to L. This explains the differences in the radionuclide behaviour in Figure 40. ^{18}F has highest branching ratio, therefore the tracer was tracked with more locations per second. ^{64}Cu has the lowest positron emission branching ratio, thus it produced the least number of location points per unit of time.

A set of decay experiments was also performed to determine the changes in location error during the tracer's decay. The experiments were carried out with a tracer which had an initial activity of 60 µCi. The tracer was placed at the centre of the view of field of the PET camera, and a 2 minute scan was completed for every half-life of the tracer until the activity dropped below 1 µCi. The ^{68}Ga and ^{64}Cu tracers were both tested for comparison.

The data obtained from the decay experiment were processed by taking $N = 50$ and $f = 70\%$. The results are shown in Figures 41 and 42. One second of data was taken for the calculation of the r.m.s. location error. A smaller N value than in previous tests was chosen for all activities of the tracer, to ensure that the tracer location was triangulated based on the same number events at both high and low activity.

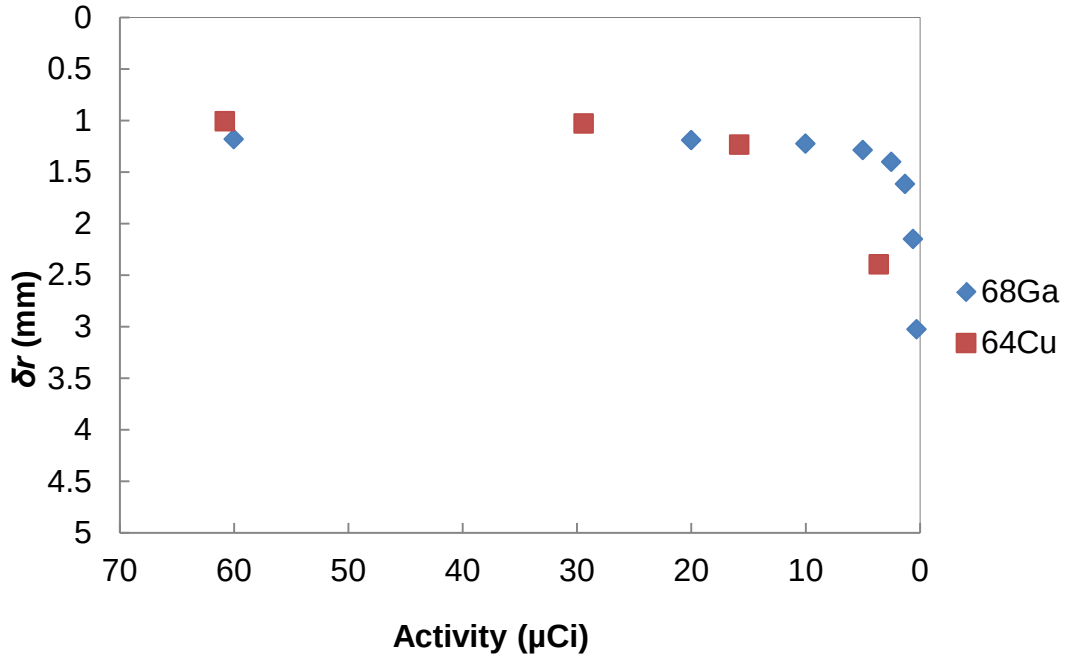

Figure 41: r.m.s. location error versus tracer activity for ^{68}Ga and ^{64}Cu tracers (at N = 50, f_{opt} = 70)[11].

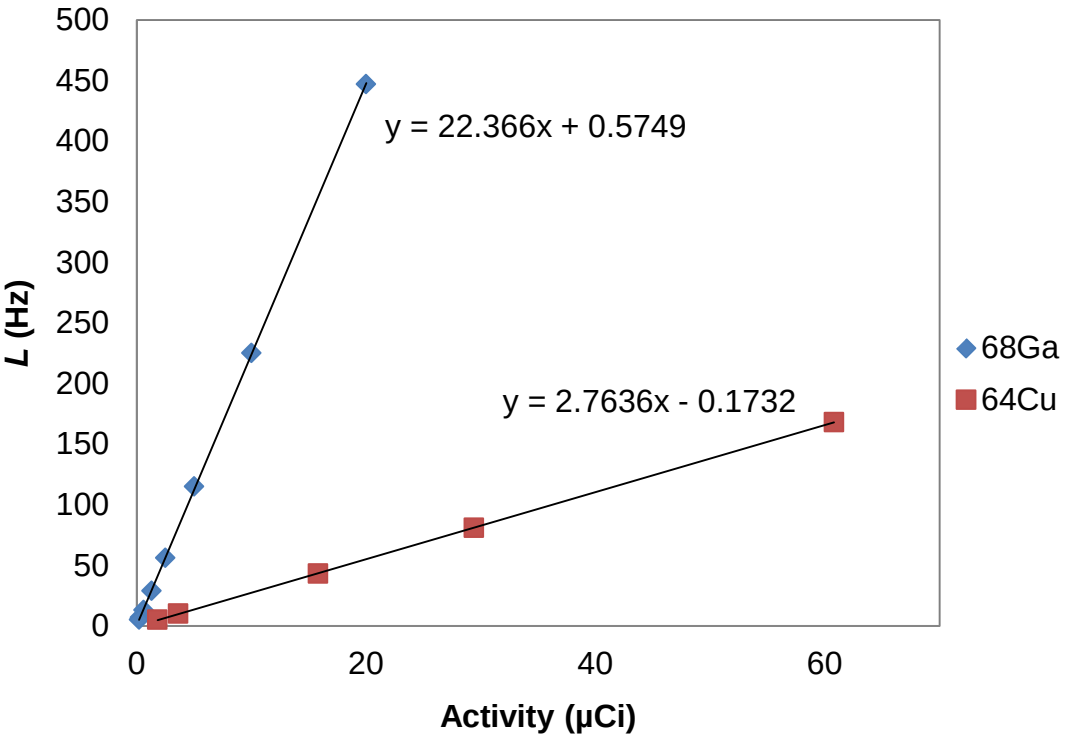

Figure 42: Number of locations per second versus tracer activity for ^{68}Ga and ^{64}Cu tracers (at N = 50, f_{opt} = 70).

[11] The axes are inverted in this diagram, because it shows a better concept how the error increases with the decreasing of tracer activity.

Figure 41 shows r.m.s. location error against tracer activity. The ^{64}Cu and ^{68}Ga tracers had similar location errors when the tracer activities were large enough, namely about 1 mm for ^{64}Cu and 1.1 mm for ^{68}Ga. However, the r.m.s. location errors increased sharply when the activity dropped below 5 μCi, and more quickly for ^{64}Cu than ^{68}Ga. The tracers would be considered completely useless when the location error was larger than 2.5 mm; at this point, the ^{64}Cu tracer was at 3 μCi, and the ^{68}Ga tracer was at about 0.5 μCi. Figure 42 shows number of location points per second against tracer activity. It shows that, at the same activity, the ^{68}Ga tracer produced more location points per unit of time than ^{64}Cu. Both of these results can be explained by the smaller branching ratio for β^+ decay for ^{64}Cu. They show that at lower tracer activity, ^{68}Ga still maintains relative low location error.

A similar set of measurements was performed using a tracer fixed to a rotatory disk at 1 Hz speed. Each run was recorded for 2 minutes. The tracer tracking was started at initial tracer activity of 60 μCi, and successive runs were recorded after every half-life until the activity was 1 μCi. The data were analysed using $N = 50$, $f = 50$. The final calculated r.m.s. location errors were plotted against tracer activities. A trend line was added for both tracers. A smaller N and f were taken as the tracer was moving, to achieve a higher number of location points per unit of time and reduce the number of corrupt events. ^{68}Ga and ^{64}Cu tracers were tested for comparison.

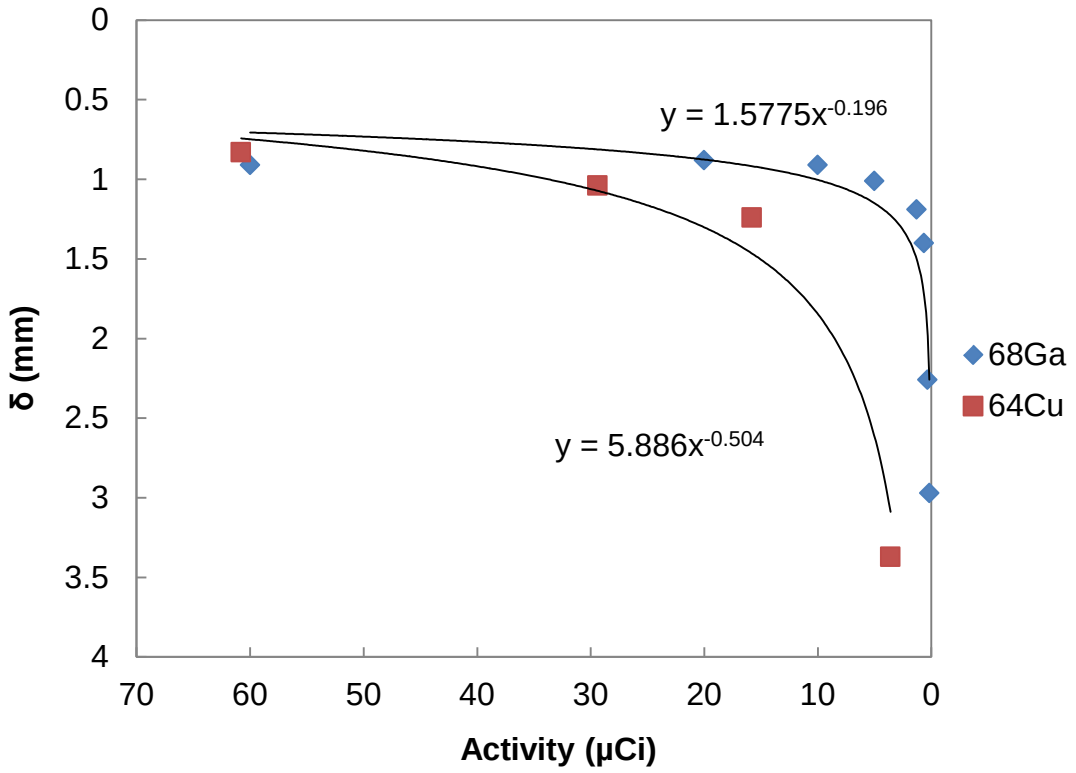

Figure 43: r.m.s. location error versus tracer activity for ^{68}Ga and ^{64}Cu tracer on a rotatory disk at 1 Hz .

Figure 43 shows that the positions of both the ^{68}Ga and ^{64}Cu tracers were measured with similar r.m.s. location errors at 60 µCi. The location error of the ^{68}Ga tracer remained constant until the activity dropped below 10 µCi; it then increased and became quite high at lower than 0.5 µCi, at this activity, ^{68}Ga became no longer usable. The location error of the ^{64}Cu tracer dropped slightly until 10 µCi, and after tracer activity dropped below 5 µCi, the error became so large which the tracer no longer usable.

As discussed previously, ^{64}Cu has a lower positron emission branching ratio than ^{68}Ga, thus ^{64}Cu emits fewer 511 keV gamma rays than ^{68}Ga per second. Different count rates were observed for the two tracers over the experimental runs: the number of 511 keV gamma rays emitted from ^{68}Ga was four times higher than ^{64}Cu. The PEPT measurements started at an activity of 60 µCi, at which level the location errors for both radionuclides were similar as there were sufficient LORs to calculate the tracer position at the limit of the PEPT measurement (1 mm). With decay, the differences in location error became more significant, with a higher location error for the ^{64}Cu tracer due to the lower position emission branching ratio. However, because

of the long half-life of ^{64}Cu relative to ^{68}Ga, the useable time of the copper tracer was much longer than that of the ^{68}Ga tracer.

4.4 Summary

In this chapter, different ion-exchange resins were labelled with ^{64}Cu in order to determine whether it is possible to fabricate ^{64}Cu tracers via the ion-exchange method. Purolite S930 chelating was chosen as the primary candidate due to its high copper selectivity. Three other commonly used resins were tested in the experiment for comparison. After the ^{64}Cu was successfully loaded onto the ion-exchange resins, leaching tests were performed to determine if the tracer would leach in certain aqueous environments. Finally PEPT experiments were conducted by using button sources to track the efficiency of ^{64}Cu compared with three other commonly used radionuclides.

From the results, the loading of ^{64}Cu on cation exchange and chelating resins was shown to be possible. Purolite S930 chelating resin had the highest labelling efficiency compared to Purolite S950 chelating resin and AG50-X2 strong cation exchange resin. This was as expected, as Purolite S930 has high copper selectivity. In leaching tests performed with labelled Purolite S930 resin particles, the tracer did not leach in aqueous environments with in a pH range of 3 to 13[12].

The ^{64}Cu tracer was tracked with PEPT in stationary and rotating disk experiments. The raw data were triangulated with different N and f values, to determine how this would affect the tracking efficiency. The results were compared to tracers labelled with the radionuclides ^{18}F, ^{68}Ga, ^{22}Na, because ^{64}Cu has a lower positron emission branching ratio than thesis radionuclides. In a stationary position in the centre of the field of view of the camera, the location of the ^{64}Cu tracer was measured with a similar r.m.s. location error as the other radionuclide tracers. However the ^{64}Cu tracer produced fewer location points per unit of time due to the lower branching ratio for positron emission as compared to the other radionuclides. In a PEPT application this would result in a lower tracking efficiency of tracers moving at high speeds, but this effect could be countered by using a higher activity of ^{64}Cu on the tracer. The 60 μCi

[12] The leaching test was only performed for 20 minutes as this test was designed at the early stage of the research, however, it would be ideal to extend the test time to few hours.

^{64}Cu tracer was measured with the same location error as the ^{68}Ga tracer on a disk rotating at 1 Hz. As the radionuclides decayed, the location error increased rapidly for ^{64}Cu, but due to the longer half-life of ^{64}Cu it provided a much longer tracking time than the ^{68}Ga tracer.

CHAPTER 5 CONCLUSION

Positron emission particle tracking (PEPT) is a non-invasive technique used for obtaining dynamic information of particle flow within industrial equipment. The technique tracks a tracer labelled with a positron emitting radionuclide ("PET radionuclide") moving within the field-of-view of a modified PET scanner. The pairs of collinear 0.511 MeV gamma rays released in the decay of the PET radionuclide are detected in coincidence and the location of the tracer is triangulated. The establishment of the PEPT Cape Town laboratory at iThemba LABS in South Africa provides a good research opportunity in the fields of tracer labelling, location algorithm development and a wider range of PEPT applications. The lab uses the radionuclides ^{68}Ga and ^{18}F for making tracers on a daily basis; however the short half-life of these radionuclides compared to the length of a PEPT experiment limits their application. The main disadvantage is that the short half-life of radionuclides reduces the tracer tracking time to two or three hours, with an increase in location error as the radionuclide decays.

^{64}Cu is a potential radionuclide for PEPT as it decays by positron emission and has a longer half-life of 12 hours. It is co-produced in the ^{67}Ga production process at the RPD at iThemba LABS. Normally, the radioactive copper is considered as unwanted waste, and is removed completely into waste solution by the ^{67}Ga production process. A novel separation method was developed several years ago by Dolley *et al.* [44] which allowed all copper nuclides to be separated from the production waste. This provides the opportunity to obtain high purity ^{64}Cu for PEPT measurements and to recycle radioactive waste.

In this thesis ^{64}Cu was separated from the ^{67}Ga production waste solution by valuating and modifying the ion-exchange procedure of Dolley *et al.* [44]. A tracer labelling procedure was developed to fabricate tracer particles for PEPT tests. The labelled tracer proved to be very stable in weakly acidic, natural and weakly basic aqueous environments. The detection efficiency of the tracer labelled with ^{64}Cu was measured in the Siemens HR++ PET camera, and the location error and frequency of the tracer compared with tracers labelled with other commonly used PET radionuclides. The ^{64}Cu tracer was shown to be a good PEPT tracer when a sufficient amount of activity was labelled onto the tracer particle.

Improving the copper separation process of Dolley *et al.* [44] began by performing a gamma spectrum of ^{67}Ga waste solution with an HPGe detector. This indicated the presence of many contaminate radionuclides, including ^{62}Zn, ^{65}Zn, ^{69}Zn, ^{56}Co, ^{57}Co, ^{58}Co, as well as the copper radionuclides ^{64}Cu and ^{67}Cu. There were also large amounts of "cold" zinc and titanium ions in solution. The process to separate radioactive copper from the waste solution was improved by using a smaller column and a much shorter period of time. Throughout the experiment, elution profiles of the washing and unloading steps were obtained to minimise the volumes of acid solutions used in these steps. In a second gamma spectrum, the final purified copper solution showed very high purity. A small amount of ^{67}Cu remained in the solution as it could not be separated from ^{64}Cu via chemical methods. However, ^{67}Cu has gamma emissions at lower energies than the detection window of most PET scanners, and will have minimal effect on the detection efficiency of a tracer labelled with this purified copper solution.

Different resins were selected to test the labelling efficiency of the purified copper solution. Purolite S930 chelating resin showed the highest labelling efficiency compared with the other two resins, Purolite S950 chelating resin and AG 50W-X2 cation exchange resin. The labelling results were similar in magnitude to those achieved with ^{68}Ga under comparable experimental conditions. A leaching test was also performed, and showed that the ^{64}Cu remained adsorbed on the tracer in a pH range of 3 to 13. This suggests the ^{64}Cu tracers are suitable for PEPT studies, and will work in a wide range of media.

PEPT experiments were performed to track the ^{64}Cu labelled resin tracer in stationary and rotating positions in the PET camera. Analysis of the tracking data showed that the copper tracer is suitable for PEPT, as it could be located frequently enough to follow a tracer moving at high speed on a rotating disk, and it could be located to r.m.s of 1.80 mm which is sufficient accuracy for most PEPT applications. In comparison to tracers labelled with other radionuclides (^{18}F, ^{22}Na and ^{68}Ga), the tracer labelled with ^{64}Cu showed fewer location points per unit of time. This can be explained by the low positron emission branching ratio of the radionuclide. In a PEPT test, ^{64}Cu tracers would lead to large location errors when tracer activity dropped to below 3 µCi at a stationary position and 5 µCi in a moving position. In comparison, ^{68}Ga reached the same error at 0.5 µCi in a moving position. However, this can be

overcome by using a tracer with higher activity. From a practical perspective, the majority of tracer particles made for PEPT are labelled with approximately 1 mCi activity. In this case, under the ideal situation ^{68}Ga tracer would provide 10 half-lives when the activity drops down to useless level, which gave about over 10 hours tracking time; if this also applied to ^{64}Cu tracer, it would take about eight half-lives for it to drop down below 5 μCi, which would give about 100 hours of tracer life time. This is much longer than any labelled tracers used in PEPT experiments previously at PEPT Cape Town. Tracers labelled with ^{64}Cu are therefore most beneficial for PEPT experiments that require long tracking times.

Overall, this research has developed a viable procedure to produce a longer lived tracer for PEPT studies and it has increased the variety of tracers that can be used in PEPT Cape Town. However, due to the limited ^{64}Cu supply and the potential lab contamination, the ^{64}Cu tracer had not been tested in the real PEPT experiments during this study. Further investigation is needed.

REFERENCES

[1] D. J. Parker and X. Fan, “Positron emission particle tracking—Application and labelling techniques,” *Particuology*, vol. 6, no. 1, pp. 16–23, Feb. 2008.

[2] X. Fan, D. J. Parker, and M. D. Smith, “Enhancing 18F uptake in a single particle for positron emission particle tracking through modification of solid surface chemistry,” *Nucl. Instruments Methods Phys. Res. Sect. A Accel. Spectrometers, Detect. Assoc. Equip.*, vol. 558, no. 2, pp. 542–546, Mar. 2006.

[3] X. Fan, D. J. Parker, and M. D. Smith, “Labelling a single particle for positron emission particle tracking using direct activation and ion-exchange techniques,” *Nucl. Instruments Methods Phys. Res. Sect. A Accel. Spectrometers, Detect. Assoc. Equip.*, vol. 562, no. 1, pp. 345–350, Jun. 2006.

[4] J. Jones and J. Bridgwater, “A case study of particle mixing in a ploughshare mixer using positron emission particle tracking,” *Int. J. Miner. Process.*, vol. 53, pp. 29–38, 1998.

[5] B. F. C. Laurent, J. Bridgwater, and D. J. Parker, “Convection and segregation in a horizontal mixer,” *Powder Technol.*, vol. 123, no. 1, pp. 9–18, 2002.

[6] Z. Yang, X. Fan, S. Bakalis, D. J. Parker, and P. J. Fryer, “A method for characterising solids translational and rotational motions using Multiple-Positron Emission Particle Tracking (Multiple-PEPT),” *Int. J. Multiph. Flow*, vol. 34, no. 12, pp. 1152–1160, Dec. 2008.

[7] S. Bakalis, P. W. Cox, A. B. Russell, D. J. Parker, and P. J. Fryer, “Development and use of positron emitting particle tracking (PEPT) for velocity measurements in viscous fluids in pilot scale equipment,” *Chem. Eng. Sci.*, vol. 61, no. 6, pp. 1864–1877, Mar. 2006.

[8] H. P. Kuo, P. C. Knight, D. J. Parker, M. J. Adams, and J. P. K. Seville, “Discrete element simulations of a high-shear mixer,” *Adv. Powder Technol.*, vol. 15, no. 3, pp. 297–309, Jun. 2004.

[9] D. V. V Kallon, I. Govender, and A. N. Mainza, “Circulation rate modelling of mill charge using position emission particle tracking,” *Miner. Eng.*, vol. 24, no. 3–4, pp. 282–289, Feb. 2011.

[10] I. Govender, G. B. Tupper, and A. N. Mainza, “Towards a mechanistic model for slurry transport in tumbling mills,” *Miner. Eng.*, vol. 24, no. 3–4, pp. 230–235, Feb. 2011.

[11] M. A. Green, C. J. Mathias, L. R. Willis, R. K. Handa, J. L. Lacy, M. A. Miller, and G. D. Hutchins, “Assessment of Cu-ETS as a PET radiopharmaceutical for

evaluation of regional renal perfusion.," *Nucl. Med. Biol.*, vol. 34, no. 3, pp. 247–255, Apr. 2007.

[12] K. Tamura, H. Kurihara, K. Yonemori, H. Tsuda, J. Suzuki, Y. Kono, N. Honda, M. Kodaira, H. Yamamoto, M. Yunokawa, C. Shimizu, K. Hasegawa, Y. Kanayama, S. Nozaki, T. Kinoshita, Y. Wada, S. Tazawa, K. Takahashi, Y. Watanabe, and Y. Fujiwara, "64Cu-DOTA-trastuzumab PET imaging in patients with HER2-positive breast cancer.," *J. Nucl. Med.*, vol. 54, no. 11, pp. 1869–1875, Nov. 2013.

[13] B. M. Paterson, P. Roselt, D. Denoyer, C. Cullinane, D. Binns, W. Noonan, C. M. Jeffery, R. I. Price, J. M. White, R. J. Hicks, and P. S. Donnelly, "PET imaging of tumours with a 64Cu labeled macrobicyclic cage amine ligand tethered to Tyr3-octreotate," *Dalt. Trans.*, vol. 43, no. 3, pp. 1386–1396, 2014.

[14] D. Parker, C. Broadbent, P. Fowles, M. Hawkesworth, and P. McNeil, "Positron emission particle tracking-a technique for studying flow within engineering equipment," *Nucl. Instruments Methods Phys. Res. Sect. A Accel. Spectrometers, Detect. Assoc. Equip.*, vol. 326, pp. 592–607, 1993.

[15] C. R. Bemrose, P. Fowles, M. R. Hawkesworth, and M. A. O'Dwyer, "Application of positron emission tomography to particulate flow measurement in chemical engineering processes," *Nucl. Instruments Methods Phys. Res. Sect. A Accel. Spectrometers, Detect. Assoc. Equip.*, vol. 273, no. 2–3, pp. 874–880, 1988.

[16] M. R. M. Hawkesworth, D. J. D. Parker, P. Fowles, J. F. Crilly, N. L. Jefferies, and G. Jonkers, "Nonmedical applications of a positron camera," *Nucl. Instruments Methods Phys. Res. Sect. A Accel. Spectrometers, Detect. Assoc. Equip.*, vol. 310, no. 1–2, pp. 423–434, Dec. 1991.

[17] D. Parker and M. Hawkesworth, "Industrial positron-based imaging: principles and applications," *Nucl. Instruments Methods Phys. Res. Sect. A Accel. Spectrometers, Detect. Assoc. Equip.*, vol. 348, pp. 583–592, 1994.

[18] P. Zanzonico, "Positron Emission Tomography: A Review of Basic Principles, Scanner Design and Performance, and Current Systems," *Semin. Nucl. Med.*, vol. 34, no. 2, pp. 87–111, 2004.

[19] M. R. Hawkesworth, M. A. O'Dwyer, J. Walker, P. Fowles, J. Heritage, P. A. E. Stewart, R. C. Witcomb, J. E. Bateman, J. F. Connolly, and R. Stephenson, "A positron camera for industrial application," *Nucl. Instruments Methods Phys. Res. Sect. A Accel. Spectrometers, Detect. Assoc. Equip.*, vol. 253, no. 1, pp. 145–157, 1986.

[20] D. Parker, R. Forster, P. Fowles, and P. Takhar, "Positron emission particle tracking using the new Birmingham positron camera," *Nucl. Instruments Methods Phys. Res. Sect. A Accel. Spectrometers, Detect. Assoc. Equip.*, vol. 477, pp. 540–545, 2002.

[21] R. D. Wildman, S. Blackburn, D. M. Benton, P. A. McNeil, and D. J. Parker, "Investigation of paste flow using positron emission particle tracking," *Powder Technol.*, vol. 103, pp. 220–229, 1999.

[22] A. Buffler and I. Govender, "PEPT Cape Town: a new positron emission particle tracking facility at iThemba LABS," in *Proceedings of International Topical Meeting on Nuclear Research Applications and Utilization of Accelerators*, 2009, pp. 1–8.

[23] D. J. Parker, D. A. Allen, D. M. Benton, P. Fowles, P. A. McNeil, M. Tan, and T. D. Beynon, "Developments in particle tracking using the Birmingham Positron Camera," *Nucl. Instruments Methods Phys. Res. Sect. A Accel. Spectrometers, Detect. Assoc. Equip.*, vol. 392, pp. 421–426, 1997.

[24] D. J. Parker, T. W. Leadbeater, X. Fan, M. N. Hausard, A. Ingram, and Z. Yang, "Positron emission particle tracking using a modular positron camera," *Nucl. Instruments Methods Phys. Res. A*, vol. 604, no. 1–2, pp. 339–342, Jun. 2009.

[25] T. J. Spinks, T. Jones, P. M. Bloomfield, D. L. Bailey, M. Miller, D. Hogg, W. F. Jones, K. Vaigneur, K. Reed, J. Young, D. Newport, C. Moyers, M. E. Casey, and R. Nutt, "Physical characteristics of the ECAT EXACT3D positron tomograph," *Phys. Med. Biol.*, vol. 45, pp. 2601–2618, 2000.

[26] A. M. Alessio, P. E. Kinahan, P. M. Cheng, H. Vesselle, and J. S. Karp, "PET/CT scanner instrumentation, challenges, and solutions.," *Radiol. Clin. North Am.*, vol. 42, no. 6, pp. 1017–32, vii, Nov. 2004.

[27] T. S. Volkwyn, A. Buffler, I. Govender, J.-P. Franzidis, A. J. Morrison, A. Odo, N. P. van der Meulen, and C. Vermeulen, "Studies of the effect of tracer activity on time-averaged positron emission particle tracking measurements on tumbling mills at PEPT Cape Town," *Miner. Eng.*, vol. 24, no. 3–4, pp. 261–266, Feb. 2011.

[28] L. Gelmini, R. W. Hilts, R. H. Petrucci, and R. K. Wismer, *General Chemistry: Principles and Modern Applications. Selected solutions manual*. Prentice Hall PTR, 2002.

[29] R. Krause-Rehberg, N. van der Walt, L. Büttner, and F. Börner, "A 22Na positron source for use in UHV," *Nucl. Instruments Methods Phys. Res. Sect. B Beam Interact. with Mater. Atoms*, vol. 221, pp. 165–167, Jul. 2004.

[30] J. Zweit, A. M. Smith, S. Downey, and H. L. Sharma, "Excitation functions for deuteron induced reactions in natural nickel: Production of no-carrier-added 64Cu from enriched 64Ni targets for positron emission tomography," *Int. J. Radiat. Appl. Instrumentation. Part A. Appl. Radiat. Isot.*, vol. 42, no. 2, pp. 193–197, 1991.

[31] T. Stoll, S. Kastleiner, and Y. Shubin, "Excitation functions of proton induced reactions on 68Zn from threshold up to 71 MeV, with specific reference to the production of 67Cu," *Radiochim Acta*, vol. 90, pp. 309–313, 2002.

[32] X. Hou, U. Jacobsen, and J. C. Jørgensen, “Separation of no-carrier-added 64Cu from a proton irradiated 64Ni enriched nickel target.,” *Appl. Radiat. Isot.*, vol. 57, no. 6, pp. 773–7, Dec. 2002.

[33] K. Hilgers, T. Stoll, Y. Skakun, H. . Coenen, and S. . Qaim, “Cross-section measurements of the nuclear reactions natZn(d,x)64Cu, 66Zn(d,α)64Cu and 68Zn(p,αn)64Cu for production of 64Cu and technical developments for small-scale production of 67Cu via the 70Zn(p,α)67Cu process,” *Appl. Radiat. Isot.*, vol. 59, no. 5–6, pp. 343–351, Nov. 2003.

[34] L. Daraban, K. Abbas, F. Simonelli, R. Adam-Rebeles, and N. Gibson, “Experimental study of excitation functions for the deuteron induced reactions 64Zn(d,2p)64Cu and 64Zn(d,alphan)61Cu using the stacked-foil technique.,” *Appl. Radiat. Isot.*, vol. 66, no. 2, pp. 261–4, Feb. 2008.

[35] S. Watanabe, Y. Iida, N. Suzui, T. Katabuchi, S. Ishii, N. Kawachi, H. Hanaoka, S. Matsuhashi, K. Endo, and N. S. Ishioka, “Production of no-carrier-added 64Cu and applications to molecular imaging by PET and PETIS as a biomedical tracer,” *J. Radioanal. Nucl. Chem.*, vol. 280, no. 1, pp. 199–205, Mar. 2009.

[36] F. Szelecsényi, G. F. Steyn, Z. Kovács, C. Vermeulen, N. P. van der Meulen, S. G. Dolley, T. N. van der Walt, K. Suzuki, and K. Mukai, “Investigation of the 66Zn(p,2pn)64Cu and 68Zn(p,x)64Cu nuclear processes up to 100 MeV: Production of 64Cu,” *Nucl. Instruments Methods Phys. Res. Sect. B Beam Interact. with Mater. Atoms*, vol. 240, no. 3, pp. 625–637, Nov. 2005.

[37] A. K. Dasgupta, L. F. Mausner, and S. C. Srivastava, “A new separation procedure for 67Cu from proton irradiated Zn,” *Int. J. Radiat. Appl. Instrumentation. Part A. Appl. Radiat. Isot.*, vol. 42, no. 4, pp. 371–376, 1991.

[38] R. D. Neirinckx, “Simultaneous production of 67Cu, 64Cu and 67Ga and labelling of bleomycin with 67Cu or 64Cu,” *Int. J. Appl. Radiat. Isot.*, vol. 28, no. 9, pp. 802–804, 1977.

[39] E. L. Hetherington, P. J. Sorby, and J. Camakaris, “The preparation of high specific activity copper-64 for medical diagnosis,” *Int. J. Radiat. Appl. Instrumentation. Part A. Appl. Radiat. Isot.*, vol. 37, no. 12, pp. 1242–1243, 1986.

[40] T. E. Boothe, E. Tavano, J. Munoz, and S. Carroll, “Coproduction of copper-64 with gallium-67 using protons on zinc-68,” *J. Label. Compd. Radiopharm.*, vol. 30, no. 1, p. 108, 1991.

[41] S. Mirzadeh and F. F. Knapp, “Spontaneous Electrochemical Separation of Carrier-free Copper-64 and Copper-67 from Zinc Targets,” *Radiochim Acta*, vol. 57, pp. 193–199, 1992.

[42] R. Schwarzbach, K. Zimmermann, P. Bläuenstein, A. Smith, and P. A. Schubiger, “Development of a simple and selective separation of 67Cu from

irradiated zinc for use in antibody labelling: a comparison of methods.," *Appl. Radiat. Isot.*, vol. 46, no. 5, pp. 329–336, May 1995.

[43] S. V Smith, D. J. Water, and N. D. Bartolo, "Separation of 64Cu from 67Ga waste products using anion exchange and low acid aqueous/organic mixtures," *Radiochim Acta*, vol. 75, pp. 65–68, 1996.

[44] S. Dolley and T. Van Der Walt, "The production and isolation of Cu-64 and Cu-67 from zinc target materialand other radionuclides," *Czechoslov. J. Phys.*, vol. 56, pp. 6–9, 2006.

[45] K. Cole, A. Buffler, J. J. Cilliers, I. Govender, J. Y. Y. Heng, C. Liu, D. J. Parker, U. V. Shah, M. van Heerden, and X. Fan, "A surface coating method to modify tracers for positron emission particle tracking (PEPT) measurements of froth flotation," *Powder Technol.*, vol. 263, pp. 26–30, Sep. 2014.

[46] C. E. Harland, *Ion Exchange: Theory and Practice*. Royal Society of Chemistry, 1994.

[47] Bio-Rad, "Cation Exchange Resins Instruction Manual." Bio-Rad, 2012.

[48] Cong Liu, "Testing and development of radiolabelling techniques using Purolite S950 resin for Positron Emission Particle Tracking," 2010.

[49] A. P. Van Der Westhuizen, I. Govender, A. N. Mainza, and J. Rubenstein, "Tracking the motion of media particles inside an IsaMill using PEPT," *Miner. Eng.*, vol. 24, no. 3–4, pp. 195–204, Feb. 2011.

[50] Cong Liu, "Further development of the radiolabelling of particles with 68Ga and 18F for positron emission particle tracking (PEPT) measurements," Cape Peninsula University of Technology, 2012.

[51] R. Jones, J. Kahovec, R. Stepto, and E. Wilks, "Definitions of Terms Relating to Reactions of Polymers and to Functional Polymeric Materials (2003)," vol. 76, no. 4, pp. 889–906, 2004.

[52] V. Der Meulen, "Elements pn AG MP-50 cation exchange resin in nitric acid and citric acid," Stellenbosch University, 2003.

[53] J. Fries Getrost, H., *Organic reagents for trace analysis*. Darmstadt [W. Germany]: E. Merck, 1977.

[54] M. E. Phelps, *PET: Physics, Instrumentation, and Scanners*. Springer, 2006.

[55] K. E. Cole, A. Buffler, N. P. van der Meulen, J. J. Cilliers, J.-P. Franzidis, I. Govender, C. Liu, and M. R. van Heerden, "Positron emission particle tracking measurements with 50 micron tracers," *Chem. Eng. Sci.*, vol. 75, pp. 235–242, Jun. 2012.

[56] I. C. Resin, "Purolite S930 / 4888," 2015.

[57] A. Moradi, “Imaging techniques to study nickel-root interactions of the Ni hyperaccumulator plant Berkheya coddii,” Swiss Federal Institute of Technology Zurich, 2008.

[58] S. Kiyomiya, H. Nakanishi, H. Uchida, A. Tsuji, S. Nishiyama, M. Futatsubashi, H. Tsukada, N. S. Ishioka, S. Watanabe, T. Ito, C. Mizuniwa, A. Osa, S. Matsuhashi, S. Hashimoto, T. Sekine, and S. Mori, “Real time visualization of 13N-translocation in rice under different environmental conditions using positron emitting Ttacer imaging system.,” *Plant Physiol.*, vol. 125, pp. 1743–1753, 2001.

[59] P. Hu, Y. G. Yin, S. Ishikawa, N. Suzui, N. Kawachi, S. Fujimaki, M. Igura, C. Yuan, J. Huang, Z. Li, T. Makino, Y. Luo, P. Christie, and L. Wu, “Nitrate facilitates cadmium uptake, transport and accumulation in the hyperaccumulator Sedum plumbizincicola,” *Environ. Sci. Pollut. Res.*, vol. 20, no. 9, pp. 6306–6316, Sep. 2013.

[60] M. Bickell, “Investigations into a positron emission imaging algorithm,” University of Cape Town, 2012.

[61] S. Clemens, M. G. Palmgren, and U. Krämer, “A long way ahead: understanding and engineering plant metal accumulation.,” *Trends Plant Sci.*, vol. 7, no. 7, pp. 309–15, Jul. 2002.

APPENDIX: PET IMAGING OF PLANTS

PET is a nuclear technique normally used for the study of the human or animal body. However, in recent years, there has been a trend to use PET as a tool for studies of plant physiology [57]–[59]. ^{64}Cu was separated for the tracer fabrication of tracer particles for PEPT experiments in this study; however, it also provides an interesting opportunity for PET imaging if used in the liquid form. Its longer half-life should enable the collection of data over the duration of water uptake cycles in plants, and the chemical property of radioactive copper would be precipitated in the bio-cycle of the hyperaccumulation in plants; presenting an opportunity to investigate the

hyperaccumulation process in plants. This appendix describes a preliminary experiment performed in PEPT plant imaging to test the potential use of ^{64}Cu.

5.1 Experimental method

Since ^{64}Cu has long half-life which makes it difficult for the operator to conduct ^{64}Cu solution experiment in PEPT laboratory. The risk of contamination is quite high. Thus, the experimental section was spilt into two parts. Firstly, ^{68}Ga was used in the plant imaging in order to practice the safety procedure of such experiment. Then, the ^{64}Cu plant imaging experiment was performed in the second part.

5.1.1 Tests with ^{68}Ga

The experimental procedure with ^{68}Ga was performed as follows. A white lily flower was purchased from a local market. The lily shoot was cut from the stem to make it approximately 300 mm in length. The flower was soaked in 50 mL of water to keep it alive while preparing the tracer. A few drops of blue dye (blue ink) were added to the solution as an indicator to see the movement of water in the plant structure. The ^{68}Ga/^{68}Ge generator was eluted with 3 mL 0.6 M HCl solution and the amount of activity in the eluate was measured in an ionization chamber (CRC-25 R, *Capintec Inc.*). Enough activity was taken from the generator to ensure 1 mCi of ^{68}Ga remained after the heating and transporting process. The solution was then transferred into a Teflon beaker on a hotplate, and heated at 250 ^{o}C until dryness. The residual activity was dissolved by adding 5 mL water. Then the liquid was transported to the PEPT laboratory, and added to the plant water. A 60 W incandescent lamp was placed 30 cm above the plant to mimic sunlight. The plant was taken out of the solution for a 2 minute scan in the PET camera at intervals of 30, 60, 120 and 180 minutes.

The same experimental procedure was performed with a *Torenia Kauai* plant. The plant was purchased from the Stodel plant nursery. It was supplied in a soil pot; the soil was completely removed from the plant to expose the root. The root of the plant was soaked in a solution containing 1 mCi of ^{68}Ga as described above. The plant was taken out of the solution for a 2 minute scan in the PET camera at intervals of 30, 60, 120 and 180 minutes.

5.1.2 Tests with ^{64}Cu

The ^{64}Cu plant imaging experiment was performed with two tomato plants, where one was left at its complete height of 500 mm and a second had the roots removed with a total height of 350 mm. Both tomato plants were soaked in 50 mL water with a few drops of blue dye (blue ink) added to the solution as indicator. 1.1 mCi of purified ^{64}Cu solution was heated in a Teflon beaker on a hotplate to complete dryness to remove 5 M HNO_3. Then 5 mL water was added to pick up the residual activity. The liquid tracer was transported to the PEPT laboratory, and added to the water supply of the plants. A 60 W incandescent lamp was placed 30 cm above the plant to mimic sunlight. Each plant was taken out the solution for a 2 minute scan in the PET camera after 5 hours soaking, and the root was cut off the first tomato plant before scanning.

^{64}Cu offers a longer imaging time than the other radionuclides used at PEPT Cape Town, such as ^{18}F and ^{68}Ga. This may cause a potential radiation safety concern when operating in the PEPT lab. In designing the PET imaging experiments, two sets of practice experiments were performed without any activity to minimise the risk of severe contamination to the laboratory and user.

5.2 Results and discussion

Firstly ^{68}Ga was used to test two different types of plant. In the second part, a ^{64}Cu plant imaging experiment was performed with tomato plants.

5.2.1 ^{68}Ga PET plant imaging

The acquired binary data were analysed using the line density algorithm [60] with a voxel size of 2 x 2 x 2 mm^3 to produce the final PET image. In the experiment, the eluted ^{68}Ga was contained in 0.6 M HCl solution; therefore a drying process was added to remove the acid from the solution. In order to enable the flow of water and mineral nutrients in the plant, an incandescent light was placed on top of the plant to improve the transpiration process.

Comparing the acquired data from different tracer absorption times, the data set obtained after two hours of absorption produced the best images. This was sufficient

time for the absorption to occur, but not long enough for the decay of a substantial fraction of the initial activity of ^{68}Ga. The blue dye added in solution also provided an indication of the mass flow in the plant. After 1.5 hours, blue dots appeared on the edges of the lily flower petals (Figure 44).

Figure 44: Blue dots appeared at the edge of the lily flower after 1.5 hours soking.

This indicated that the time for mineral nutrient transport from the bottom of the lily shoot to the top of the flower petals was 1.5 hours. Since there were no roots attached to the flower, the major driving force of mass flow was transpiration. The capillary effect also played a part, but it was not the primary factor. During this process, water evaporated from the stomata, the opening pores on plant leaves, which created potential differences in water content within the plant. Then this force drove water from root up to leaves via the xylem. The process can be seen in the images shown in Figure 45.

Figure 45: Blue ink flow through the xylem of lily stem.

Figure 46 shows the PET images of ^{68}Ga absorption in the lily flower after two hours. Different concentrations of ^{68}Ga were detected in different parts of the plant body, therefore different scales were used to highlight the absorption in different sections of the plant. The PET images are presented in three separate slices. The image at the top left is a sum over vertical 2D slices of the 3D PET data between *Z* values of -117 mm to -69 mm with values below a line density of 150 (threshold) not shown. The image in top right is the sum of slices from -67 mm to -29 mm on the *Z*-axis, with a threshold of 200 mm. The image at bottom is a sum of slices from -27 mm to +11 mm on the *z*-axis.

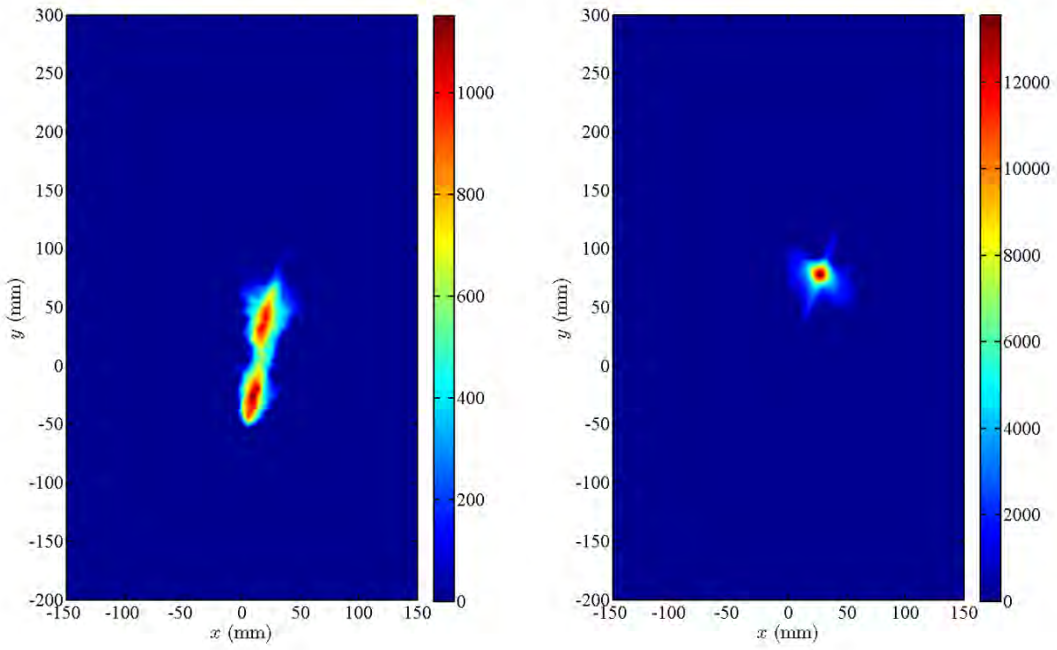

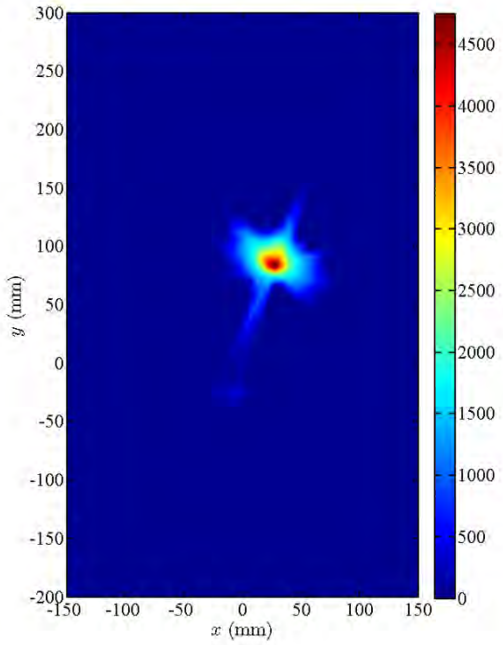

Figure 46: PET images of a lily flower: (top left) stem of the flower, (top right) flower pedicel, (bottom) PET images overlapped on lily flower.

The images show that ^{68}Ga ions were absorbed and distributed throughout the entirety of the lily flower. A threshold value was applied to eliminate the background noise. According to the line density, the concentration of ^{68}Ga was highest in the flower pedicel, and the stem retained a low concentration of ^{68}Ga. A possible explanation for this would be that the major driving force for ^{68}Ga absorption is transpiration, which happens when water evaporates through the stomata on plant leaves (or in this case, on flower petals). Therefore the ^{68}Ga was absorbed into the plant with the water flow. For the short duration of tracer absorption, the selective absorption of ^{68}Ga ions was minimal. When water evaporated from the top of the lily flower, ^{68}Ga remained behind in the plant, and therefore caused the high gallium concentration in the flower pedicel. Since there are no stomata on the surface of the plant stem and the water was only transported through xylems inside the stem, the gallium should be lower in the stem than the in other parts of the plant.

Figure 47 shows the PET images of ^{68}Ga absorption in *Torenia Kauai* plant. This particular plant was purchased because it was the same size as the field of view of the PET camera. The PET data was recorded after two hours of soaking in the tracer solution, and the image is a sum of several 2 mm slices at the central *Z*-axis of the

camera. It shows that after two hours, the gallium was mostly absorbed into the roots of the plant. Very small amounts of gallium reached the stem, which can be seen in the faint colour at the top of the root which represents the stems. An observation was made throughout the experiment: the blue colour slowly faded away in the soaking solution. The picture at the bottom of Figure 47 shows that a large amount of dye was absorbed by the roots as it changed into blue from its original white colour. After careful examination of the stems and flowers of the plant, there was only small amount of blue dye in the body of the plant.

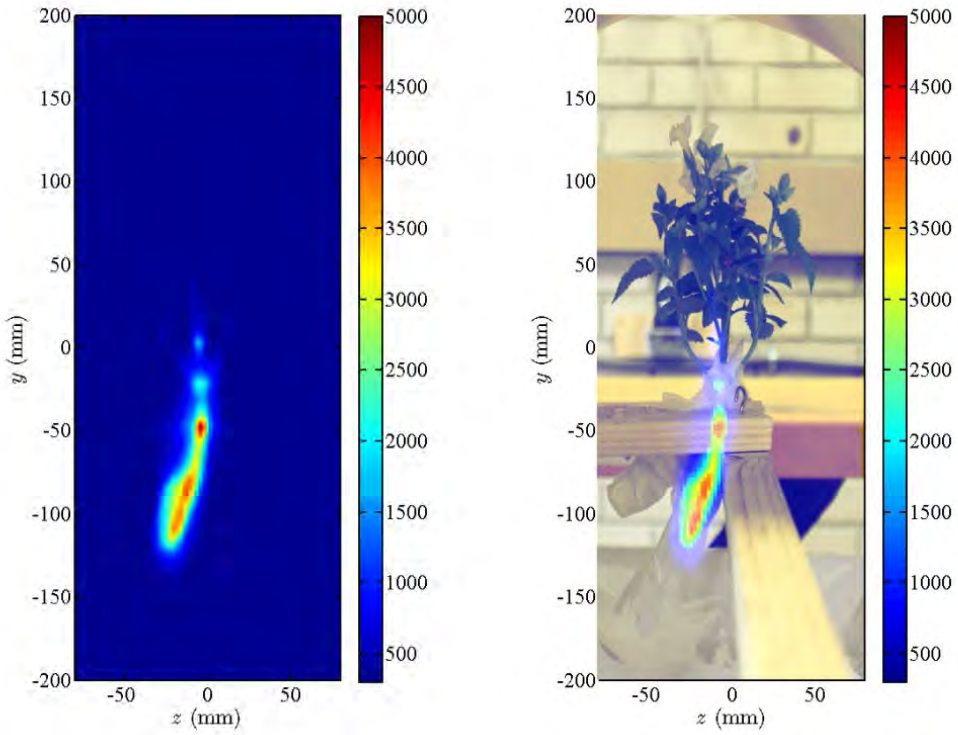

Figure 47: PET image of *Torenia Kauai* plant: (top left) PET image of plant, (top right) PET image overlapped on plant picture in scanner, (bottom) plant after scanning.

This phenomenon can be explained from the mechanism of xylem transport. The plant root epidermis and cortex are permeable for solutes, but the cell walls of the endodermal cell layer act as a barrier for diffusion into the vascular system. In general, the solutes have to get into the root before they can enter the xylem. The transport of ions into the xylem is a tightly controlled process, and is mediated by membrane transport proteins [61]. Thus entry of metal ions into the plant xylem is a slow process. Two hours would only allow a small amount of gallium ions into the plant body, and the large amount of radiation absorbed in the root obscures any ^{68}Ga in the stems.

5.2.2 ^{64}Cu PET plant imaging

The final purified copper was contained in a 5 M nitric acid solution, and although the plant absorption was performed with less strict botanical controls (e.g. tap water was used instead nutrient solution), the high acid concentration would have damaged plant cells. Thus a drying procedure was added to remove the acid.

Figure 48 shows the ^{64}Cu PET images of a tomato plant, which were chosen for their ability to absorb a large amount of water. The tomato shoot and tomato plant with root were soaked in ^{64}Cu water for about five hours. The previous ^{68}Ga PET experiments showed that plant roots absorbed a large amount of radionuclide which interfered with

the scanning result. Therefore the root of the tomato plant was cut off before scanning, with the aim of improving the final image. The acquired data were analysed with the line density algorithm, and images are presented in the *Y* and *Z*-axes, over a 2D slice at an *x* value of 13 mm.

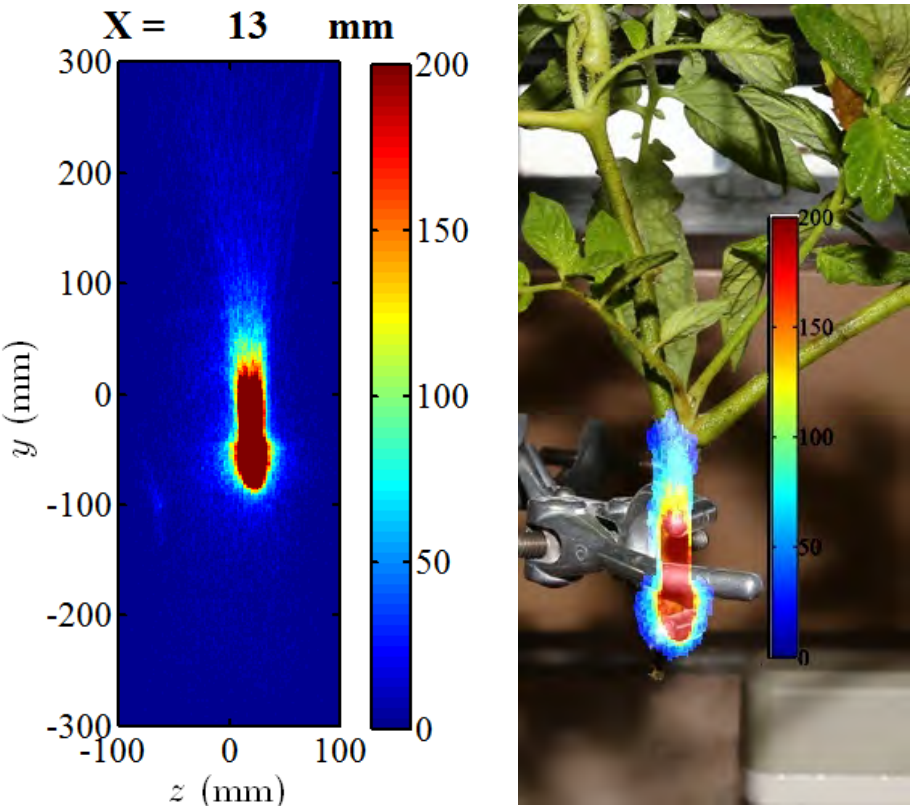

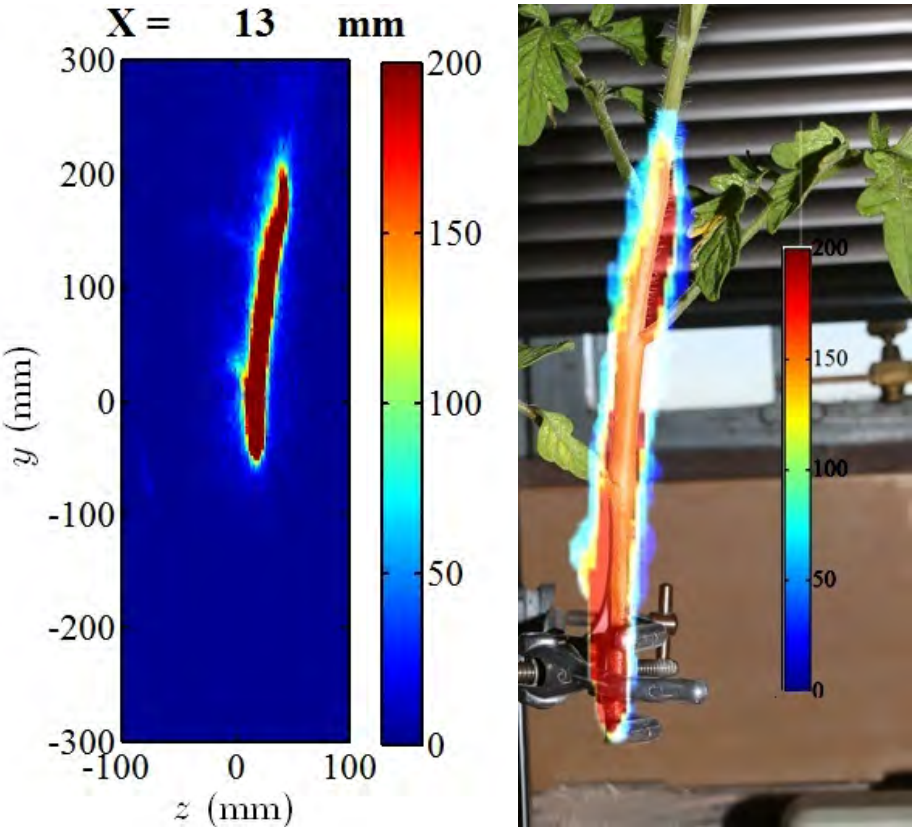

Figure 48: ^{64}Cu PET plant images: (top) tomato plant shoot, (bottom) tomato plant with root, with root cut off for scanning.

The ^{64}Cu PET imaging results show that the ^{64}Cu was successfully absorbed onto the tomato plant, and the longer soaking time produced more detail in the image of the plant stem. The tomato shoot had more branches, and most of the activity accumulated in the bottom part of the plant, with the concentration of copper decreasing with height. There was very little activity detected in the branches. The sample plant with root, on the other hand, showed a similar result as the shoot, where most of copper activity was detected in the main stem and only a small amount in the branches. Both of the PET images were overlapped with pictures of the plant, and the PET images were re-sized to fit the scale.

5.3 Conclusion

This section described how PET plant imaging experiments were performed with both ^{68}Ga and ^{64}Cu radionuclides. The purpose of the experiments was to provide some preliminary indications of how to apply PET imaging techniques in the field of plant studies. Both of these radionuclides showed promising imaging results. Liquid ^{68}Ga

tracers can be used for about two hours of PET imaging, and the longer lived ^{64}Cu tracers can be used for a much longer experiment duration for PET plant imaging. It is worth noting that due to the time restraints in the PEPT lab, the copper experiment was only performed for five hours, but the total duration for a ^{64}Cu tracer for PET plant studies could be as long as about 24 hours.